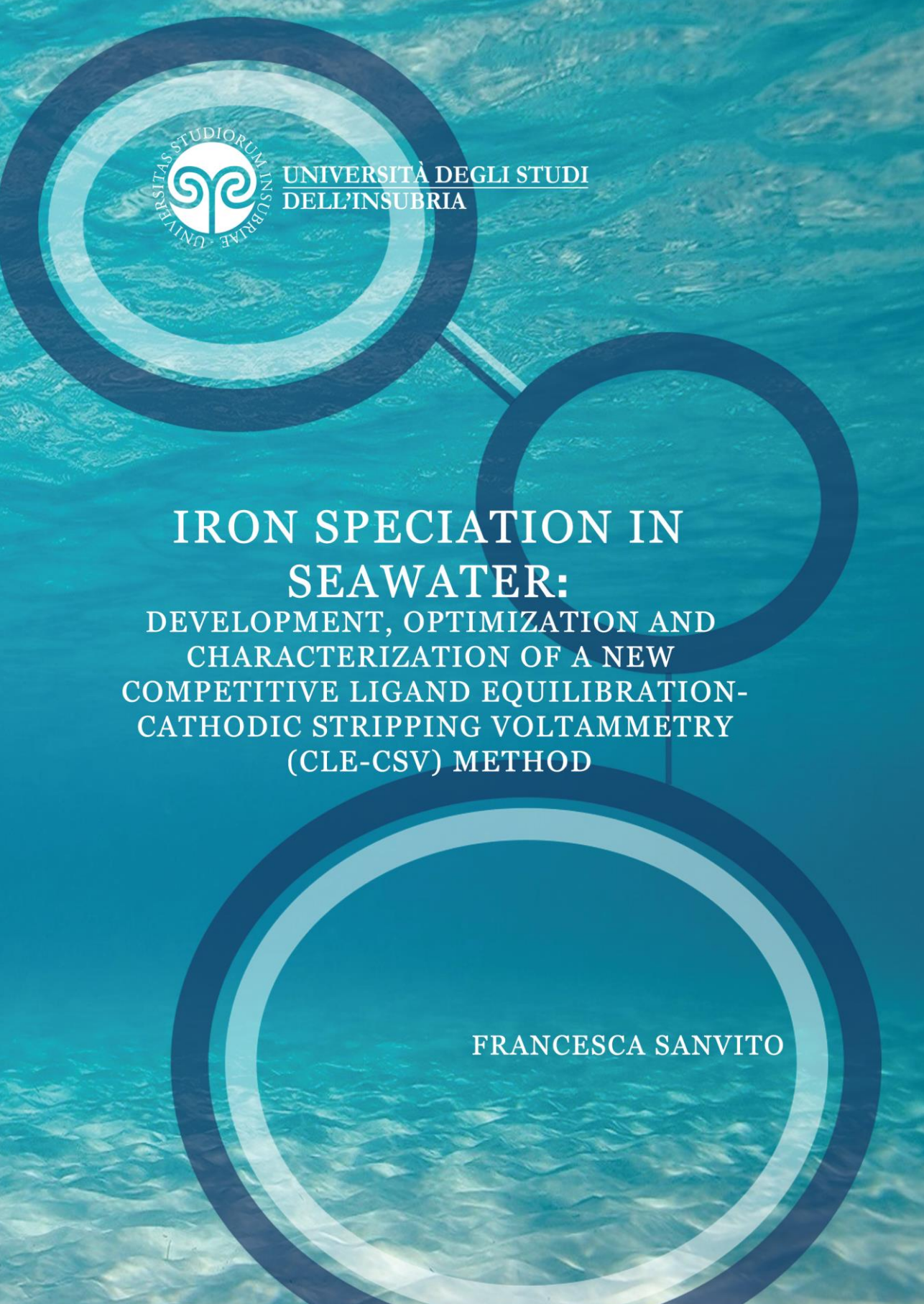

IRON SPECIATION IN SEAWATER:

DEVELOPMENT, OPTIMIZATION AND CHARACTERIZATION OF A NEW COMPETITIVE LIGAND EQUILIBRATION-CATHODIC STRIPPING VOLTAMMETRY (CLE-CSV) METHOD

FRANCESCA SANVITO

UNIVERSITÀ DEGLI STUDI
DELL'INSUBRIA

Department of Science and High Technology

IRON SPECIATION IN SEAWATER: DEVELOPMENT, OPTIMIZATION AND CHARACTERIZATION OF A NEW COMPETITIVE LIGAND EQUILIBRATION-CATHODIC STRIPPING VOLTAMMETRY (CLE-CSV) METHOD

By Francesca Sanvito

A dissertation in partial fulfillment of the requirements for the degree of Doctor of Philosophy in
Chemical and Environmental Sciences

XXXIII Cycle

Committee in charge:
Professor Sylvia G. Sander
Professor Pascal Salaun
Professor Andrea Pozzi

Supervisor:
Professor Damiano Monticelli

To You

“Whatever you can do, or dream you can, begin it. Boldness has genius, power, and magic in it. Begin it now.”

Johann Wolfgang von Goethe

“What you get when you arrive at your destination is not as important as what you become by reaching it.”

Epitteto

INDEX

ABSTRACT

Iron speciation in seawater is of the utmost importance in understanding the biogeochemical cycle of this element, in view of its central role in regulating the primary productivity of the oceanic environment and its connection to global planetary cycles. The Competitive Ligand Equilibration-Cathodic Stripping Voltammetry (CLE-CSV) methods, often with the catalytic enhancement of the signal, are fit for this purpose, as they allow to study the organic speciation of the metal by determining the organic iron binding ligands concentration and their stability constants for the metal itself. These methods avoid any sample separation or pretreatment step, and show acceptable detection capabilities and robustness towards the saline matrix.

The aim of the present PhD project was the development, optimization and characterization of a new method based on the CLE-CSV technique, characterized by optimal detection capabilities (sensitivity and limit of detection) and by an easy-to-use instrumental configuration. In fact, several methods experienced a development during the last 20 years, but each of them was characterized by the presence of important drawbacks as poor sensitivity, too long analysis time requirement and also, in some cases, by the use of a suspected carcinogenic species as catalytic enhancer.

In the present work, 2,3-dihydroxynaphthalene and atmospheric oxygen were employed as iron chelator and catalytic enhancer, respectively, as they ensure the best analytical performances.

A new hardware configuration was firstly developed, leading to an overall simplification of the system: a silver wire pseudoreference was installed replacing the traditional Ag/AgCl 3 M KCl reference electrode and atmospheric

oxygen was directly introduced into the close analysis cell by an air pump. An extensive optimization procedure was accordingly performed, and the detection capabilities were carefully evaluated: fully satisfactory analytical performances for trace and ultratrace iron determination were achieved.

A comprehensive approach to the characterization of an adsorptive cathodic stripping voltammetry with catalytic enhancement followed. The focus of this second part of the work was on the understanding of the chemical features and processes involved. The consecutive effects of the studied features on the analytical signal were evaluated to appreciate possible limitations and future directions for the method improvements. Accordingly, the 2,3-dihydroxynaphthalene degradation and the Fe-DHN complex stoichiometry were studied and their consequences on the speciation procedure evaluated. The stoichiometry of the FeDHN complex was also determined as it plays a major role in the speciation data treatment. Furthermore, the thermodynamics of the ligand and the complex simultaneous adsorption onto the electrode surface was considered to evaluate a possible competition between these two species. As the final step of this part of the work, the electron transfer kinetics (k^0) and catalytic enhancement (k'_{cat}) were studied to completely characterize the electrode reaction, i.e., to give full insight into the exact mechanism responsible for the analytical sensitivity.

The new CLE-CSV method was subsequently developed. Firstly, the side reaction coefficients for the FeDHN complex were calibrated against the EDTA and the conditional stability constants calculated. The method was successfully validated in UV digested seawater using diethylenetriaminepentaacetic acid (DTPA), deferoxamine (DFO), and protoporphyrin IX (PPIX). It was proved that good detection capabilities also for humic acid (HA) could be achieved. The analysis of six seawater samples from a Ross Sea water column (Antarctica) was then performed, demonstrating the fit for purpose for the detection of trace concentrations of organic iron binding ligands in seawater.

Lastly, as a further development of the technique, the pH buffer which is usually

employed to perform the voltammetric analysis in seawater was removed. The latter innovation was enabled by the natural pH buffer capacity of seawater due to the presence of the $CO_2/HCO_3^-/CO_3^{2-}$ system. The application of the unbuffered method resulted in statistically indifferent values for both the side reaction coefficients and conditional stability constants with respect to the buffered method. Again, the unbuffered method was successfully validated in UV digested seawater using both an artificial and a natural ligand and then applied to the same six seawater samples from the Ross Sea water column. The proposed unbuffered approach may demonstrate relevant to already existing speciation procedures for iron, resulting in a correct determination of complexing capacity and stability constant of organic iron binding ligands at ambient pH.

The new method, both in its buffered and unbuffered version, achieved a tenfold sample size reduction and a tenfold increase in the analytical sensitivity compared with other methods employing 2,3-dihydroxynaphthalene. Furthermore, the analysis time was halved with respect to the fastest method reported in the literature as half an hour resulted enough to measure a twelve points titration.

LIST OF ACRONYMS IN ALPHABETIC ORDER

AdCSV: adsorptive cathodic stripping voltammetry
CLE-CSV: competitive ligand equilibration – cathodic stripping voltammetry
CV: cyclic voltammetry
DA: domoic acid
DFO: deferoxamine
DHN: 2,3-dihydroxynaphthalene
DPD: NN-dimethyl-p-phenylenediamine
DTPA: diethylenetriaminepentaacetic acid
EDTA: ethylenediaminetetraacetic acid
EPS: exopolysaccharides
FA: fulvic acid
FI: flow injection
HA: humic acid
HEPPS: 4-(2-hydroxyethyl)-1-piperazinepropanesulfonic acid
HMDE: hanging mercury drop
HNLC: high nutrient low chlorophyll
1H-NMR: proton nuclear magnetic resonance
HS: humic substances
IARC: International Agency for Research on Cancer
ICP-MS: inductively coupled plasma - mass spectrometry
LOD: limit of detection
NN: 1-nitroso-2-naphthol
PPIX: protoporphyrin IX
RSD%: percentage relative standard deviation
RT: reverse titration

S/N: signal to noise ratio
SA: salicylaldoxime
SAFe: sampling and analysis of iron
SqW: square wave
SW: seawater
TAC: 2-(2-thiazolylazo)-p-cresol
UV: ultraviolet
UV-SW: ultraviolet digested seawater
UV-Vis: ultraviolet-visible
WHO: World Health Organization

LIST OF SYMBOLS IN ALPHABETIC ORDER

A: electrode surface area

α: symmetry factor

$\alpha_{Fe'L}$: side reaction coefficient for the Fe'L complex

β: adsorption constant

β_1: stability constant of the ML2 species

β_2: stability constant of the ML3 species

c: concentration

C_L: total organic iron binding ligand concentration

γ: catalytic parameter

ΔE_p: difference between anodic and cathodic peak

$E^{0:}$ standard potential

E_p: peak potential

F: Faraday constant

f: square-wave frequency

f_{max}: critical value of the square-wave frequency

Γ: electrode surface coverage

Γ_{max}: maximum electrode surface coverage

i: peak current

$i_{p,a}/i_{p,c}$: anodic/cathodic peak current

k: kinetic constant

K: stability constant of the ML complex

k^0: standard electrochemical rate constant

k_{cat}: catalytic constant

$K'_{Fe'L}$: conditional stability constant for the Fe'L complex

λ: kinetic parameter

L: organic iron binding ligand

L_{add}: iron chelator employed in a AdCSV analysis

n: number of electrons exchanged during an electrode reaction

Q: charge exchanged during an electrode reaction

S: sensitivity

v_a/v_c: rate of the anodic/cathodic reaction

ψ_p: net dimensionless peak current

$\psi_{p,a}/\psi_{p,c}$: dimensionless anodic/cathodic peak current

ω: dimensionless kinetic parameter

ω_{max}: critical dimensionless kinetic parameter

[Fe']: inorganic iron concentration

$[Fe^{3+}]$: free iron concentration

[FeL]: iron concentration complexed by organic iron binding ligand

$[Fe_{labile}]$: iron concentration released from the FeL complexes upon the addition of Ladd and inorganic iron

[L']: concentration of organic iron binding ligand not complexed by iron

[M]: metal concentration

1 INTRODUCTION

Iron determination and speciation in seawater are tasks of the utmost importance for chemical oceanographers. Iron, in fact, plays an important role in regulating the primary productivity of the oceanic system[1]. Since 1990, when the first "Iron Hypothesis" was formulated[2–4], it is clear that iron limitation reduces the phytoplankton community activity which consists on the synthesis of chlorophyll by photosynthetic processes.

More than 30% of the surface waters of the oceans are known as the "high nutrient low chlorophyll" (HNLC) regions[5]. In these areas, despite the high concentrations of macronutrients as nitrate and phosphate, low chlorophyll concentrations are found as a consequence of a low phytoplankton biomass. To date, this phenomenon is acknowledged to be a result of the iron limitation. Therefore, the relevance of this limitation on the determination of the global atmospheric CO2 level and, hence, on the regulation of the global climate has been thoroughly investigated[2,6,7]. Low iron concentrations, in fact, could affect the ability of the phytoplankton which acts as a sink for CO2 and transports part of it to the deep ocean by the so-called "biological pump" process[6].

In this complex context, the Iron hypothesis has been investigated by both small-scale[3,8–11] and mesoscale Fe-enrichment experiments[5,12–21]. The first, based on incubation bottle experiments, led to controversial results, as they did not

demonstrate that iron enrichment stimulates the phytoplankton growth[22]. Several limitations were found in these experiments, especially in recreating the oceanic environment: the walls of the containers are just one example affecting the simulation of the natural environment. For this reason, the small-scale experiments were not the best to describe the processes that happen in nature and the large-scale experiments were then set-up[13]. These were based on in situ mesoscale iron enrichment experiments: large areas of the ocean were fertilized with a controlled amount of iron sulfate, and simultaneously sulfur hexafluoride, SF_6, was added as inert tracer. Iron concentration was largely increased and its effect on chemical, physical and biological properties of seawater was monitored for days. Several large-scale experiments were performed in different regions of the oceans during the last decades: the IRONEX I and II[12,13] in the equatorial Pacific south of the Galapagos Islands, the FeeP[14] in the North Atlantic Ocean and the LOHAFEX[5] in the South Atlantic Ocean are just a few examples.

Nevertheless, the latest studies include more efficient modelling of the global earth system and suggest that even an efficient fertilization, which results in an increased phytoplankton activity, would have a limited impact on the global climate compared to other climate drivers[23,24]. In addition, recently introduced models have hypothesized the possible limiting ability of other micronutrients on the phytoplankton activity when iron is bounded by organic species[25] (see "Iron Speciation" and "Iron Cycle and Bioavailability" paragraphs of this chapter for more information). Apart from these controversies, a deep comprehension of iron biogeochemical cycle and its linking to the other cycles in seawater would represent a giant step in the direction of the complete understanding of the regulatory processes in this natural environment.

These knowledge gaps led to the development of the GEOTRACES program (www.geotraces.org)[26]. Since 2005, in fact, the main purpose of the GEOTRACES program is to achieve a complete understanding of marine biogeochemical cycles of trace metals and their isotopes, motivated by their crucial role in many aspects of oceanography.

Regarding iron, more than 20000 data were collected about its total concentration in seawater as of 2016[7], while data collected about its speciation were only around 1700, as of the same year[27]. The latter discrepancy is mostly due to the labor intensive and time-consuming analytical procedures developed up to now for iron speciation in seawater.

From the analytical chemist's point of view, iron determination and speciation in seawater are challenging tasks as they require methods characterized by extreme detection capabilities in terms of sensitivity and limits of detection, usually below 1 nM, preventing the high risk of sample contamination. Regarding the total iron determination, several methods experienced a great development during the last decade, increasing the detection capabilities and simplifying the analytical protocols. On the other hand, the same advancements were not achieved for the speciation analysis, as methods developed up to now show quite poor sensitivity and are characterized by long analysis time strongly limiting sample throughput.

1.1 Iron in seawater

1.1.1 Iron Speciation

Iron speciation is of the utmost importance in understanding its behavior and bioavailability in the oceanic environment. Fractionation will be presented first, followed by the description of the speciation on a chemical species-based approach, as it relies on well-known chemical concepts, as oxidation states, thermodynamics and kinetic laws and inorganic/organic domains.

Before moving to the description of the main topic of the paragraph, an introduction to the forms of iron in seawater and its solubility in this matrix is required.

Iron dimensional fractionation is usually defined following physical separation by commercial filters (Figure 1.1)[28].

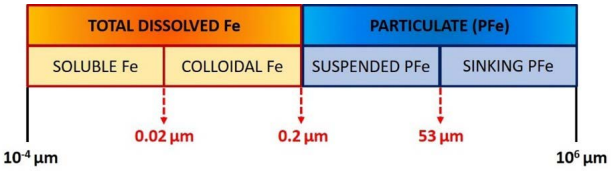

Figure 1.1: Operational definitions used in chemical oceanography for iron fractions based on the filter pore size.

The particulate iron is the fraction retained by a filter with a 0.2 µm pore size. Within the latter, the fraction smaller than 53 µm, which is composed of the suspended particles, is separated by the fraction larger than 53 µm, which instead contains the sinking particles. The 53 µm value is only dictated by the commercially available filters. The fraction which is not retained by a 0.2 µm pore size filter is called total dissolved iron[28]. No living organisms are generally present in this fraction, whereas many different chemical species are very common. Moreover, thanks to a filter with a pore size of 0.02 µm or by a cross-flow filtration with a membrane cut-off of 1 kDa[29,30], the retentate containing the colloidal iron can be separated by the permeate which, instead, contains the soluble iron. Actually, the colloidal iron cannot be directly measured, but it

is deduced from the difference between the total dissolved iron and the soluble fraction. The knowledge about the physical separation of iron in seawater has been improved by using other techniques in addition to the filtration with trace metal clean membranes, such as the ultrafiltration or the flow field flow fractioning coupled to ultra-violet (UV) and inductively coupled plasma-mass spectrometry (ICP-MS)[30,31].

Moving to iron chemical species in seawater, the oxidation state, inorganic and organic complexes should be considered: both the ferrous, Fe(III), and ferric(II) oxidation states exist in seawater. Fe(III) and Fe(II) are the oxidizer and the reducer, respectively, of the redox couple Fe(III)/Fe(II) characterized by the standard potential E^0=0.771V. The latter is modified in seawater by the complexation with several ligands resulting in a wide range of redox potentials for the Fe(III)L/Fe(II)L couple. As a consequence, the ability of iron to fine-tune its redox potential make this element essential for all the living organisms.

In the presence of oxygen, Fe(III) is the stable state, showing high reactivity, thermodynamic stability, and very low concentrations as free Fe^{3+}. Inorganic complexes of Fe^{3+} include $Fe(OH)_4^-$, $Fe(OH)_3$, $Fe(OH)_2^+$, $Fe(OH)^{2+}$ as iron(III) is characterized by a strong affinity for the hydroxide ion.

Iron inorganic and organic speciation in seawater defines its solubility in this natural environment and, for this reason, it has been always presented in relation to this topic. In particular, the measurement for the iron solubility in seawater represented a challenging task for many years. In principle, it could be calculated considering the thermodynamic equilibria and summing the concentrations of the different dissolved forms for a determined total iron concentration at a given pH and temperature. The first approach was proposed by Byrne et al. in 1976[32]: by using filtration and dialysis techniques, the prevalence of the $Fe(OH)_2^+$ and $Fe(OH)_3$ species was suggested. Later, in 1996, Kuma et al.[33] studied the iron solubility both in coastal and oceanic water and compared it to the solubility in seawater preliminarily UV irradiated to remove all the organic matter. These experiments confirmed the prevalence of the $Fe(OH)_2^+$ species and led to

calculated solubility products log*K_{SO} in the range of 4.8-5.0 for coastal water and 4.4-4.6 for oceanic water. Moreover, a medium solubility value between 0.3 and 0.6 nM was found in the mixed layer, with the minima between 0.15 and 0.2 nM at depths of 50-200 m. Besides, in 2002, Liu et al.[34] studied the solubility for a wide range of pH (2-9), temperature (5°C-50°C) and salinity (0-36). At the same conditions (salinity=36, pH = 8 and T= 25°C) the 0.3-0.6 nM solubility found was in good agreement with the previous work[33]. Moreover, it was demonstrated that solubility increases with the temperature decrease, and decreases with the salinity decrease. These results were confirmed by Schlosser et al[35] in 2012, who studied the solubility of iron in the Southern Ocean and found values between 0.4 and 1.5 nM correlated to the temperature.

In this context, the inorganic iron speciation in seawater is mostly studied in synthetic seawater to determine the solubility of the metal in this natural environment[32–34]. It primarily involves hydrolysis reactions (equation 1.1).

$$Fe^{3+} + nH_2O \xleftrightarrow{\beta^*} Fe(OH)_n^{(3-n)+} + nH^+ \quad (1.1)$$

(n integer between 1 and 4)

with precipitation of amorphous $Fe_n(OH)_{3-n}$ xH2O and consecutive transformations into more stable forms such as hematite, goethite, and lepidocrocite. Also, the complexation of the metal with major ions must be considered for a complete evaluation of the inorganic speciation.

The conditional stability constant β* can be experimentally determined or theoretically calculated considering the thermodynamic constants at the ionic strength I=0 and applying a correction for the activity coefficient for each ion[36].

Iron solubility studies have demonstrated that the solubility of iron in seawater considerably decreases to 0.1 nM ore less when the sample is pretreated with UV-digestion[33], proving that natural organic Fe(III) ligands increase the metal solubility. In this context, in 1995, Van den Berg[37] proved that at least the 99% of the total iron is bounded by organic ligands. Seemingly these ligands are present everywhere in the marine environment, from the costal to open ocean

and from the surface down to the deep waters. Organic Fe-binding ligands are divided into classes (denoted as L_i, with i=1, 2, 3) following their binding strengths: L_1 groups the stronger ligands characterized by a $\log K'_{Fe'L1}$ >12 (with $K'_{Fe'L}$ conditional stability constant for the iron-ligand complex (from now on referred to as FeL)), L_2 groups ligands with $11<\log K'_{Fe'L2}<12$, and L_3 is the class for the weaker ligands characterized by a $\log K'_{Fe'L3}$ <11. These differences by orders of magnitude are dictated by the chemical structures and different nature of the species. Actually, there are several geochemical models that can be used to classify the organic matter in this natural environment. Just as an example, the NICA-Dunnan model[38–40] is commonly used to describe the distribution of proton and metal binding to humic substances (see above for major information about these species). In particular, this model, which is based on a continuous site distribution, states that the distribution of the metal-binding functional groups follows statistical rules and the pk'_s are distributed normally along the molecule[38–40].

Several small organic Fe-binding ligands have been identified up to now: in particular, siderophores are the species of major interest (Figure 1.2-a and 1.2-b). Siderophores are compounds produced by both terrestrial and marine heterotrophic and cyanobacteria to sequester iron from their environment[41–43]. Nevertheless, the siderophore uptake is not specific: they can be used by a bacterial species even though they are produced by another one[44]. Their production is more significant in regions where the organic carbon concentration is high enough to promote the bacterial productivity[45]; nevertheless, it has been suggested that many siderophores classes are not present in different water masses due to their photochemical lability[46,47]. By incubation experiments, it has been proved that all the siderophores are characterized by the presence of the catechol, hydroxamic or α-hydrocarboxylic acid groups[48] and by high stability constants. Among these, the deferoxamine, DFO, (Figure 1.2-c) is a common example of siderophores. The chemical structure of many marine siderophores also contains one or more fatty acid chains bonded to the iron-chelating head

group[5,49–56] that strongly influence the biogeochemistry of siderophores.

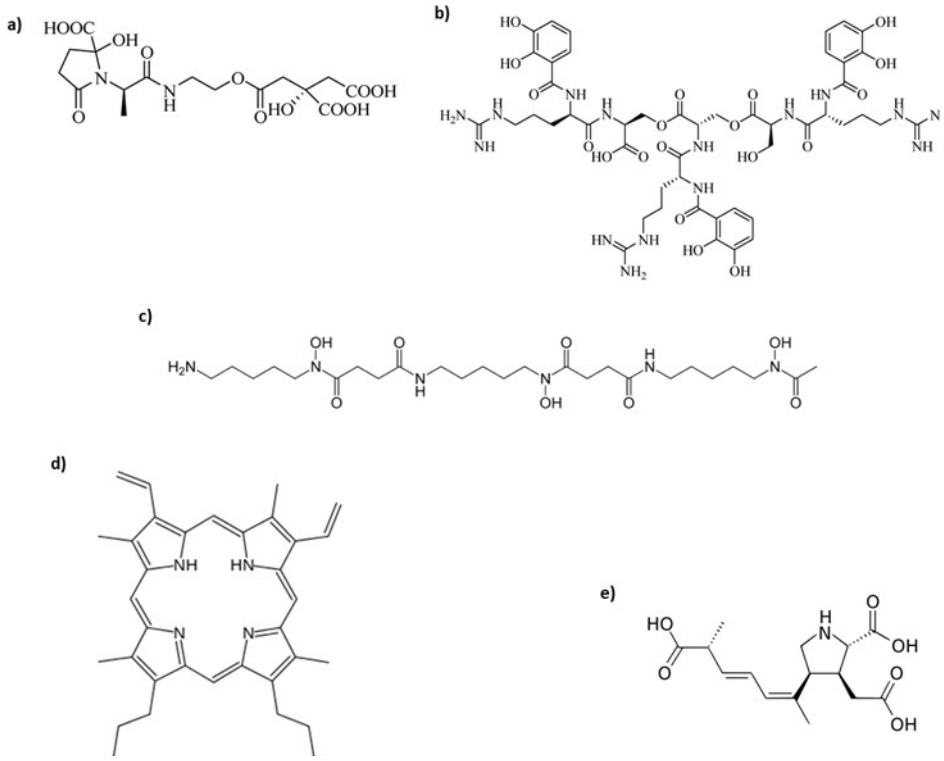

Figure 1.2: Examples of the small defined organic Fe-binding ligands: a), b) c) siderophores; c) deferoxamine; d) protoporphyrin IX; e) domoic acid.

Porphyrins (Figure 1.2-d) are another biologically produced class of molecules suggested as organic Fe-binding ligands[57,58]. They include chlorophylls and their breakdown products and hemes. Due to their low solubility in seawater at pH 8, porphyrins are thought not to be a large part of the organic Fe-binding ligands, despite the ability to spontaneously complex Fe(III) in solution[30,59].

Furthermore, domoic acid (Figure 1.2-e), which is an algal toxin, can complex iron in seawater, even though it is one of the weaker ligands with $\log K'_{Fe'DA}=8.7$[60]. So, even though domoic acid is not one of the most common organic Fe-binding

ligands, it plays an important role in the biogeochemical cycle of this element in seawater.

More recently, it has been proved that molecules characterized by larger dimensions, lower binding capacity for iron, but relatively higher concentrations in seawater contribute to the complexation of iron in the oceanic environment. In particular, humic substances (HS), saccharides and exopolysaccharides (EPS) are the most common classes of this kind of ligands. Humic substances, i.e. fulvic and humic acids (FA and HA, respectively Figure 1.3-a and 1.3-b) are refractory terrestrial, freshwater or marine substances and they persist into the deep ocean. On the other hand, EPS are mostly produced in the surface water and they are more associated with the phytoplankton activity. They are composed of neutral sugars and contain acidic polysaccharides like uronic acids.

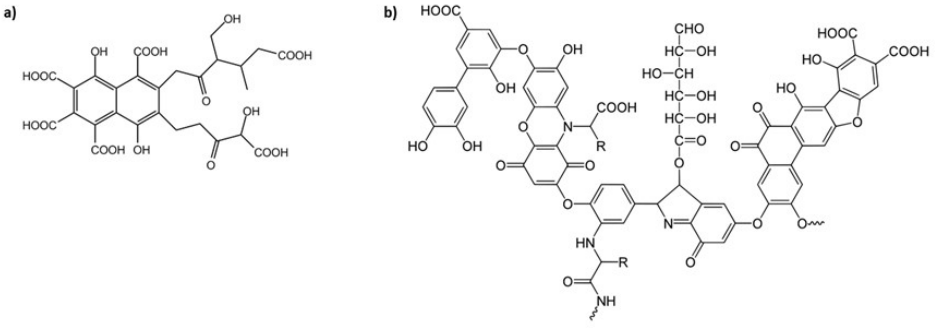

Figure1.3: Larger less defined organic Fe-binding ligands in seawater: a) example of a fulvic acid and b) general structure of humic acids

Moreover, exopolysaccharides represent a significant part of the dissolved and colloidal organic matter[61,62]. The two classes, HS and EPS, are characterized by similar properties being both oxygen rich[63] and their complexes with iron more stable at high pH.

To conclude, the organic iron speciation in seawater plays a fundamental role, as the organic Fe complexes are dominant in this environment and has important implications on the iron bioavailability and redox speciation as well as on its

solubility.

1.1.2 Iron sources in seawater

External iron sources contribute to the total iron concentration in seawater and alleviate the iron limitation, mostly in Fe-limited regions. Part of it, in fact, is lost due to the sedimental burial of the particulate fraction. At steady state, in fact, the residence time of iron in seawater, which is thought to be between 200 and 500 years, is calculated considering both the mean dissolved iron concentration in the oceans and the total external iron inputs.

For many years, dust deposition has been considered as the most important external iron source[64]. The dust iron, which is originated mainly from regions with enhanced soil aridity as North Africa or the Arabian Peninsula, is deposited on the ocean surface after its uplift from the terrestrial system and atmospheric transport. The latter can cover long distances so that dust is exposed to chemical transformations that can influence iron speciation and solubility in seawater.

Rivers are another relevant external iron source as they transport a large amount of the metal through the suspended sediments[65,66]. In these sediments, iron is mostly present as particles or colloids and the flocculation phenomenon causes a significant loss in iron concentration in the estuary zone[67]. This is the reason why riverine iron supply, which is relevant for the total iron concentration of coastal water, is considered negligible for the open ocean.

More recently, it has been proved that hydrothermalism along the mid-ocean ridges and back-arc basins has a significant impact on the iron supply[68–72]. New models, in fact, demonstrated that the hydrothermal iron has a longer residence time[70,73] contrary to what previously believed, i.e. that iron rapidly precipitates as solid minerals when the plume mixes with seawater[74]. In fact, despite the relevant mechanism is yet under study, it has been hypothesized that the hydrothermal iron is stabilized by complexation with organic species[69,75,76] or transported by nanoparticles[77,78].

Lastly, in the high latitude regions, glaciers, iceberg and sea ice are other

important iron sources. In fact, the meltwater of glaciers interacts with the sediments underneath them[79] and iron concentrations may be increased by the mechanical and chemical weathering that occurred therein. Moreover, icebergs, which are also rich in terrigenous material, melt during their equatorward transport and are a potential source of iron to the open ocean.

1.1.3 Iron cycle and bioavailability

The simplified iron cycle includes the uptake by microorganisms and the consecutive flux of sinking and subducted organic matter into deeper waters, basically until either iron is solubilized back into oceanic waters or iron containing particles settle on the ocean floor.

The description of the biogeochemical cycle of iron in the oceanic system is complicated as many different processes and chemical and biological species must be considered.

Generally, the so-called "internal Fe cycle" is supplied by inputs and generates outputs (Figure 1.4) after going through a multitude of different processes involving all the iron forms previously described.

Most of them are biologically controlled processes while only a few, as the dissolution, the precipitation, the photochemical or the redox processes are abiotic.

Figure 1.4: Scheme of iron cycling in seawater involving external iron sources as inputs and sinks as outputs

This is the reason why the definition of a biological iron demand is mandatory for the description of the iron cycle, both for phytoplankton and heterotrophs. The first take up iron for their physiological functioning, whereas heterotrophic species are responsible for the remineralization of the organic carbon, a process which can return particulate iron into dissolved species.

The rapid cycle of iron uptake and consequent regeneration driven by a range of biological mechanisms, called "ferrous wheel", plays a fundamental role in

the biogeochemical cycle of iron in seawater[80]. In particular, the importance of the ferrous wheel is based on the rapid mobilization of the biogenic iron pool with consequences on the bioavailability of this metal. Inside the ferrous wheel, heterotrophic organisms use siderophores to acquire iron[81,82]; moreover, microzooplankton[83–85], mesozooplankton[86,87], viruses[88] and heterotrophic bacteria83 can rapidly recycle particulate biogenic iron in the surface water. On the other hand, phytoplankton can also use colloidal iron directly for photosynthetic processes[89].

Figure 1.5 represents a simplified scheme of the iron cycle in the ocean, taking into account all the iron forms, the external iron sources as inputs and both the biotic and abiotic processes involved.

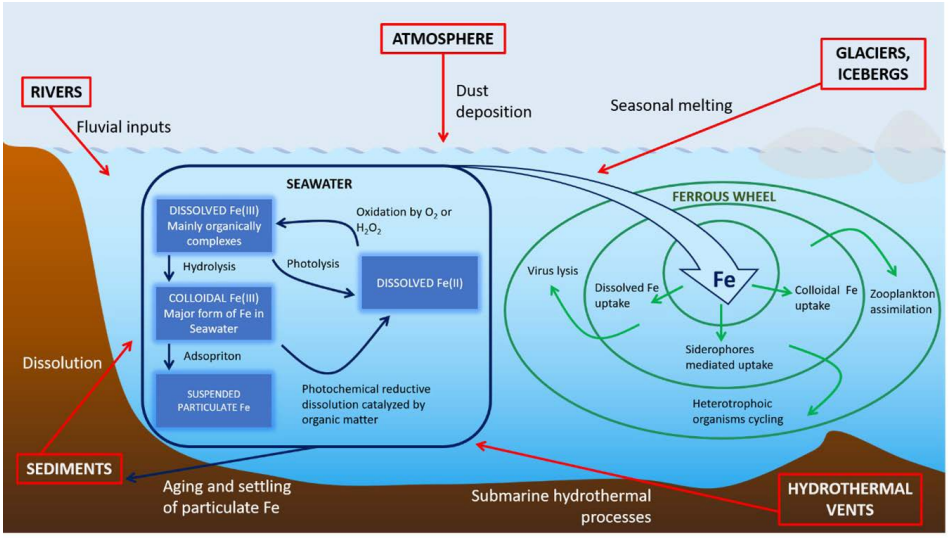

Figure1.5: Iron biogeochemical cycle in the oceanic system. The red boxes show the external iron sources. The blue box represents all the iron forms and the abiotic processes while in the green circle the ferrous wheel involving all the biologically controlled processes by phytoplankton and heterotrophic organisms is shown.

The organic Fe-binding ligands cycles are also of the utmost importance in this context. In fact, recently, an ocean biogeochemistry model with a dynamic pool[25] of ligands has been studied and its links to the iron cycle assessed. The model

predicts that iron availability in seawater is enhanced by the production of organic Fe-binding ligands, demonstrating the connection between ligand and metal ion cycles. Moreover, this study hypothesizes that the microbial production, fueled by external iron sources, produce ligands supporting iron solubility and lead to the consumption of other micronutrients until these become the limiting factor for the primary productivity.

1.2 Analytical Methods

The determination and speciation of iron in seawater challenge the analytical chemist to develop methods characterized by extreme detection capabilities in terms of sensitivity, selectivity and limit of detection.

Several methods for the determination of the total dissolved iron concentration, based on different techniques and chemical principles, experienced a great development.

Spectrophotometric methods[90,91], for example, have been thorough developed and studied. They involve ligands able to selectively bind iron or to specific redox state of the metal that produce a color compound with high molar adsorptivity. Moreover, methods based on the iron catalytic ability on reactions that can be monitored by spectrophotometry have been developed. The catalytic effect of Fe(III) on the NN,-dimethyl-p-phenylenediamine (DPD) by the hydrogen peroxide[91,92] is just an example. The latter, which provides a 25 pM limit of detection (LOD), initially required a flow-injection (FI) preconcentration on 8-HQ microcolumns and was later modified by the introduction of an online preconcentration on NTA chelating resin at pH 1.7 making the method suitable for shipboard determination.

Chemiluminescence[93,94] is also one of the most used methods in this field. It is often coupled to flow injection and requires a preconcentration on 8-HQ microcolumns. This method bases its functioning on the catalytic oxidation of brilliant sulfoflavin[95] or luminol[96] and its performances have been greatly improved by Obata et al.[97] reaching a 10 pM LOD. Chemiluminescence is so

used thanks to its robustness and portability and low const instrumentation required. Moreover, it allows rapid analysis minimizing the high risk of sample contamination. Nevertheless, despite its applicability to redox speciation measurements, it cannot be used for the organic speciation analysis due to many unknown factors involved in iron chelation on the microcolumn.

Since the 1970s-1980s, also mass spectrometry methods have been studied and used for the total iron determination in seawater. All these methods require a sample preconcentration by solvent extraction or on-line chelating column. The most common extraction method is based on the chelation with ammonium 1-pyrrolidinedithiocarbamate (APDC) and diethylammonium diethyldithiocarbamate (DDDC), double extraction into chloroform and back-extraction in nitric acid[98]. The latter, coupled with GFAAS[99], allows a 30 pM limit of detection. Lots of extraction methods coupled both with GFAAS and ICP-MS have been developed[100–104], but the best performances in terms of limit of detection are obtained by the $MgOH_2$ coprecipitation followed by ICP-MS analysis.

In this context, to date, one of the most used method for the detection of the total iron concentration employs the SeaFAST system (see http://www.icpms.com/pdf/seaFAST_REE_ICPMS_Element2.pdf for the commercially available system) coupled to an ICP-MS analysis. The former is a fully automated online system which employs a resin with ethylenediaminetriacetic acid and iminodiacetic acid functional groups to metals while anions and alkali and alkaline earth cations are washed out.

Neverhteless, the only methods avoiding the preconcentration steps are the electrochemical techniques based on the Adsorptive Cathodic Stripping Voltammetry (AdCSV). Besides being the only method avoiding any sample pretreatment, in fact, voltammetric techniques are characterized by significant advantages: they exploit a relatively low cost, compact and portable instrumentation which can be easily installed in on-ship laboratories.

The latter methods use a Hanging Mercury Drop Electrode (HMDE) and require the introduction of an artificial Fe-binding ligand into the analysis cell. The so-

formed complex adsorbs onto the mercury drop surface during the so-called deposition time and a potential scan towards the cathodic direction follows. The current is measured during the potential scan and the height of the complex reduction peak is directly proportional to the iron concentration.

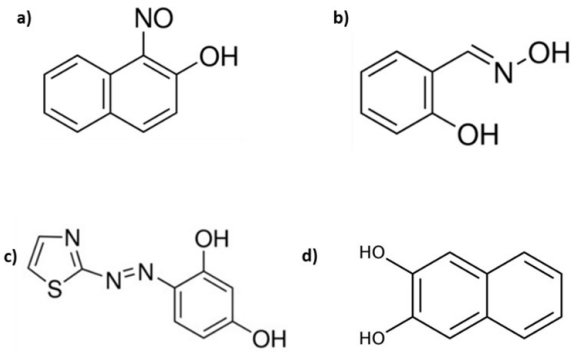

Figure1.6: species used as ligand for iron in the Adsorptive Stripping Voltammetry determination of the metal in seawater: a) 1-nitroso-2-naphthol, b) salicylaldoxime, c) 2-(2-thiazolylazo)-p-cresol and d)

Several ligands have been employed as iron chelator: 1-nitroso-2-naphthol (NN)[105–108] (Figure 1.6-a), salicylaldoxime[109] (Figure 1.6-b) , 2-(2-thiazolylazo)-p-cresol (TAC)[110] (Figure 1.6-c) and 2,3-dihydroxynaphthalene (DHN)111 (Figure 1.6-d).

Besides the traditional methods, starting from 1992[107], also catalyzed methods have been developed and applied. They consist on the introduction of an oxidizing species into the cell and the Fe(III) complex works as a sort of "*electron shuttle*" as it transfers electrons to the oxidizing species during the analysis. This phenomenon causes an enhancement of the peak current resulting in higher sensitivity and, in general, in better analytical performances. Bromate[110,111] and hydrogen peroxide[105] are the common oxidizer used in this context.

The most recent AdCSV method developed for the total dissolved iron concentration exploits DHN as the ligand and atmospheric oxygen as catalyzer[112]. It is characterized by the great improvement of using a microcell instead of the

traditional 10 mL cell which apparently causes an increase in the analytical sensitivity, showing on the other hand instability of the signals. Furthermore, recent developments[113] extremely simplify the sample pretreatment. In fact, it has been demonstrated that the seawater UV-digestion required to remove all the organic matter for the total iron determination can be avoided and totally replaced by a 24 hours acidification followed to a neutralization before performing the analysis.

Besides presenting some benefits for the determination of the total dissolved iron concentration, AdCSV are at the utmost importance in the oceanography field mostly because they represent the unique techniques showing results for the organic iron speciation in seawater.

In particular, the Competitive Ligand Equilibration scheme coupled to the Cathodic Stripping Voltammetry (CLE-CSV) has been developed to study the interaction of metal with organic ligands[105,114]. The latter procedure is based on the competition between the organic Fe-binding ligands present in seawater samples and the artificial ligand used during the analysis. Accordingly, the determination of the organic Fe-binding ligands concentration CL and their conditional stability constant for iron K'_{FeL} can be determined (see chapter 4 for details about the procedure).

As in the case of the total iron determination, also in this context, several artificial ligands for iron and oxidizer for the catalytic enhancement were employed and their performances evaluated.

1-nitroso-2-naphthol (NN) was the first historically used both without[115,116] and with the catalytic effect of hydrogen peroxide[105] or bromate[117], showing poor detection capabilities with a 1.5 $nA \cdot nM^{-1} \cdot min^{-1}$ maximum sensitivity when bromate is used[117]. In 2000, 2-(2-thiazolylazo)-p-cresol (TAC) was tested[110] and gave the high sensitivity value of 17 $nA \cdot nM^{-1} \cdot min^{-1}$ although a deposition time between 120 and 600 s was mandatory.

To date, the method with salicylaldoxime as ligand and atmospheric oxygen as catalytic enhancer is the most exploited. It shows sensitivity values between 2.6

and 4.4 $nA \cdot nM^{-1} \cdot min^{-1}$ which increases up to 180 $nA \cdot nM^{-1} \cdot min^{-1}$ when an around seven times higher mercury drop surface is used. 2,3-dihydroxynapthalene (DHN) can be also employed as a ligand and both uncatalyzed and catalyzed by bromate[118,119] methods have been developed.

Accordingly, the choice of the most performing ligand is crucial in this context to prevent the drawbacks typical of these methods. In particular, too long analysis time should be avoided ensuring, on the other hand, sensitivity values satisfactory for the trace and ultratrace determination. Moreover, it should be also considered that these kinds of methods can detect several classes of organic ligands; consecutively, interferences should be avoided, and data carefully treated.

1.3 Aim of the thesis

The main purpose of this project is to develop a new, better performing and easier to use method for iron speciation in seawater following the competitive ligand equilibration – cathodic stripping voltammetry (CLE-CSV) scheme. As explained in the previous section, in fact, several methods employing different iron ligands were developed during the last 20 years, but each of them has its drawbacks. The use of NN required high analysis times resulting in a poor sensitivity[105,106,115,116]. SA[120,121] has a only 5 $nA \cdot nM^{-1} \cdot min^{-1}$ for 30 µM ligand concentration and better analytical performances were obtained only employing a huge mercury drop as the electrode[122,123]. On the other hand, an acceptable sensitivity was reached with TAC[110], but huge deposition time (up to 600 seconds) were needed. Furthermore, also the use of DHN[118,124] resulted in poor sensitivity and, in this case, only the use of bromate as catalytic enhancer was experimented.

More in general, iron speciation methods developed up to now were characterized by poor sensitivity, too high time analysis requirement and also, in some cases, by the use of a suspected carcinogenic species as catalytic enhancer.

In this complex context, the method developed in 2015 by Caprara et al.[112] was chosen as the starting point of the project. The latter used DHN as the ligand and

atmospheric oxygen as the oxidant and was characterized by the introduction of the microanalysis, 1 milliliter sample cell. The choice of this method was basically due to its promising analytical performances both in terms of sensitivity (49 $nA \cdot nM^{-1} \cdot min^{-1}$ for 10 µM DHN in seawater) and limit of detection (5 pM) obtained using atmospheric oxygen instead of bromate as catalytic enhancer. Moreover, the tenfold sample size reduction allowed using the microcell seemed perfectly suitable for the CLE-CSV scheme which usually required more than 100 mL of sample for each analysis. On the other hand, the Caprara et al. method, was characterized by a drift in the analytical signal, especially for high ligand concentrations, and, mostly, by an instrumental configuration which resulted difficult to use and set-up. The small microcell, in fact should have hosted the three electrodes configuration and the stirrer, and the latter configuration was difficult to set-up because of the black support. Thus, firstly a new instrumental configuration should be developed, as these two problems should be avoided before developing the speciation method. Parallel to this, as extreme detection capabilities as required, a deep knowledge of the method in terms of its chemical and electrochemical feature is considered mandatory. In particular, the main interest should be focused on which parameters could control and thus positively influence the analytical sensitivity. Accordingly, a protocol for the characterization of a AdCSV method should be suggested as it seems to be missing in literature up to now.

Therefore, the development of the new CLE-CSV method for iron speciation in seawater should follow these two steps. Applying the new instrumental configuration (chapter 2) and controlling the method thanks to its characterization (chapter 3), in fact, a performing and easy to use method should be expected (chapter 4).

2 HARDWARE SET-UP, OPTIMIZATION AND VALIDATION[1]

The development of a new hardware configuration for the Competitive Ligand Equilibration-Cathodic Stripping voltammetry (CLE-CSV) is described in this chapter. In particular, this first step started form the most recent development by Caprara et al.[112] for total iron determination, as it was characterized by promising analytical performances together with a reduction of the employed chemicals. The latter procedure was based on the use of 2,3-dihydroxynaphthalene as the ligand for iron and atmospheric oxygen instead of bromate for the catalytic enhancement of the signal. Moreover, a 0.5-1 mL microcell was for the first time introduced and led to a lower sample requirement to carry out each analysis (Figure 2.1). Therefore, the traditional cell was replaced by a Delrin (polyoxymethylene, POM) microcell support characterized by the presence of four holes that allowed a continuous flux of oxygen to the samples as needed for the catalytic enhancement. The latter instrumental configuration required a particular attention when used, especially during its set-up, as the small microcell should host three electrodes (working, counter and reference) and the

[1] Partially reproduced and adapted with permission of from Fostering and Understanding Iron Detection at the Ultratrace Level by Adsorptive Stripping Voltammetry with Catalytic Enhancement, Electroanalysis 2019, 31 (2) (https://doi.org/10.1002/elan.201800675). Copyright © 2019 Wiley-VCH Verlag GmbH& Co. KGaA, Weinheim.

stirrer, and the bottom of the Delrin support should be installed at the perfect height with respect to the stand.

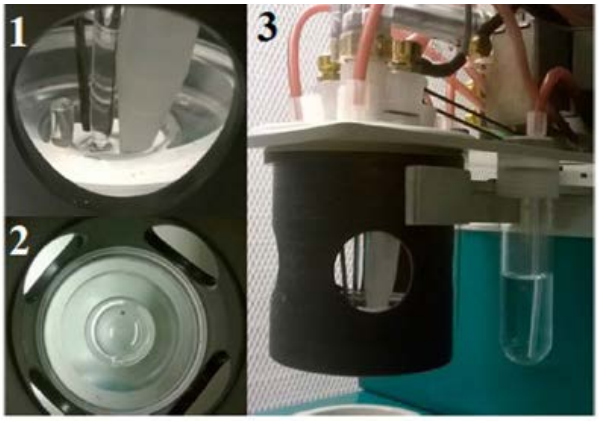

Figure 2.1: Images of the voltammetric configuration developed by Caprara et al. (directly from[112]). View of the microcell through one of the four holes (1) and from above (2). Overview of the voltammetric system (3).

Despite the high sensitivity reached by this method, up to 550 $nA \cdot nM^{-1} \cdot min^{-1}$ and 150 $nA \cdot nM^{-1} \cdot min^{-1}$ for ultrapure water and seawater, respectively, obtained at high 2,3-dihydroxynaphthalene concentrations, an important deterioration of the signal stability and baseline was observed when moving from 10 to 500 µM DHN. In fact, as reported in[112], although ensuring the best analytical sensitivity ever registered with a cathodic stripping voltammetry method, the signal was constantly rising leading to a poor reproducibility. External pollution as a consequence of the Delrin open support was supposed to be a reason for such behavior. Furthermore, the leaching phenomenon of the KCl filling solution of the reference electrode through the porous ceramic frit was thought to be an additional possible source of sample contamination.

The following chapter will focus on the setup, optimization and validation of a new hardware configuration that may overcome the previously described problems, and, more generally, lead to the development of a fast, easy to use

and reproducible method for iron speciation, without compromising the already described good analytical performances.

2.1 Hardware development

The first step in the development of the new hardware configuration was focused on the introduction of two substantial modifications to the previously described one, in the attempt to limit the signal instability.

Firstly, a *pseudoreference* (literally "*pseudo*" = false[125]) was installed to replace the traditional Ag/AgCl/3M KCl reference electrode. To date few information is known about pseudoreference electrodes, as their applications are limited in the literature. The main disadvantage of a pseudoreference, in fact, is the lack of the thermodynamic equilibrium which avoids the determination of its potential. Moreover, it can work only over a limited range of conditions of pH and temperature. Nevertheless, the application of a pseudoreference to the analysis of seawater samples seemed reliable, as the pH, ionic composition, and temperature are constant during all the voltammetric analysis and among all the experiments. In this context, a 5 cm silver wire with a 1 mm diameter and characterized by a 99.9% purity was employed as a pseudoreference electrode (Figure 2.2) by direct electrical connection with the stand.

The use of the silver wire pseudoreference led to several benefits. First, the leaching phenomenon of the KCl filling solution of the traditional Ag/AgCl/3M KCl electrode through the porous frit into the sample112 was avoided. In this way, no contamination due to this species could occur, making the removal of the long purification step of the potassium chloride filling solution, which required consecutive overnight equilibrations with an ion-

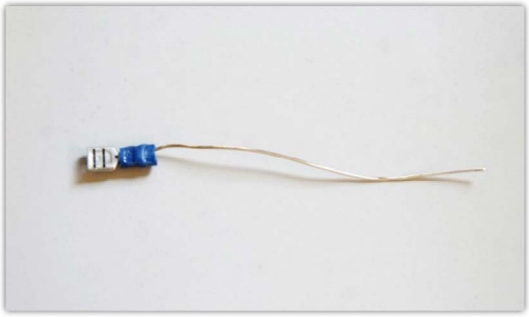

Figure 2.2: Image of the silver wire pseudoreference (Sigma-Aldrich; 99.9% purity; 1 mm diameter).

exchange resin, namely Chelex®, possible. Furthermore, the possible increase in the sample volume, which could be not-negligible using the microcell, was prevented. Secondly, the pseudoreference, thanks to its five times smaller diameter, fitted better into the microcell which should host the three electrodes (working, reference, and counter) and the stirrer, with respect to the traditional Ag/AgCl reference. Actually, the employment of a pseudoreference electrode in ultratrace element detection was not reported in the literature and its effect on the analytical signal was accordingly carefully evaluated. In particular, an around 120 mV shift of the peak potential towards the cathodic direction was evident using the pseudoreference, as it moved from -0.572 V to -0.690 V (Figure 2.3).

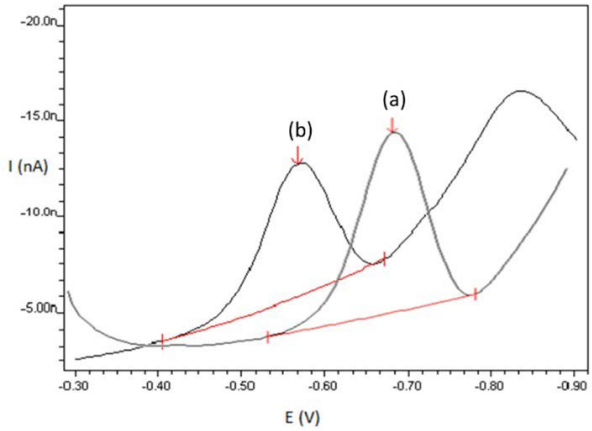

Figure 2.3: Peak shift towards the cathodic direction using the pseudoreference (a) and the Ag/AgCl reference electrode (b) in ultrapure water. Experimental: ultrapure water; 10 mM HEPPS buffer pH 8.0; 10 µM DHN; 0.5 nM Fe. Square-wave voltammetry: 30 s deposition time; -0.4 V deposition potential; 10 Hz square-wave frequency; 0.05 $V \cdot s^{-1}$ scan rate; 90 mV half width for both the peaks.

The latter effect could be due to the formation of silver(I) oxide, Ag_2O, at the silver surface during the analysis. This hypothesis was formulated considering that the standard potential E^0 of the ½ Ag_2O/Ag couple against the Standard Hydrogen Electrode (SHE) is +0.344 V, whereas the potential of the Ag/AgCl/3 M KCl reference electrode is +0.210 V. Notwithstanding the potential of the

pseudoreference cannot be exactly calculated because of its nature[125], it is important that it keeps constant during the experiment under suitably selected and constant conditions (pH, ionic composition, temperature). Such stability was experimentally demonstrated by the iron peak potential being constant during prolonged experiments like the titrations reported in chapter 4.

The second substantial modification with respect to the initial instrumental configuration was the use of a small air pump for the introduction of atmospheric oxygen as the catalytic enhancer of the signal. The air pump was located under the laminar flow hood to provide a continuous constant flux of clean air. Moreover, air was directly introduced into the close analysis cell by feeding the nitrogen line which is normally used for the purging step during traditional measurements. Nevertheless, the nitrogen connection to the HMDE (Hanging Mercury Drop Electrode) working electrode was maintained to guarantee its correct functioning. The catalytic enhancement by an oxidizer on the analytical signal is mandatory in this context, as the iron concentration in the oceanic natural environment is in the nM-pM range (see the Introduction chapter for more information) and high detection capabilities are required. The choice of atmospheric oxygen as the sensitivity enhancer instead of BrO_3^- was dictated by the promising analytical performances obtained by Caprara et al.[112] as well as the latter reagent being classified as a suspected carcinogenic for humans (2B group by the International Agency for Research on Cancer (IARC) of the World Health Organization (WHO)). Moreover, the use of atmospheric oxygen avoided the purification step of the chemical used as catalytic enhancer going towards a further simplification of the procedure and an important time saving. The new hardware configuration is shown in Figure 2.4.

2.2 Method optimization, sensitivity, and figures of merit

Before testing the analytical performances of the new hardware configuration, an optimization of the instrumental parameters was mandatory as for the first time

a pseudoreference was used together with the air pump for the introduction of atmospheric oxygen. Therefore, all the measurements reported in the following section have been performed employing them. Firstly, the influence of the square-wave (SqW) frequency and of the DHN concentration on the signal was simultaneously evaluated by studying the trend of the peak current vs. the frequency itself for DHN concentrations between 1 and 100 µM (figure 2.5).

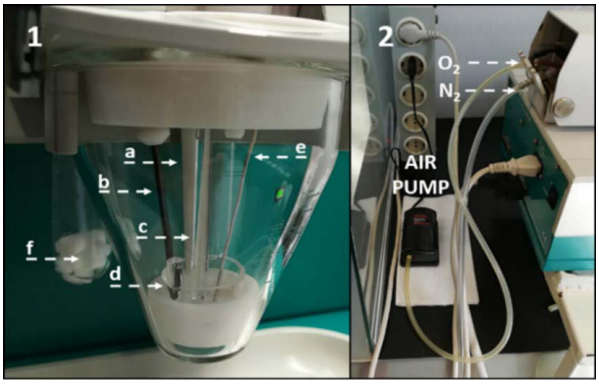

Figure 2.4: Image of the new hardware configuration (directly from[126]). Overview of the system (1: a) stirrer, b) counter electrode, c) HMDE, d) microcell and its support, e) silver wire pseudoreference, f) humidification chamber). Air pump and gas connection (2).

For all the studied ligand concentrations the peak current increased with the square-wave frequency. Nevertheless, the square-wave frequency of 10 Hz ensured the best signal to noise (S/N) ratio and, consequently the best analytical performances, as problems connected to the peak shape and the background current were found when SqW frequencies higher than 25 Hz were employed. In particular, the peak widening and the background current increased with the square-wave frequency leading to a deterioration of the S/N ratio. The peak widening is commonly due to the increasing peak potential separation between the

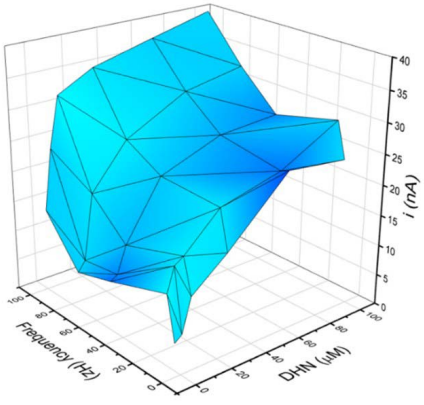

Figure 2.5: Trend of the peak current with the square-wave frequency and the DHN concentration. Experimental: ultrapure water; 10 mM HEPPS buffer pH 8.0; 0.3 nM Fe. Square-wave voltammetry: 30 s deposition time; -0.4 V deposition potential.

forward and backward components of a square-wave voltammogram for quasireversible and irreversible systems[127,128]. In this context, in fact, we are in the presence of a quasireversible reaction (see chapter 3 for a thorough discussion on this topic). On the other hand, the growing background current is a consequence of the capacitive current increase due to the increase of the scan speed. Therefore, as in the case of the previous work[112], the square-wave frequency of 10 Hz was employed from now on for all the measurements. The effect of the deposition potential on the signal was also considered: a previous work[112] have set it to -0.1 V, as this value allowed the best analytical performances. In this context the trend of the peak current was studied as a function of the deposition potential in ultrapure water. In particular, the FeDHN reduction peak current showed a growing trend with the deposition potential up to a maximum for -0.4 V, and then it started to decrease for more negative potentials (Figure 2.6). Actually, the differences in the peak current obtained with deposition potentials between -0.2 V and -0.4 V are minimal.

However, the deposition potential of -0.4 V was adopted from this point on, as it granted the highest peak current. The influence of the deposition time on the signal was, lastly, studied.

Several experiments involving two different DHN concentrations,

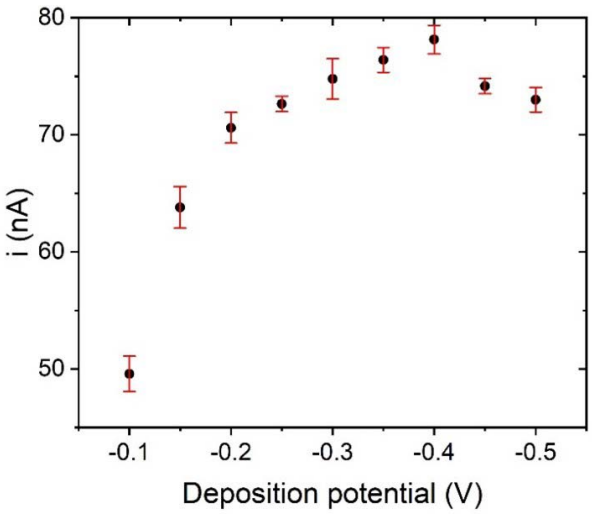

Figure 2.6: Trend of the peak current with the deposition potential. Data are expressed as medium value (black points) ± standard deviation of three replicates measurements (red error bars). Experimental: ultrapure water; 10 mM HEPPS buffer pH 8.0; 10 μM DHN; 0.5 nM Fe. Square-wave voltammetry: 30 s time; 10 Hz square wave frequency; 0.05 $V \cdot s^{-1}$ scan rate.

namely 5 and 30 µM, were carried out using both the traditional 10 mL analysis cell and the microcell. The peak current was measured for increasing deposition time, from 30 to 240 s (figure 2.7).

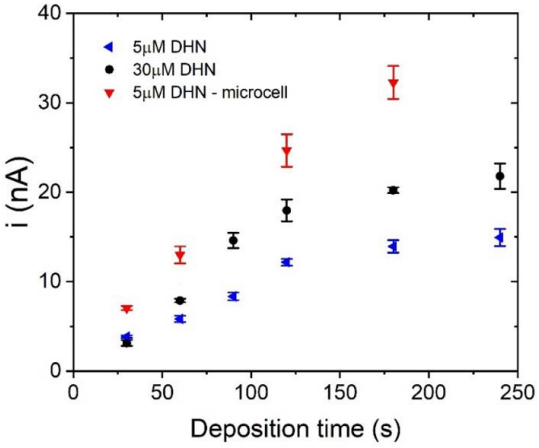

Figure 2.7: Trend of the peak current with the deposition time for both the microcell and the standard cell. Data are expressed as medium value (points) ± standard deviation of three replicates measurements (error bars). Experimental: ultrapure water; 10 mM HEPPS buffer pH 8.0; 5 and 30 µM DHN, 0.3 nM Fe. Square-wave voltammetry: -0.4 V deposition potential; 10 Hz square-wave frequency; 0.05 V·s^{-1} scan rate.

The peak current vs. deposition time deviated from linearity after 120 seconds deposition time. In addition, regarding the use of the microcell, the smaller distance between the stirrer and the mercury drop of the working electrode affected the results. In fact, longer deposition time increases the probability of the drop detachment from the electrode capillary and deposition times higher than 60 seconds are difficult to apply when the microcell is used (see above and section 3.4.3 of Chapter 3 for an explanation of the higher current obtained with it).

Following the optimization of the instrumental parameters, the analytical sensitivity (sensitivity=slope of the calibration line/deposition time) was thoroughly studied for several DHN concentrations and using different sample

salinity (Figure 2.8).

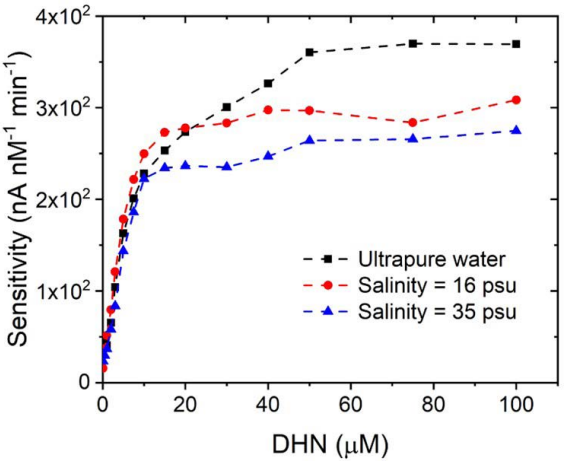

Figure 2.8: Trend of the sensitivity with the DHN concentration in ultrapure water and seawater samples with different salinity values. Experimental: 10 mM HEPPS buffer pH 8.0; 0.3 nM Fe added to calibrate the sensitivity. Square-wave voltammetry: -0.4 V deposition potential; 10 Hz square-wave frequency; 0.05 V·s^{-1} scan rate.

The trend of the sensitivity with the DHN concentration was the same for all the matrices: it increased up to a maximum and then it levelled off for the highest DHN concentration Moreover, for each DHN concentration the sensitivity decreased with the matrix salinity (the reasons for this will be discussed in the following chapter). Regarding the limit of detection (LOD) of the technique, calculated as $3s_{BLANK}/slope$ of the calibration line, non-distinguishable values were found for a wide range of DHN concentrations. In particular, LODs in the range 9.7 to 16 pM for both ultrapure water and seawater for DHN concentrations between 1 and 100 µM were determined. The similarity in LOD values was a clear indication that the reproducibility of the signal is proportional to the signal itself, resulting in a constant S/N ratio. A comparison between the latter results and the sensitivity and LODs values reported in[112] is mandatory to assess the analytical performances of the new method. Moreover, the limit of linearity

(LOL) of the method was estimated as 0.8 nM and 1 nM in ultrapure water and seawater, respectively. Regarding the analytical sensitivities, a slight increase was observed when the new hardware configuration was employed (e.g. 150 $nA \cdot nM^{-1} \cdot min^{-1}$ vs 220 $nA \cdot nM^{-1} \cdot min^{-1}$ for 10 µM DHN and in ultrapure water in[112] and in this work, respectively). As far as the LOD is concerned, a similar value around 10 pM was obtained in ultrapure water for 10 µM DHN concentration. Nevertheless, it should be highlighted that the latter LOD was obtained in[112] only for 10 µM DHN, whereas it deteriorates with increased DHN concentrations due to the growing instability of the signal. As opposite, the present method featured the same limit of detection for a wide range of DHN concentration. The latter evidence confirmed that the signal instability evidenced by the previously developed instrumental configuration[112] was avoided thanks to simultaneous use of the silver wire pseudoreference and of the air pump for the introduction of the atmospheric oxygen into the close analysis cell as they avoided any sample contamination.

Lastly, a brief discussion about the selectivity of the method is required. Since its first development in 2001[111], the method seemed extremely selective towards Fe, as only vanadium showed a partial interference in the voltammograms acquired for iron detection in seawater[113]. The new developments led to a great improvement in the selectivity as also the vanadium peak was not present in any of the voltammograms. The latter is possibly caused by the combination of two different phenomena. Firstly, the height of the vanadium peak could be reduced by a less efficient catalytic effect triggered by hydrogen peroxide with respect to the previously employed bromate ion[118]. Secondly, the hydrogen peroxide reduction peak is positioned right at negative potentials of the iron one and could completely overlap the vanadium peak.

Furthermore, the previously introduced modifications, i.e. the pseudoreference and the air pump, were tested also using the standard 10 mL cell from Metrohm. The same trend in the sensitivity vs. DHN concentration was found for the two the sample volume meaning that the new instrumental configuration is suited

for both 1 and 10 mL (Figure 2.9).

Nevertheless, for all the studied ligand concentration, the sensitivity was higher using the microcell with respect to the traditional cell (Figure 2.6). This evidence could be due to a higher flux caused by a more efficient stirring in the microcell (refer to chapter 3 (section 3.4.3) for a deeper discussion).

As a final remark, the introduced modifications led to a significant simplification of the instrumental configuration. In fact, the microcell was directly introduced into the standard 10 mL cell only using a Teflon support, and the 1 mm diameter of the pseudoreference better fitted into the small cell together with the working and counter electrodes and the stirrer. The analytical performances obtained were comparable to the ones of the previously developed method[112], avoiding, on the other hand, the signal drift. Accordingly, the method seemed fully exploitable for the trace and ultratrace determination of iron in seawater and its analytical performances promising for the metal speciation in this complex environmental matrix.

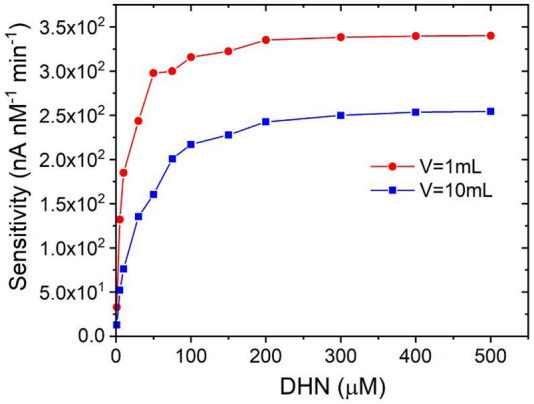

Figure 2.9: Trend of sensitivity vs. DHN concentration for 1 and 10 mL sample volume. Experimental: ultrapure water; 10 mM HEPPS buffer pH 8.0; 0.3 nM Fe added to calibrate the sensitivity. Square-wave voltammetry: -0.4 V deposition potential; 10 Hz square-wave frequency; 0.05 V·s^{-1} scan rate.

2.3 Validation

As the final step for the new hardware configuration set-up, its performances were assessed by analyzing the seawater sample SAFe D2 collected in the framework of the SAFe (Sampling and Analysis of Fe) program129. The latter was characterized by the consensus value of 0.91±0.022 nM for the total iron

concentration. The seawater sample, which was treated as thorough explained in the "Materials & methods chapter (section 6.3.4.1), was 10x diluted test the method for the detection of ultratrace levels of the metal. The determination was repeated four times and gave an average value of 1.01±0.16 nM (medium value of the four replicates ± standard deviation) after the subtraction of 0.070±0.006nM which corresponded to the blank iron concentration 0.070±0.006nM (ultrapure water, buffer, HCl and NaOH). The obtained result was not statistically different from the consensus value at the 95% confidence interval; moreover, the method resulted reproducible with an 8% relative standard deviation of the mean (RSD%).

3 METHOD CHARACTERIZATION[2]

Despite the promising analytical performances in terms of detection capabilities obtained by the new hardware configuration, several features of the method were unclear. A thorough knowledge of the chemical features and of the phenomena occurring during the analysis would lead to a better understanding of the chemical bases of the method. Thus, the degradation of the 2,3-dihydroxynaphthalene was studied and the complex stoichiometry evaluated. On the other hand, the adsorption of the species onto the electrode surface was considered and the electron transfer kinetics and the catalytic mechanism simultaneously characterized. The latter would in turn provide control of the performances and limitations of the methods for both total iron detection and speciation. Moreover, it should be highlighted that information on the characterization of catalytically enhanced Adsorptive Cathodic stripping Voltammetry (AdCSV) methods are sparse and usually a thorough investigation of newly introduced methods is not performed. In this context, all the investigations reported in this chapter led to a complete knowledge of the (AdCSV) method for iron detection and speciation

[2]Fully reproduced and adapted with permission of Elsevier from Strategies for the Characterization and Optimization of Adsorptive Stripping Voltammetry with Catalytic Enhancement for Ultratrace Element Determination: The Case of Iron 2,3-Dihydroxynaphthalene Complex with Catalytic Enhancement by Atmospheric Oxygen, Electrochimica Acta 2019, 321, 134653 (https://doi.org/10.1016/j.electacta.2019.134653). Copyright 0013-4686/

in seawater, thus providing a general protocol for the characterization of AdCSV methods for the detection and speciation of a metal at the ultratrace level.

3.1 Theoretical background

In the following section all the methods and procedures used for the characterization of the catalytically enhanced AdCSV technique will be presented. The equation used to fit experimental data will be also reported.

3.1.1 Ligand degradation

Different techniques can be employed to determine the degradation rate of a chemical species. In this context spectroscopic and spectrometric methods play a major role. In particular, the UV-Vis spectroscopy and the proton nuclear magnetic resonance spectrometry (1H-NMR) were employed to study the degradation of the 2,3-dihydroxynaphthtalene by the acquisition of several spectra in a given time frame. Experimental data were treated using the zero (eq. 3.1), first (eq. 3.2) and pseudo-first (eq.3.3) kinetic models.

$rate=-d[A]/dt=k$ (3.1)

$rate=-d[A]/dt=k[A]$ (3.2)

$rate=k[A][B]=k'[A]$ (3.3)

With $k'=k_{obs}=k[B]_0$; $[k']=s^{-1}$

The pseudo-first kinetic model is mostly used as an approximation for second order (equation 3.3) reactions involving two different species if the concentration of one of them can be considered constant; under this condition, the reaction rate depends only on the concentration of the non-constant chemical species.

3.1.2 Complex stoichiometry

The stoichiometry of a complex can be established using different techniques. The most common and simple ones require the use of the UV-Vis spectroscopy basing their functioning on the Beer-Lambert's law. However, these methods

can be used only if the complex adsorbs in a spectral range characterized by the absence of any interference caused by the presence of the ligand. The *Job's method*, also called the *method of continuous variation*[130,131] plays a major role in this context. It is based on the absorbance measurement of several solutions characterized by different ratios between the concentrations of the metal and the ligand keeping the sum of them constant. The stoichiometric ratio value of the complex is then determined by the maximum of the graph obtained plotting the absorbance vs. the *[L]/[M]* ratio (*[L]*: ligand concentration; *[M]*: metal concentration). Otherwise, a second method, called *mole-ratio method*, can be applied to determine the stoichiometry of a complex. Contrary to the method previously described, the latter is based on the absorbance measurements of UV-Vis spectra of solutions containing increasing ligand concentrations keeping the metal ion one constant. In this case, the graph of the absorbance vs. the *[L]/[M]* ratio is a curve which reaches a plateau in the correspondence of the complex stoichiometric ratio. In particular, the curved trend of the absorbance vs. *[L]/[M]* ratio holds only for high complex formation constant K (*log(K)>6*)[132], whereas ambiguous results can be obtained for lower log(K) values[133]. Despite their ease of use, these methods are characterized by an important limitation which make them not completely versatile. In fact, they can be used only when the metal ion and the ligand concentrations are high (in the range of molar-millimolar) and differ at most by an order of magnitude. When this requirement is not fulfilled, a different approach based on the square-wave voltammetry (SqW) can be employed. The latter is based on the acquisition of voltammograms for solutions with increasing ligand concentration and constant metal concentration. The stability constant of a ML, ML_2 and ML_3 complex, and therefore the complex stoichiometry, is estimated by fitting the peak current plotted against the ligand concentration with equation 3.4.[120]

$$i=i_{max}\cdot(K[L]/(K[L]+\beta_1[L]^2+\beta_2[L]^3+1)) \quad (3.4)$$

The latter equation is the general form when the 1:1 only is electroactive and all the three species form; if more than one species is electroactive, then they

should be added to the numerator of the equation and if one or more species do not form, they should be removed from the denominator. Few examples of the modified equation follow (equations 3.5-3.7; see equations A.1-A.6 of the Appendix for all the forms of equation 3.4).

$i=i_{max}\cdot(K[L]/(K[L]+1))$ (3.5) (only the 1:1 complex forms and is electroactive)

$i=i_{max}\cdot(K[L]/(K[L]+\beta_1 [L]^2+1))$ (3.6) (The 1:1 and 1:2 species form but only the 1:1 one is electroactive)

$i=i_{max}\cdot((K[L]+\beta_1 [L]^2)/(K[L]+\beta_1 [L]^2+1))$ (3.7) (The 1:1 and 1:2 species form and are electroactive)

3.1.3 Adsorption

The AdCSV technique is based on the adsorption of the complex onto the surface of the Hanging Mercury Drop Electrode (HMDE) used as the working electrode. Thermodynamic information (maximum electrode surface coverage and adsorption equilibrium constant) can be easily obtained using the linear sweep voltammetry or, alternatively, the cyclic voltammetry. The first step for the adsorption phenomenon characterization is the determination of the amount of the exchanged charge Q during the electrode reaction. The latter is calculated by integration of the reduction peak of the adsorbed species for each voltammogram. The surface coverage is then calculated following equation 3.8.

$Q=nFA\Gamma$ (3.8)

(Where Q: amount of exchanged charge; n: number of the electrons exchanged during the electrode reaction; F: Faraday constant = 96485 C·mol^{-1}; A: electrode surface area; Γ: electrode surface coverage expressed as moles concentration of adsorbed molecules per surface area unit). The Henry (equation 3.9) or the Langmuir (equation 3.10) isotherm models are then employed to model the Γ vs. concentration data in order to obtain the adsorption thermodynamic parameters[134,135].

$\Gamma/\Gamma_{max} = \beta \cdot c$ (3.9)

$(\Gamma/\Gamma_{max})/(1-(\Gamma/\Gamma_{max})) = \beta \cdot c$ (3.10)

(Where Γ_{max}: maximum surface coverage; β: adsorption equilibrium constant; *c*: species concentration in solution).

The above equations are successfully used to model the data of a monocomponent system, that is a system characterized by the adsorption of only one species onto the electrode surface. More complex systems are better described by the multicomponent Langmuir isotherm model (equation 3.11) which can be also used for the description of a competitive adsorption between two or more species onto the same electrode surface[136,137].

$\Gamma_i = (\beta_i \cdot \Gamma_{maxi}) \cdot c_i / (1 + \sum_{j=1}^{N} c_j \cdot \beta_j)$ (3.11)

3.1.4 Electron transfer reaction

Important information about the electrode reaction is obtained studying the kinetics of the electron transfer reaction. In this context, cyclic voltammetry (CV) is useful to determine the kinetic parameters, that are the standard electrochemical rate constant (k^0) and the symmetry factor (α). These parameters can be calculated only if the number of electrons exchanged during the reaction (*n*) is well-known. The latter is calculated taking into account the mid-height width $\delta_{0.5}$ of the cathodic peak, which should be 90.6/n mV for a totally reversible reaction or 62.5/(1-α)n mV for a totally irreversible reaction[138]. Subsequentially, the standard electrochemical rate constant k^0 and the symmetry factor α can be experimentally determined following equations 3.12 and 3.13 if the difference between the anodic and cathodic peaks potentials ΔE_p is larger than 200/n mV[138].

$E_p = E_j - (RT/\alpha nF) \cdot \ln(\alpha/|m|)$ for the cathodic reaction (3.12)

$E_p = E_j + (RT/((1-\alpha)nF)) \cdot \ln((1-\alpha)/|m|)$ for the anodic reaction (3.13)

With $m = (RT/F)(k^0/nv)$ (3.14)

(Where *v*: reaction rate for the anodic or the cathodic reaction).

Accordingly, a graph of $E_p = f[\log(v)]$ is used for the calculation of the kinetic

parameters k^0 and α. In particular, the latter gives two straight lines characterized by a -2.3RT/αnF slope for the cathodic reaction and a 2.3RT/(1-α)nF ones for the anodic reaction; the reaction rates for the anodic and cathodic processes (v_c and v_a, respectively) are subsequentially deduced by the intersection of the two straight lines with the x-axis of the graph. Alternatively, the symmetry factor α can be calculated following equation 3.15.

$$\alpha/(1-\alpha)=v_a/v_c \quad (3.15)$$

Otherwise, the standard electrochemical rate constant can be calculated from the anodic and cathodic reaction rates, following equation 3.16.

$$k^0=(\alpha n F v_c)/RT=((1-\alpha)nFv_a)/RT \quad (3.16)$$

The latter equation can be applied only if the ΔE_p>200 mV condition is verified. Contrarily, when the latter condition is not fulfilled, square-wave voltammetry is employed to estimate the standard electrochemical rate constant and the symmetry factor. In particular, the symmetry factor is roughly calculated considering the split between the forward and the backward components of the square-wave voltammogram as the related ratio of the peak heights is a function of α according to equation 3.17.

$$i_{(p,c)}/i_{(p,a)} = 5.64e^{-3.46\alpha} \quad (3.17)$$

(Where $i_{p,c}$: cathodic peak current; $i_{p,a}$: anodic peak current)

The function of the net dimensionless current ψ_p (ψ_p is the heights of the peak of the square-wave scan, i.e $\psi_p = \psi_{p,a}-\psi_{p,c}$) against the square-wave frequency is subsequentially employed to estimate the standard electrochemical rate constant k^0. ψ_p, in fact, is related to the dimensionless kinetic parameter ω, which is the ratio between the standard electrochemical rate constant and the square-wave frequency ($\omega=k^0/f$), by a parabolic function. The dimensionless kinetic parameter is also useful to estimate the electrode reaction mechanism: if $log(\omega)<-2$, the reaction is totally irreversible and, on the other hand, if $log(\omega)>2$, the reaction is totally reversible; within the latter range ($-2<log(\omega)<2$) the reaction is considered quasireversible. Therefore, the peak current is measured at different square-

wave frequency and its function against log(1/f) shows a trend characterized by a sharp maximum, called "*quasireversible maximum*", positioned in the so-called "*quasireversible region*". Each surface electrode reaction is characterized by a critical frequency fmax in correspondence of the quasireversible maximum. The latter frequency produces the highest dimensionless peak current so that the standard electrochemical rate constant can be calculated according to equation 3.18.

$k^0=\omega_{max} \cdot f_{max}$ (3.18)

The ωmax value is a function of the symmetry factor, the square-wave amplitude and the number of electrons exchanged during the redox reaction; if all of these parameters are well-know, the ωmax value can be easly found in Table 3.1[127].
The theory here described refers to simple confined surface processes where the contribution of the mass transfer phenomena during the stripping step is negligible and all the experimental system is approximated as being free of surface lateral interaction.

ω_{max}					
	nE_{sw}/mV				
α	15	25	30	40	50
0.9	1.43	1.35	1.38	1.33	1.26
0.8	1.32	1.30	1.25	1.17	1.08
0.7	1.31	1.26	1.20	1.10	0.97
0.6	1.29	1.20	1.16	1.04	0.90
0.5	1.28	1.19	1.13	1.01	0.88
0.4	1.27	1.18	1.13	1.02	0.89
0.3	1.26	1.22	1.17	1.04	0.94
0.2	1.25	1.24	1.19	1.12	1.04

Table 3.1: Values of the critical dimensionless kinetic parameter as a function of the symmetry factor α, of the number of electrons exchanged during the electron transfer reaction n, and of the square-wave amplitude E_{sw} (table from[127]).

3.1.5 Catalytic reaction mechanism

The catalytic cathodic stripping voltammetry methods base their functioning on the introduction of an oxidizing species into the analysis cell. The latter species re-generate via a re-oxidation process the metal complex, which adsorbs onto the electrode surface, after being reduced during the electron-transfer process. As a matter of fact, the metal complex catalyzes the electron- transfer reaction from the electrode to the oxidizing species working as an electron shuttle.

These methods are deeply studied and applied as they ensure an enhancement of the signal and, consequently, of the analytical sensitivity, also for a totally irreversible reaction[139]. Generally, in the case of a species free to diffuse in the solution, the peak current is directly proportional to the square root of the oxidizing species concentration[140]. The same cannot be said for the surface catalytic mechanisms, as a general expression for the peak current vs. oxidant concentration cannot be derived for all the different conditions[141]. In particular, when the preceding electron- transfer reaction is close to be totally reversible, i.e. the kinetic parameter $\lambda \geq 0.7$ (see the following paragraph of this section for more information), the function of the peak current vs. oxidizing species concentrations is characterized by a linear trend; otherwise a non-linear trend is related to quasireversible electron-transfer reactions[141]. As in the case of the system studied in the present thesis (see section 3.4.2 of this chapter for the data about the electron transfer kinetics), the linear trend of the peak current vs. the oxidizing species concentration follows equation 3.19.

$$i_p = k_{cat} \cdot [Complex] \cdot [Oxidizing\ species]_{(electrode\ surface)} \quad (3.19)$$

According to equation 3.19, as the sensitivity linearly increases with the oxidizing species concentration, a linear plot of the peak current vs. oxidizing species concentration can be employed for the estimation of the catalytic constant kcat. If the concentration of the oxidizing species is unknown, the apparent catalytic constant k'cat is also defined following equation 3.20.

$$k'_{cat} = k_{cat} \cdot [Oxidizing\ species]_{(electrode\ surface)} \quad (3.20)$$

3.1.6 Electrode reaction mechanism

The characterization of the reaction mechanism requires the use of square-wave voltammetry. In particular, the aspect of the square-wave voltammograms are determined by the kinetic parameter λ (equation 3.21) and the catalytic parameter γ (equation 3.22)[139].

$$\lambda = k^0 / f \quad (3.21)$$

$\gamma = k'_{cat}/f$ (3.22)

(Where k^0: standard electrochemical rate constant; k'_{cat}: apparent catalytic constant; f: square-wave frequency).

The kinetic parameter describes the reversibility of the reaction and, in particular, the effect of the electron transfer kinetics on the voltammograms aspect: the reaction is considered totally reversible for $log(\lambda)>1$, and totally irreversible for $log(\lambda)<-1.5$. Within this range ($-1.5<log(\lambda)<1$), the reaction is quasireversible. If the quasireversible condition if fulfilled and $log(\lambda)<0.7$, the dimensionless peak current ψp is described by a complex function of the catalytic parameter; otherwise, if $log(\lambda)\geq 0.7$, the function of ψ_p vs. γ is characterized by a linear trend. Moreover, also the ratio between the catalytic and the kinetic constants gives important information: the trend of ψ_p vs. $log(1/f)$ is characterized by the presence of the quasireversible maximum if $k'_{cat}/k^0 \leq 0.15$; in this case, the reaction is mainly controlled by the charge transfer process. On the other hand, if $k'_{cat}/k^0 \geq 0.5$, the function of the dimensionless current vs. $log(1/f)$ is a non-linear sigmoid without the quasireversible maximum and the effect of the catalytic reaction prevails.

3.2 Protocol for the characterization of a catalytically enhanced AdCSV method

In the following section, two schemes reporting the steps required for the characterization of the chemical features (figure 3.1) and the electrode reaction mechanism (figure 3.2) are reported.

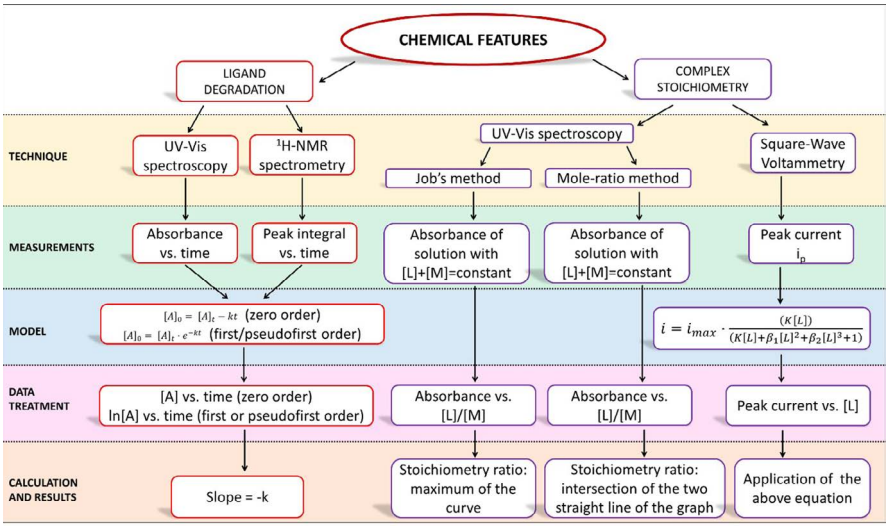

Figure 3.1: Procedures required to characterize the degradation of a species used as ligand of the AdCSV method analyte, and the complex stoichiometry.

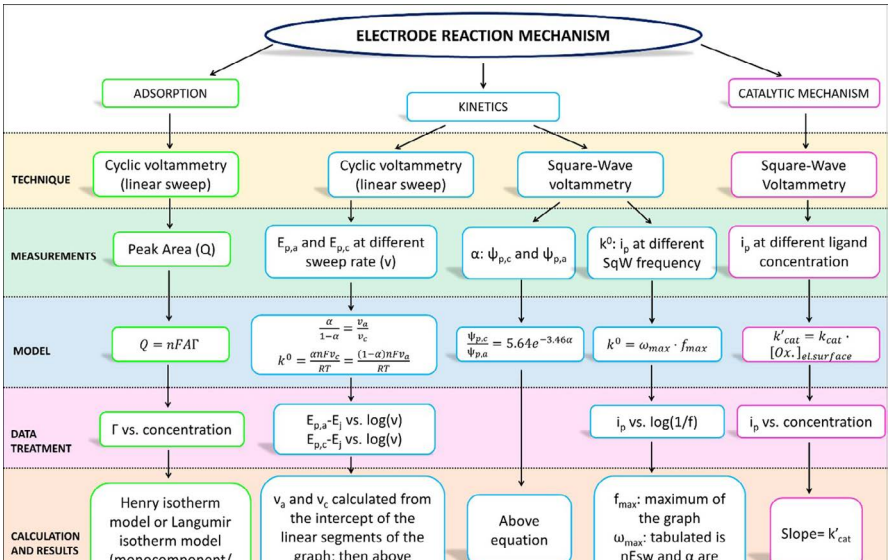

Figure 3.2: Procedures for the characterization of the adsorption of a species onto the electrode surface, of the electrode reaction kinetics and of the catalytic mechanism, if involved, of a general AdCSV method.

All the procedures reported were used in the present thesis to characterize the AdCSV method for iron determination and speciation in seawater. Nevertheless, the reported schemes can be also considered as a protocol for the characterization of the AdCSV techniques for the detection of a metal at trace and ultratrace levels in different kind of matrices.

3.3 Characterization of the chemical features

3.3.1 Degradation of 2,3-dihydroxynaphthalene

The slow degradation of 2,3-dihydroxynaphatlene (DHN) at alkaline pH values in aerated solutions was highlighted in a previous work[113], and it is clearly observable as a pink and then light brown color develops in alkaline DHN solutions. The degradation of the ligand used to complex the metal could generally cause a loss in the analytical sensitivity and other adverse effects; this phenomenon takes on particular importance for the speciation analysis procedure, which require an overnight equilibration time of solutions containing the ligand at pH 8. These are the reasons why a comprehension of this phenomenon and the conditions under which it occurs is mandatory. According to the evidence of a change in the color of DHN solutions, UV-Vis spectroscopy was at first employed to study the DHN degradation. The adsorption spectra of DHN aerated solutions at different pH values are reported in figure 3.3.

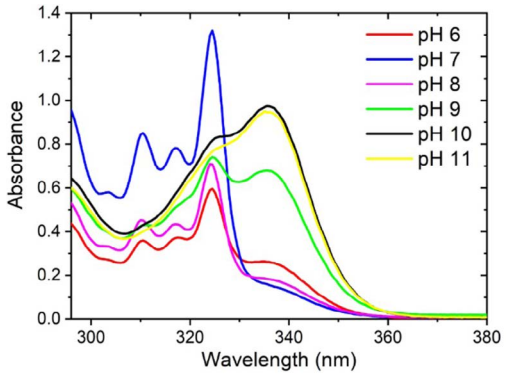

Figure 3.3: Adsorption spectra of 2,3-dihydroxy-naphthalene aerated solutions at pH values between 6 and 11. Experimental: 0.2 mM DHN except pH 4 which required 0.4 mM DHN concentration; 1 nm bandwidth; 0.2 s integration time, 0.5 nm data range; 150 nm·min^{-1} scan rate; 298.15 K constant temperature. See Table A.1 of the Appendix for the measurements of temperature and pH at the beginning and at the end of each kinetic test.

Kinetic tests demonstrated that the peak at around 335 nm steadily decreased with time, evidencing a fast and first order kinetics characterized by a degradation half-life times ($t_{1/2}$) between 37 minutes and 660 minutes moving from pH 7 to 11 (see Table 3.2 for all the $t_{1/2}$ values).

pH	Half-life time (min)	pH	Half-life time (min)
6	Constant absorbance	9	135
7	37	10	420
8	103	11	660

Table 3.2: Half-live times of the species characterized by the peak at 335 nm for pH values between 6 and 11.

Moreover, the kinetic tests at pH 8 was repeated in absence of oxygen: no variation in the spectra were found during all the test (see figure 3.4), confirming that the degradation of the ligand is caused by the presence of O_2. ^{1}H-NMR spectrometry was then used to confirm the degradation rate of the 2,3-dihydroxynaphthtalene but preliminary experiments evidenced a much slower kinetics; therefore, the fast degradation rate related to the peak at 335 nm was attributed to an impurity contained in the DHN, and the appearance of the peak in the visible region and the consecutive color of solutions were attributed to its degradation and

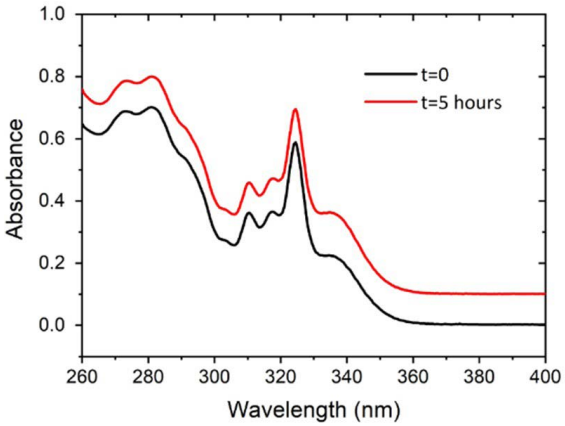

Figure 3.4: Adsorption spectra of 2,3-dihydroxynaphthalene solution prepared under nitrogen at the beginning and at the end of the kinetic test (t=5 hours). The spectra are shown with 0.3 offset on the y-axis. Experimental: 0.2 mM DHN, pH=8; 1 nm bandwidth; 0.2 s integration time, 0.5 nm data range; 150 nm·min-1 scan rate; 298.15 K constant temperature.

not to the degradation of the DHN itself. In this context the UV-Vis spectroscopy failed in the attempt to describe the degradation phenomenon of the ligand and the ^{1}H-NMR was preferred. In particular, ^{1}H-NMR tests were conducted at the natural pH value of the DHN stock solutions (around 5) to study their degradation in time, and at pH 8 as it is the pH value used to apply the AdCSV method for iron determination and speciation in seawater with the DHN. Both the solutions used during this step were prepared by dissolution of the adequate amount of the solid reagent in ultrapure water and setting the pH at the proper value (8.0) by adding NaOH. Moreover, ^{1}H-NMR spectra were acquired for 315 and 402 hours for pH 5 and pH 8, respectively, with time intervals between 2 and 96 hours. The method of the internal standard was applied, and the dimethyl sulfoxide was employed. Figure 3.5 shows the ^{1}H-NMR spectra of the DHN at the beginning of the kinetic test at pH 8 (t=0) and at the end (t=402.5 hours).

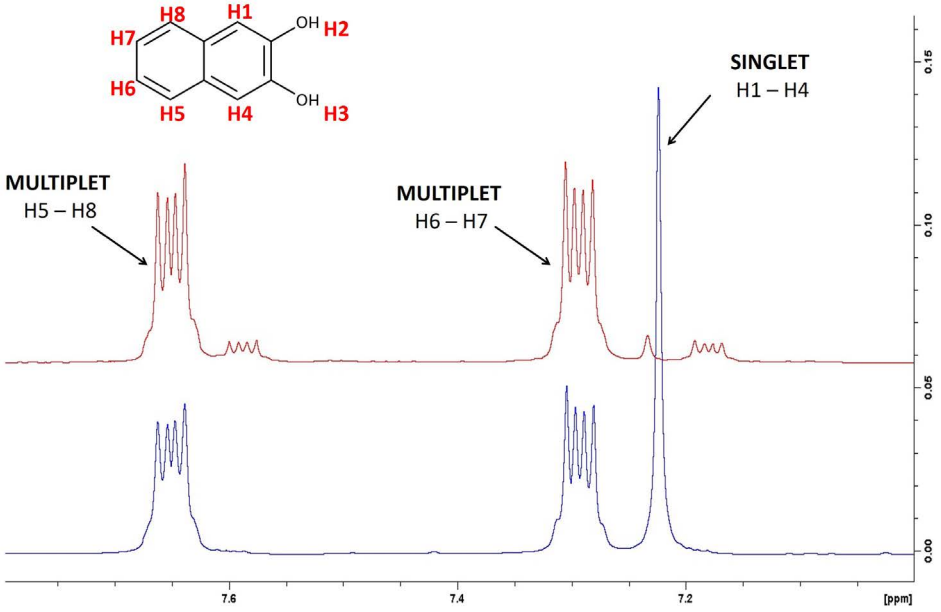

Figure 3.5: ^{1}H-NMR spectra DHN at the beginning (t=0) (blue spectrum) and at the end (t=402.5 hours) (red spectrum) of the kinetic test. Experimental 10 mM DHN; pH=8; zg acquisition sequence with 15 s delay time and 32 scans accumulated.

The simultaneous study of these spectra together with literature data[142] suggested that the reaction mechanism of the degradation phenomenon involved the 1,4 coupling of two naphthalene rings. In particular, ^{1}H-NMR spectra evidenced that the singlet at 7.31 ppm, which corresponded to hydrogen 1 and 4 of the naphthalene ring, reduced its integral, whereas multiples at 7.38 and 7.73 ppm, which corresponded to hydrogen 6-7 and 5-8, respectively, were constant with respect to the dimethyl sulfoxide singlet during all the kinetic test. According to this evidence, the kinetic law of the DHN degradation was established using the integral of the 7.31 ppm singlet. The data treatment (Figure 3.5) involved only the points up to the halving of the 2,3-dihydroxynaphthalene concentration, assuming the formation of the dimer due to the 1,4 coupling reaction although polymers with higher order and other DHN oxidation products may also form[142].

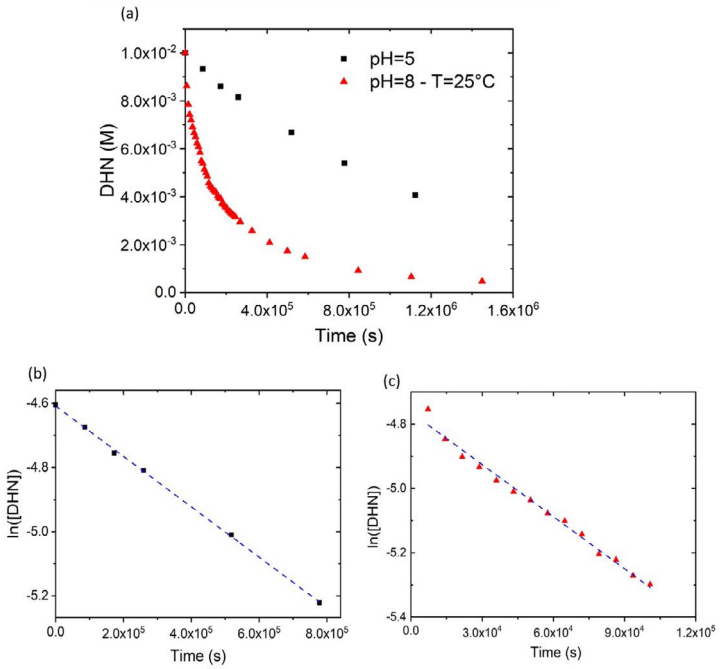

Figure 3.6: Trend of DHN concentration vs. time evidenced by the 1H-NMR spectroscopy/internal standard method for the two different conditions (a), and its linearization by logarithm function for pH=5 (b), for pH=8 and T=25°C (c).

The logarithm function was applied to linearize the concentration trend vs. time evidencing that the 2,3-dyhydroxynapthalene degradation kinetic law was first order for both the studied pH values or, possibly, pseudo-first order, as the role of atmospheric oxygen was not studied. Table 3.3 summarizes the kinetic rate constant calculated for each kinetic test. Test at pH 5 was characterized by a slower kinetics. Otherwise, test at pH 8 showed a faster kinetics characterized by an order of magnitude higher reaction rate with respect to the test conducted in acidic condition. Accordingly, these data suggested an important reduction of the sensitivity, even for relatively short time, requiring further investigation. Thus, the influence of the ligand degradation on the analytical sensitivity was studied for two DHN concentration levels (Figure 3.7).

pH	T (°C)	R^2	n	Rate Constant (s^{-1})
5	25	0.9993	6	$(7.8\pm0.1)\cdot10^{-7}$
8	25	0.9881	14	$(5.4\cdot\pm0.2)\cdot10^{-6}$

Table 3.3: Rate constant of the DHN degradation at pH 5 and 8.

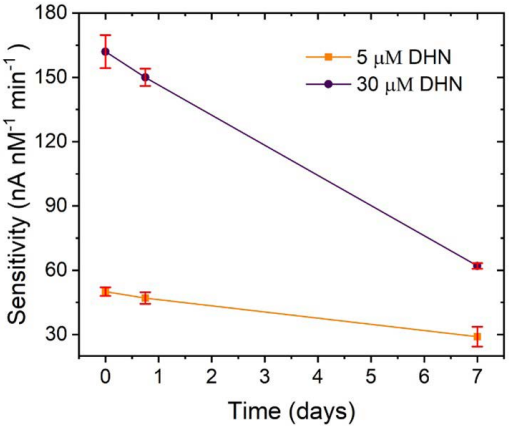

Figure 3.7: Trend of sensitivity vs. time. Experimental: ultrapure water; 10 mM HEPPS buffer pH 8.0; 5 and 30 µM DHN; 0.3 nM Fe added to calibrate the sensitivity. Square-wave voltammetry: -0.4 V deposition potential; 10 Hz square-wave frequency; 0.05 V·s^{-1} scan rate.

A decrease in the analytical sensitivity was evident, although it was not as high as the decrease in the DHN concentration (see Table 3.5 for the

detailed data).

DHN (µM)	Time of degradation	Sensitivity (nA·nM^{-1}·min^{-1})
5	New	50 ± 2.0
30	New	162 ± 7.7
5	18 hours	47 ± 2.7
30	18 hours	150 ± 4.0
5	7 days	29 ± 4.6
30	7days	62 ± 1.3

Table 3.5: Analytical sensitivity determined using the DHN at different degradation levels for both the uncatalyzed and catalyzed method.

This limited decrease in the analytical sensitivity could be an indication that the oxidized 2,3-dihydroxynaphtalene retained, at least in part, its capability to complex iron and be electroactive. Despite the analytical sensitivity not being strongly influenced by the DHN degradation, at least after 24 hours, the DHN concentration loss affected the speciation analysis that required an overnight equilibration time (see chapter 4). In an attempt to limit the DHN degradation, a kinetic test at pH 8 was repeated preserving the solution between each acquisition at T=4°C and in the dark (see Figure 3.8).

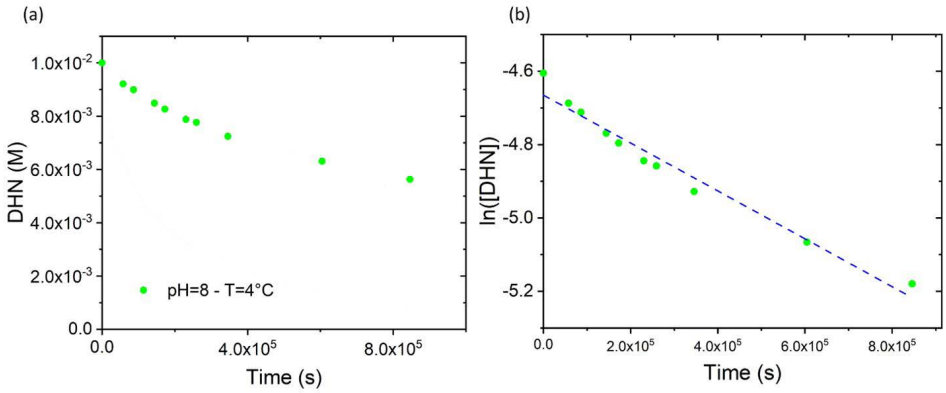

Figure 3.8: Trend of DHN concentration vs. time evidenced by the ^{1}H-NMR spectroscopy/internal standard method for pH=8 and T=4°C (a), and its linearization by logarithm function (b).

Accordingly, the ^{1}H-NMR spectra were acquired for 235 hours with time interval between 8 and 72 hours. A rate constant of $(6.5\pm0.4)\cdot10^{-7}$ s^{-1} was obtained by the linearization (R^2=0.9690) of the experimental data showing a slower kinetic with an order of magnitude lower rate constant with respect to the test at the same pH value conducted preserving the sample at room temperature (T=25°C). The latter results suggested two consequences. Firstly, during the 16 hours equilibration time required by the speciation analysis (see chapter 4), the aliquots should be stocked in a fridge to avoid the at least 33% loss in the DHN concentration. Secondly, the DHN stock solution should be refrigerated, as the lower temperature allowed a tenfold slower degradation rate. Thus, this stock solution could be reprepared weekly showing a negligible loss in its concentration.

3.3.2 Complex stoichiometry

The UV-Vis spectroscopy was firstly employed to determine the stoichiometry of the Fe-DHN complex which adsorbs onto the electrode surface, following the Job's and the mole-ratio methods130,131. Job's method, also called the method of continuous variations, was repeated for a wide range of pH values, between 2 and 10. A stoichiometric ratio of 1:1 was found for the test at pH 2, which increased up to 1:3 in alkaline conditions (Figure 3.9).

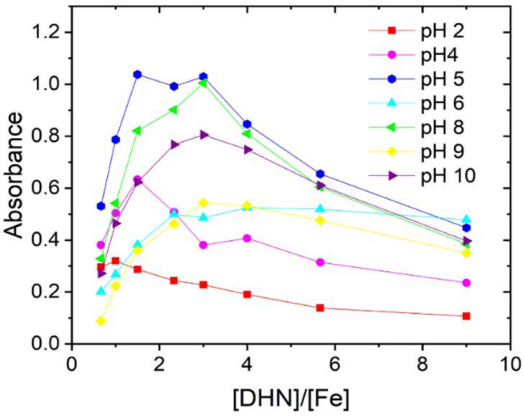

Figure 3.9: Job's plot at pH values between 2 and 11. The stoichiometry ratio value is 1:1 for pH 2 and it increases up to 1:3 for basic pH. Experimental: [DHN] between 0.1 and 1 mM; [Fe] between 0 and 0.9 mM; pH varied; 1 nm bandwidth; 0.2 s integration time, 0.5 nm data range; 150 nm·min^{-1} scan rate; 298.15 K constant temperature.

The mole-ratio method was then applied to verify the stoichiometric ratio value of the complex at

pH 8, which is the condition needed for iron determination and speciation in seawater. This experiment succeeded as the 1:3 value was found for the Fe-DHN stoichiometric ratio at pH 8 (Figure 3.10 (a)).

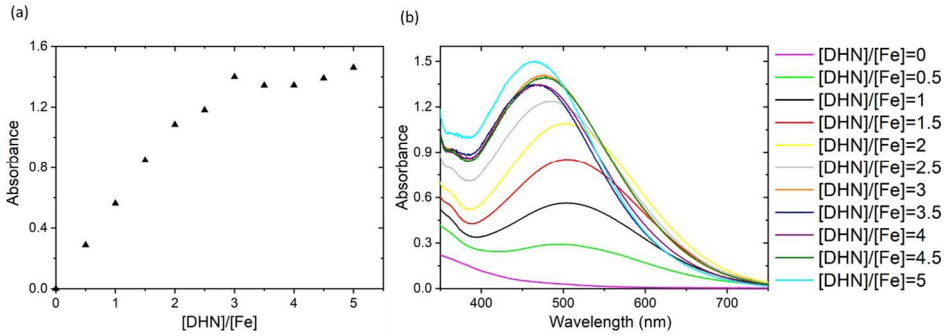

Figure 3.10: Mole-ratio plot showing the 1:3 stoichiometric ratio (a); Adsorption spectra of the mole-ratio experiment showing that λmax decreases with increasing [DHN]/[Fe] ratios. Experimental: [DHN] between 0 and 1 mM; [Fe]=0.2 mM; pH=8.0 ; 1 nm bandwidth; 0.2 s integration time, 0.5 nm data range; 150 nm·min^{-1} scan rate; 298.15 K constant temperature.

Nevertheless, the latter test showed that the λmax was higher for solutions characterized by [DHN]/[Fe]<3 with respect to solutions with [DHN]/[Fe]≥3 (Figure 3.9 (10)), suggesting the presence of a mixture of species characterized by different stoichiometric ratios. The latter methods based on the UV-Vis spectroscopy required high and similar concentrations of both the ligand and the metal to be applied. Nevertheless, the AdCSV method is used to detect trace and ultratrace levels of iron (nM-pM range), in the presence of at least two order of magnitude higher DHN concentration. For this reason, the electrochemical measurement[120] described in the 3.1.2 paragraph (peak current vs. increasing DHN concentration at a constant iron concentration) was needed to confirm the stoichiometric ratio of the complex under these conditions. In particular, the reduction peak of the Fe-DHN complex was already present in the voltammograms at the lowest 0.5 µM ligand concentration. The latter started to increase reaching a maximum in the range between 50 and 75 µM DHN, and then it levelled off for the higher concentrations. The trend of the peak current

vs. the DHN concentration, which is reported in figure 3.11, suggested the formation of only one electroactive species and probably the one characterized by the 1:1 stoichiometric ratio, as previously demonstrated by Abualhaija and van den Berg[120].

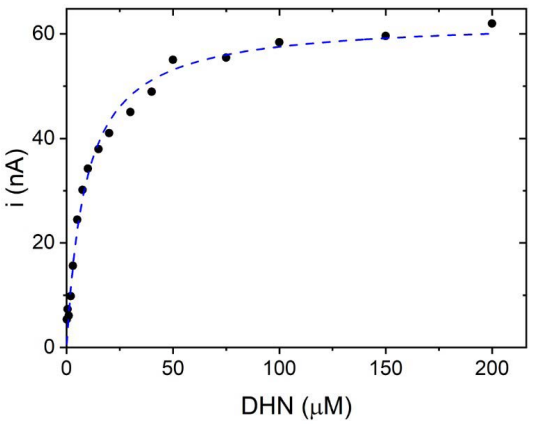

Figure 3.11: Trend of the peak current of the FeDHN reduction peak vs. DHN concentration. Experimental: ultrapure water; 10 mM HEPPS buffer pH 8.0. Square-wave voltammetry: -0.4 V deposition potential; 10 Hz square-wave frequency; 0.05 V·s^{-1} scan rate.

To confirm the hypothesis of the 1:1 complex, the experimental data (black points of Figure 3.11 were fitted with the specific form of equation 3.4. Table 3.6 reports the results of the data fitting with equation 3.5 (indicating that only the 1:1 species forms and is electroactive), 3.6 (indicating that both the 1:1 and the 1:2 species form but only the 1:1 is electroactive) and 3.7 (indicating that both the 1:1 and the 1:2 species form and are electroactive); see the Appendix for all the used equations.

Equation	i_{max}	K'	β_1	R^2
3.5	63 ± 1.3	(1.1 ± 0.9) · 10^5	/	0.9881
3.6	59 ± 2.5	(1.3 ± 0.1) · 10^5	Negative	0.9861

Table 3.6: Parameters calculated by fitting the experimental data with equation 3.5-.37.
*Not significantly different from zero (p<0.01)

The first evidence of this data treatment was that all the models involving the 1:3 complex did not converge; therefore, the formation of this species was excluded. All the models that considered the 1:1 and the 1:2 complexes lead to an around ^{105} value for the stability constant K' of the 1:1 species and a negative or a not

significantly different from zero ($p<0.01$) value for the stability constant β1 of the 1:2 species. Therefore, only the 1:1 complex formed and was electroactive under the condition typically encountered in the AdCSV method. The latter conclusion is also in good agreement with a previous work[118] which evidenced the prevalence of the 1:1 complex. This only apparent discrepancy between the results obtained with the two different techniques (UV-Vis spectroscopy and voltammetry) is easily explained by the fact that the dilution favors the formation of the species characterized by a lower stoichiometry as explained by standard equilibrium calculations. As a final remark, it should be highlighted that the use of ligand and metal concentrations different from the ones employed by the AdCSV method could lead to an erroneous identification of the species involved.

3.4 Characterization of the electrode reaction mechanism

3.4.1 Adsorption

An AdCSV method bases its functioning on the adsorption of the metal-ligand complex onto the working electrode surface and usually works in the presence of a large (at least two orders of magnitude) excess of the ligand concentration. Regarding the case of iron determination and speciation using 2,3-dihydroxynaphtalene as the complexing ligand, preliminary experiments evidenced that both the Fe-DHN complex and the DHN itself adsorbed onto the electrode surface giving a symmetric voltammetric signal at around -0.600 V and -0.050 V, respectively (Figure 3.12).

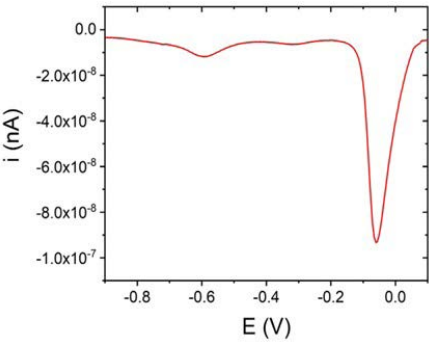

Figure 3.12: Square-wave voltammogram showing the symmetric DHN (-0.050 V) and FeDHN (-0.600 V) peaks. Experimental: ultrapure water; 10 mM HEPPS buffer pH 8.0; 30 µM DHN. Square-wave voltammetry: 30 s deposition time; -0.05 V deposition potential; 10 Hz square-wave frequency; 0.05 V·s^{-1} scan rate.

In this context a competition between the two species for the electrode surface could be possible. The latter phenomenon could result in a loss in the analytical sensitivity and, for this reason, it required a thorough investigation. The ligand adsorption in the absence of the metal was first studied. The trend of the electrode surface coverage Γ_{DHN} vs. ligand concentration is reported in Figure 3.13.

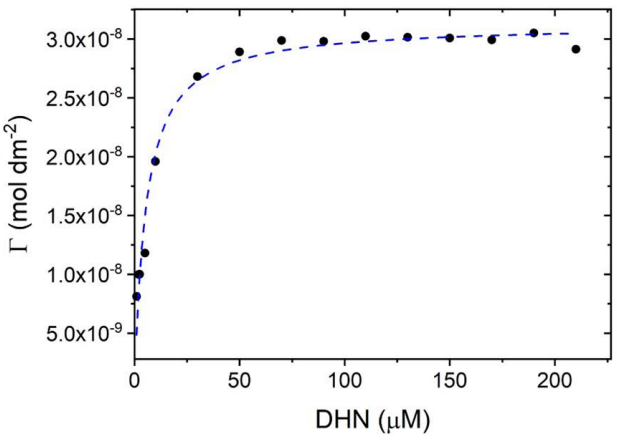

Figure 3.13: Trend of Γ (electrode surface coverage) vs. DHN concentration. The experimental data (black points) are fitted with the Langmuir isotherm model (dashed blue line). Experimental: ultrapure water; 10 mM HEPPS buffer pH 8.0. Square-wave voltammetry: 30 s deposition time; -0.05 V deposition potential; 10 Hz square-wave frequency; 0.05 V·s^{-1} scan rate.

The experimental data (black points) were fitted following the Langmuir isotherm model (dashed blue line) resulting in a $3.1 \cdot 10^{-8} \pm 6 \cdot 10^{-10}$ mol·dm^{-1} maximum surface coverage Γ_{max} and in a $(1.8 \pm 0.2) \cdot 10^{5}$ L·mol^{-1} adsorption equilibrium constant β. The same procedure, that is the calculation of the adsorption parameters for the complex in the absence of the ligand, was not possible because, as previously explained, these methods are applied in the presence of a large excess of ligand concentration. The multicomponent Langmuir isotherm model was then applied to describe the simultaneous adsorption of the Fe-DHN and the DHN species onto the electrode surface. Figure 3.14 shows the experimental data together with the fitted surface (R^2=0.9154), whereas Table 3.7 lists the calculated adsorption parameters for the two species.

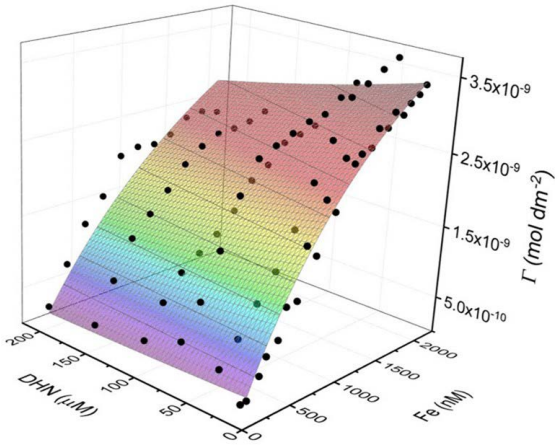

Figure 3.14: Trend of the surface coverage by FeDHN complex vs. iron and DHN concentration. The surface is modelled following the multicomponent Langmuir isotherm model. Experimental: ultrapure water; 10 mM HEPPS buffer pH 8.0. Cyclic voltammetry: 30 s deposition time; -0.4 V deposition potential; 0.05 V voltage step

Species	Γmax (mol·dm^{-1})	β (L·mol^{-1})
DHN	/*	(2.55±0.5) ·10^{3}
Fe-DHN	(6.9·10±0.6) ·10^{-9}	(5.5±0.8) ·10^{5}

Table 3.6: Adsorption parameters of the DHN and the FeDHN complex considered simultaneously by the multicomponent Langmuir isotherm model

*** The Γmax value for the DHN cannot be calculated using the multicomponent approach.**

The ligand adsorption constant calculated by fitting the experimental data with the multicomponent Langmuir isotherm model resulted two order of magnitude lower with respect to the complex one and with respect to the same parameter calculated in the absence of the complex. This meant that the ligand adsorbed around 100 times weaklier onto the electrode surface in the presence of the Fe-DHN complex than in its absence. The latter behavior suggested that the competition between the two species for the electrode surface did not occur. In particular, a reduction of the adsorption strength of the neutral ligand could be observed as a consequence of the adsorption of the complex which was, instead,

charged. The latter hypothesis could be also confirmed by the fact that in all the studied conditions the electrode surface was not saturated by the species as suggested by the experimental data trends.

3.4.2 Kinetics

Prelaminar cyclic voltammogram of the FeDHN complex was acquired to choose the proper method for the kinetic parameters' determination (see section 3.1.4 of this chapter). As the backward component of the cyclic voltammogram was missed, square-wave voltammetry was employed. In particular, the split between the forward and backward components of the square-wave voltammograms was employed to calculate the symmetry factor α following equation 3.17: a value of 0.57 was found. The latter value meant that the energy barriers of the reduction and oxidation reactions were slightly asymmetrical. On the other hand, the standard electrochemical rate constant k^0 was calculated by measuring the FeDHN reduction peak current at different square-wave frequencies. Thus, the trend of the *i/f* ratios (*i*: peak current; *f*: square-wave frequency) vs. *log(1/f)*, was used to determine the quasireversible maximum (Figure 3.15). The latter, which was the same for all the studied iron concentration, was in correspondence of f_{max}=90 Hz.

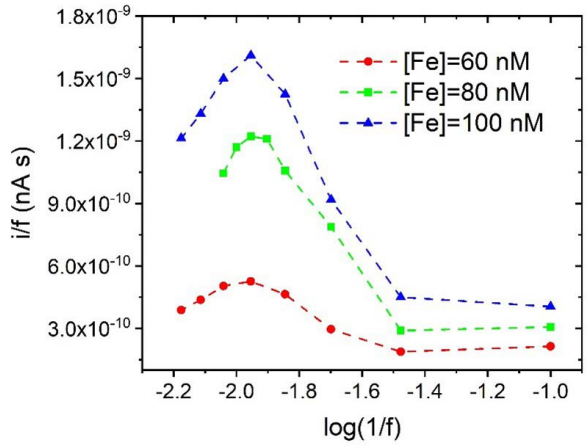

Figure 3.15: Trend of the i/f ratio vs. log(1/f). The quasireversible maximum is in the correspondence of f=90 Hz for all the iron concentration. Experimental: ultrapure water; 10 mM HEPPS buffer pH 8.0; 5 µM DHN. Square-wave voltammetry: 30 s deposition time; -0.05 V deposition potential; 10 Hz square-wave frequency; 0.05 V·s^{-1} scan rate.

Moreover, the 50 mV square-wave amplitude used to perform all the measurements and the 0.57 value of α previously determined led to the ωmax value of 0.88 (see Table 3.1). Accordingly, the standard electrochemical rate constant k0 resulted in a value of 79 s^{-1} by applying equation 3.18. The latter value was in good agreement with literature data reported for other complexes (e.g. k^0 for several molybdenum complexes is in the range between 8 and 150 s^{-1} [143,144]. Consequently, the kinetic parameter $\lambda=k^0/f$ was 7.9 for the square-wave frequency of 10 Hz, which is the typical condition used for iron determination and speciation with the DHN: *log(λ)=0.9* evidenced the quasireversibility of the Fe-DHN reduction reaction. Moreover, as in the case of the DHN itself, the high value of k^0 meant that the equilibrium, which involved only the charge transfer and re-solvation reactions, was achieved in a short-time scale.

3.4.3 Catalytic reaction mechanism

The catalyzed AdCSV methods are, as already described, widely applied in ultratrace iron determination as they allow a significant increase in the peak current and, thus, in the analytical sensitivity. In the case presented in this thesis, atmospheric oxygen was used as the oxidizing species; nevertheless, it was hypothesized that the real responsible of the catalytic enhancement of the signal was not the oxygen itself, but the hydrogen peroxide produced at the electrode surface during the deposition step at the potential of -0.4 V by the reduction of O_2. Figure 3.16 shows the suggested catalytic reaction mechanism. The apparent catalytic constant k'cat was

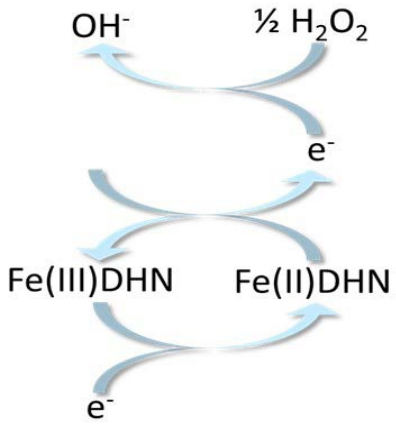

Figure 3.16: Suggested catalytic mechanism scheme. H2O2 generated at the electrode surface during the deposition step at the potential of -0.4 V by the O2 reduction, re-oxidizes the Fe(II)DHN species into the Fe(III)DHN one producing the catalytic enhancement of the peak current.

defined following equation 3.20 as $k'_{cat} = k_{cat} \cdot [H_2O_2]$. Accordingly, the sensitivity (see Figure 2.9 which reports the trend of sensitivity vs. DHN concentrations for 1 and 10 mL sample volume) for DHN concentration higher than 150 µM, condition under which all iron was complexed by the ligand, was employed for the k'_{cat} calculation following equation 3.19. Consequently, the average apparent catalytic constant resulted 168 s^{-1} and 123 s^{-1} for 1 and 10 mL cell volume, respectively. The around 1.4 higher sensitivity for the smallest cell volume could be attributed to a higher hydrogen peroxide concentration generated at the electrode surface. A more efficient stirring in the small volume, in fact, could reduce the diffusion layer and consequently cause a better diffusion of oxygen, which is the precursor of H_2O_2, towards the electrode during the deposition step. The oxygen reduction current measured during the deposition step was a confirmation of this hypothesis, as it was around 1.5 µA and constant for 1 mL analysis cell volume, whereas it decreased down to around 0.9 µA for the 10 mL one. In this case, the value of the catalytic constant kcat may be obtained only by estimation of the H_2O_2 concentration at the electrode surface. Thus, a comparison between the sensitivity values here presented and reported in a previous work, in which the effect of increasing hydrogen peroxide concentration added to the sample on the Fe-DHN reduction peak current was studied[112], could be useful. In particular, similar sensitivities were obtained for around 1 mM hydrogen peroxide concentration. Therefore, the k_{cat} values were calculated by multiplying the apparent catalytic constant values by 10^3 obtaining $1.68 \cdot 10^5$ $mol^{-1} \cdot dm^3 \cdot s^{-1}$ and $1.23 \cdot 10^5$ $mol^{-1} \cdot dm^3 \cdot s^{-1}$ for 1 mL and 10 mL sample volume, respectively. The latter values for the catalytic constant agreed with a previous work where the kcat value for a molybdenum complex in the presence of hydrogen peroxide was reported as $8 \cdot 10^4$ $mol^{-1} \cdot dm^3 \cdot s^{-1}$ [143]. At last, regarding the contribution of the catalytic effect to the electrode reaction, the ratio k'_{cat}/k^0 was 2.1. According to the theory previously explained (see section 3.1.6 of this chapter)[143], the latter value was an indication of the prevalence of the catalytic reaction effect.

3.5 Comparison with seawater

As reported in the previous chapter of this thesis (see section 2.2), the analytical sensitivity increases when the matrix salinity decreases. Understanding which parameters led to this difference among the sensitivity in ultrapure and seawater is a fundamental topic, especially for its consequences on the application of the technique to iron speciation in seawater. A comparison of the electrode reaction mechanism was required in this context. The same procedure used in the case of ultrapure was then applied for a seawater sample with a 35 psu salinity. Square-wave voltammetry was employed to determine the symmetry factor α and the standard electrochemical rate constant k^0 for the Fe-DHN reduction at the electrode surface because, as in the case of ultrapure water, ΔEp<200/n mV. The first difference evidenced by this procedure was that the calculated symmetry factor for seawater was 0.30. The latter value indicated an important asymmetry between the energy barriers of the reduction and oxidation reactions. On the other hand, the calculation of k^0 required the prior determination of the quasireversible maximum, by the application of the procedure reported in section 3.1.4 of this chapter. The trend of the *i/f* ratio vs. *log(1/f)* (see Figure 3.17) was employed to determine the quasireversible maximum.

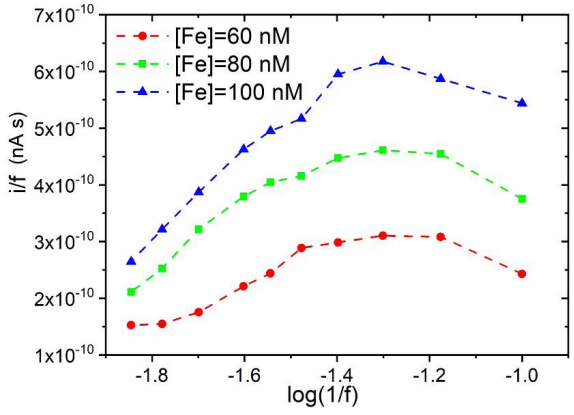

Figure 3.17: Trend of the i/f vs. log(1/f) for seawater. The quasireversible maximum is in the correspondence of f=90 Hz for all the Fe concentration. Experimental: ultrapure water; 10 mM HEPPS buffer pH 8.0; 5 µM DHN. Square-wave voltammetry: 30 s deposition time; -0.05 V deposition potential; 10 Hz square-wave frequency; 0.05 $V \cdot s^{-1}$ scan rate.

The quasireversible maximum, which was the same for the three different Fe

concentration studied was in correspondence of f_{max}=20 Hz. According to Table 3.1, this fmax value led to a k^0 of 19 $cm \cdot s^{-1}$, which was around fourfold lower with respect to the standard electrochemical rate constant for the same electron transfer reaction in ultrapure water. The latter value is a clear indication of a much slower kinetics of the electron transfer reaction in a high salinity matrix. Accordingly, the lower sensitivity found in seawater is the result of this slower kinetics as it limits the Fe-DHN peak current.

4

IRON SPECIATION[3]

Iron speciation; i.e. the distribution of the metal between different species (redox state III or II, inorganic, bund by organic ligands…), has attracted considerable attention in the last decades because it is of utmost importance in understanding the behavior of the metal in the oceanic system. From the analytical chemist's point of view, the problem of iron speciation in seawater represents a challenging task: methods characterized by extreme detection capabilities and selectivity able to detect different forms of the analyte at concentration levels often below the nM one are, in fact, required. Contrary to the methods developed for the detection of the total dissolved iron concentrations, advances in iron speciation methods were limited since the introduction of the Competitive Ligand Equilibration - Cathodic Stripping Voltammetry scheme (CLE-CSV)[105]. In fact, as extensively described in the Introduction chapter of this thesis, since the early '80s, cathodic stripping voltammetry has been employed to determine the interaction of several metals, such as Cu[145], Ni[146] and Co[147], with organic complexing ligands, but only since 1994[105] it has been applied to the problem of iron speciation in seawater.

[3]Fully reproduced and adapted with permission of Elsevier from Fast Iron Speciation in Seawater by Catalytic Competitive Ligand Equilibration-Cathodic Stripping Voltammetry with Tenfold Sample Size Reduction, Analytica Chimica Acta 2020, 1113, 9–17 (https://doi.org/10.1016/j.aca.2020.04.002). Copyright 0003-2670/© 2018 Elsevier B.V. All rights reserved.

The following chapter will be focused on the description of the development, validation, and application steps of a new method for iron speciation in seawater based on the CLE-CSV scheme which apply the hardware configuration previously developed and characterized. Firstly, the method together will be described together with the theoretical background of the data treatment. The results will be presented subsequently.

4.1 Theoretical background

The competitive ligand equilibration-cathodic stripping voltammetry (CLE-CSV) procedure allows the determination of the organic iron-binding ligands concentration in seawater and their stability constant for the metal. This method is based on the competition for iron complexation between the added artificial iron chelator, namely L_{add} (in our case the 2,3-dihydroxynaphthalene), and one (or more) organic iron binding ligand *L* present in the sample. Therefore, the analytical signal is determined by the reduction of the FeDHN complex adsorbed onto the electrode surface and depends on the competition between L_{add} and *L*. Accordingly, data required by the speciation calculations are obtained from titrations of seawater samples with growing iron concentrations whilst keeping constant the added ligand L_{add} concentration and monitoring the free iron not complexed by the organic iron-binding ligand *L*.

4.1.1 Titrations

As previously mentioned, the CLE-CSV method is based on a titration scheme. The latter consists on the addition of growing iron concentration to equivalent sample aliquots in the presence of a constant concentration of the iron chelator. Accordingly, the proper iron chelator concentration is chosen accordingly to the expected side reaction coefficient of the *FeL* complex (see section 4.1.3 of this chapter). Voltammograms are usually acquired following the order of increasing iron concentration after a time period called "*equilibration time*", as the equilibrium must be achieved before performing all the measurements.

The trend of the peak current vs. total iron concentration is peculiar of the CLE-CSV titrations and characterized by three different areas (Figure 4.1). Firstly, the current slightly increase with the Fe concentration, as in the solution there are both *L* and L_{add} that competitively complex iron. Then, the current increases more considerably when *L* starts to be saturated by iron. Subsequentially, the last part of the curve is characterized by the linear increase of the current with the total iron concentration, meaning that all *L* is saturated, and the added iron is complexed only by L_{add}.

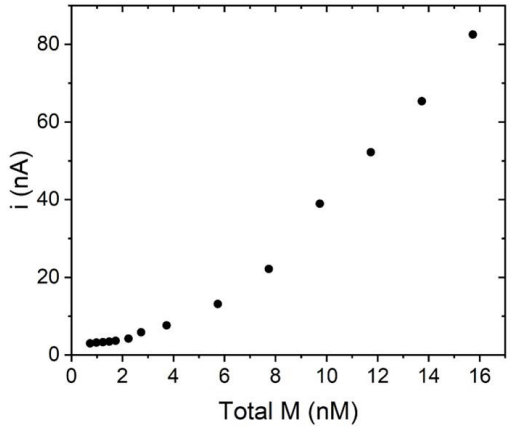

Figure 4.1: Typical trend of the peak current vs. total iron concentration for a CLE-CSV titration of a seawater sample.

4.1.2 Calibration of the side reaction coefficient

The calibration of the side reaction coefficients of the FeDHN complex is required by the data treatment of the titration procedure (see the following section). This step requires a competitive titration of a seawater sample containing a constant amount of Fe and L_{add} with increasing concentration of a ligand characterized by well-known stability constants for most metal ions. Ethylenediaminetetraacetic acid (EDTA) is often used in this context. It should be highlighted that the seawater sample used here must be UV-digested before being used to remove

all the organic matter which could interfere during the measurements. As in the case of the sample titrations, measurements are acquired after the *equilibration time*. During this step, the peak current decreases with the EDTA concentration as a consequence of the competition between the two ligands (Figure 4.2).

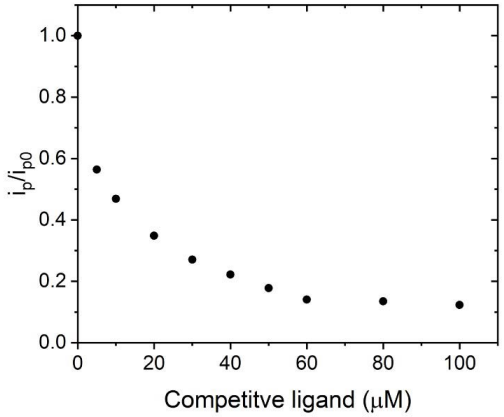

Figure 4.2: Typical trend of the current with the EDTA concentration for the calibration of the side reaction coefficient.

4.1.3 Data treatment

The theoretical basis of the speciation calculation based on titration data was firstly formulated by van den Berg and Ruzic[148–150]. In particular, a Langmuir type[148–150] linear plot (equation 4.1) is usually used to fit experimental data.

$$[Fe^{3+}]/[FeL] = [Fe^{3+}]/C_L + 1/(K'_{FeL} \cdot C_L) \quad (4.1)$$

(Where [FeL]: concentration of Fe complexed by the organic iron-binding ligand *L*; C_L: total L concentration, including both the free and the complexed species; K'_{FeL}: conditional stability constant for the *FeL* complex; see equation 4.2).

$$K'_{FeL} = [FeL]/([Fe^{3+}][L']) \quad (4.2)$$

(Where [L']: concentration of organic iron-binding ligand not complexed by iron. It comprises free [L^-] and complexes of *L* with the major cations, protons and trace metal in seawater).

It should be reminded the K'_{FeL} value is conditional upon the seawater composition in terms of calcium, magnesium and trace elements concentration, and pH and salinity conditions.

Important information can be also obtained by the plot of the ratio $[Fe^{3+}]/[FeL]$ vs $[Fe^{3+}]$ as, if the latter is linear, only a single ligand is present in the analyzed sample, whereas, if a curved trend is found, two or more organic iron-binding ligands characterize the composition of seawater. A definition of the labile iron Fe_{labile} concentration is, at this point, mandatory, to describe the theoretical basis of the method: in particular, $[Fe_{labile}]$ includes the iron released from the FeL complexes upon the addition of the artificial iron ligand L_{add} together with the inorganic iron. $[Fe_{labile}]$ is directly related to [FeL] by equation 4.3.

$$[FeL]=C_{Fe}-[Fe_{labile}] \quad (4.3)$$

Where CFe can be calculated by the mass balance (equation 4.4).

$$C_{Fe}=[Fe']+\sum[Fe(L_{add})_x]+[FeL] \quad (4.4)$$

Where [Fe'] is the concentration of the free iron(III), i.e. not complexed by the DHN or other ligands.

A more useful expression of the labile iron concentration can be obtained by substitution of equation 4.4 in equation 4.3 as follow.

$$[Fe_{labile}]=[Fe']+\sum[Fe(L_{add})_x] \quad (4.5)$$

Moreover, $[Fe^{3+}]$ is directly related to the $[Fe_{labile}]$ one (equation 4.6) by the overall side reaction coefficient α' (equation 4.7) for the complexation of iron by the added ligand Ladd and the inorganic complexation.

$$[Fe^{3+}]=([Fe_{labile}])/\alpha' \quad (4.6)$$

$$\alpha'=\alpha'_{Fe3+}+\alpha'_{Fe3+Ladd} \quad (4.7)$$

Therefore, a more convenient expression of the linearization plot (equation 4.1) is obtained by substituting the expression of $[Fe^{3+}]$ (equation 4.6) in equation 4.1, as the labile iron is measured by cathodic stripping voltammetry, rather than $[Fe^{3+}]$.

$[Fe_{labile}]/[FeL] = [Fe_{labile}]/C_L + \alpha'/(C_L \cdot K'_{FeL})$ (4.8)

The theory explained up to now is generally applied.

In the specific case of this work, in which the 2,3-dihydroxhynaphtalene was used as the added iron ligand Ladd data were treated as van den Berg reported in[118]. In particular, data were fitted with the linear equation 4.9.

$[Fe_{labile}]/[FeL] = [Fe_{labile}]/C_L + (1+\alpha_{Fe'DHN})/(C_L \cdot K'_{FeL})$ (4.9)

(Where $\alpha_{Fe'DHN}$ is the side reaction coefficient for the FeDHN complex).

The latter equation differs from equation 4.1 as the inorganic iron Fe' was consider rather than Fe^{3+}. From now on the notation Fe' will be employed as usually preferred by the oceanographic community. In this context the stability constant of the FeL complex was expressed following equation 4.10.

$K'_{Fe'L} = [Fe'L]/[Fe'][L^']$ (4.10)

(Where: [L']: DHN concentration not complex by Fe).

The inorganic side reaction coefficient $\alpha_{Fe'} = [Fe']/[Fe^{3+}] = 10^{10}$ was calculated (see the following sections) and used as before[105,118,151].

Accordingly, to the theory up to now described, two graphs were used to obtain information from the experimental data:

1) the graph of the peak current ip plotted against the total dissolved iron concentration was used to estimate the sensitivity of the technique: in particular, the sensitivity S ($nA \cdot nM^{-1}$) was calculated by di_p/dC_{Fe} of the linear final points of each titration;

2) the graph of the ratio $[Fe_{labile}]/[FeL]$ vs. $[Fe_{labile}]$ was used to calculate the organic iron-binding ligand concentration CL and its conditional stability constant for iron $K'_{Fe'L}$.

The determination of the conditional stability constant for the FeDHN complex (equation 4.11) and its side reaction (equation 4.12), was mandatory to apply the speciation procedure.

$K'_{Fe'DHN} = [Fe'DHN]/[Fe'][DHN']$ (4.11)

It should be reminded that, as CFe<<CDHN, the concentration of DHN not

complexed by iron can be approximated to the total DHN concentration.

$\alpha_{Fe'DHN}=[Fe'DHN]/[Fe'] = K'_{Fe'DHN}\cdot[DHN]$ (4.12)

The side reaction coefficient αFe'DHN was calibrated by competition with ethylenediaminetetraacetic acid (EDTA), as its stability constants for iron and most metal ions are well-known. In particular, in the absence of EDTA the concentration of the FeDHN complex followed equation 4.13, whereas, in the presence of EDTA, it could be described by equation 4.14.

$[FeDHN]_0=(\alpha_{Fe'DHN}\cdot C_{Fe})/(\alpha_{Fe'}+\alpha_{Fe'DHN})$ (4.13)

$[FeDHN]=(\alpha_{Fe'DHN}\cdot C_{Fe})/(\alpha_{Fe'}+\alpha_{Fe'DHN}+\alpha_{Fe'EDTA})$ (4.14)

(Where $\alpha_{Fe'EDTA}=K'_{Fe'EDTA}\cdot[EDTA']$ and, as in the case of DHN, because CFe<<CEDTA, the concentration of EDTA not complexed by iron [EDTA'] can be approximated to the total EDTA concentration [EDTA].)

It should be reminded that all the calculations were performed against the inorganic iron, so that $\alpha_{Fe'}$ equal to 1 could be neglected with respect to the other parameters of equation 4.13 and 4.14.

The peak current i_p obtained by voltammetric measurement was theoretically lowered as a result of the competition between DHN and EDTA. Therefore, considering that ip was described by equation 4.15, the ratio X between the signal in the presence and in the absence of EDTA resulted in equation 4.16

$i_p=S[FeDHN]$ (4.15)

$X=i_p/i_{p0}=\alpha_{Fe'DHN}/(\alpha_{Fe'DHN}+\alpha_{Fe'EDTA})$ (4.16)

The only parameter unknown in equation 4.16 is the side reaction coefficient of the FeDHN complex so that, it could be calculated by non-linear regression of X against $\alpha_{Fe'EDTA}$.

4.2 Calibration of the side reaction coefficients and the stability constant for the FeDHN complex

The side reaction coefficients for the FeDHN complex were calibrated against

the ethylenediaminetetraacetic acid (EDTA) due to its well-known stability constant for most metal ions. In particular, the $\alpha_{Fe'EDTA}$ values for different EDTA concentrations at pH 8 were previously calculated using the Visual MINTEQ software (version 3.1) which employed the equilibrium constant from the NIST database (Table 4.1).

EDTA

Species	logK	Species	logK
$HEDTA^{-3}$	10.948	$CaHEDTA^{-}$	15.97
$H2EDTA^{-2}$	17.221	$MgEDTA^{-2}$	10.58
$H3EDTA^{-}$	20.338	$MgHEDTA^{-}$	15.01
H4EDTA	29.24	$FeEDTA^{-}$	27.66
$H5EDTA^{+}$	24.052	FeHEDTA	29.17
$H6EDTA^{+2}$	23.94	$Fe(OH)EDTA^{-2}$	33.843
$CaEDTA^{-2}$	12.9		

Table 4.1: Stability constants used by the Visual MINTEQ software for the calculation of the $\alpha_{Fe'EDTA}$ values.

Moreover, the side reaction coefficients for the FeEDTA complex were calculated considering the correction for the activity coefficients of the ionic species because the contribution of the ionic strength could not be neglected as it will be explained later.

Preliminary experiments were performed to assess the equilibration time required by the procedure. The reduction peak of the FeDHN complex in the presence of a constant EDTA concentration was measured during time to estimate the time required to achieve the signal stability. Figure 4.3 shows that the signal decreased in time for the first hours of the test and became constant after an at least fifteen hours. Therefore, an overnight equilibration time was employed for all the speciation measurements from now on.

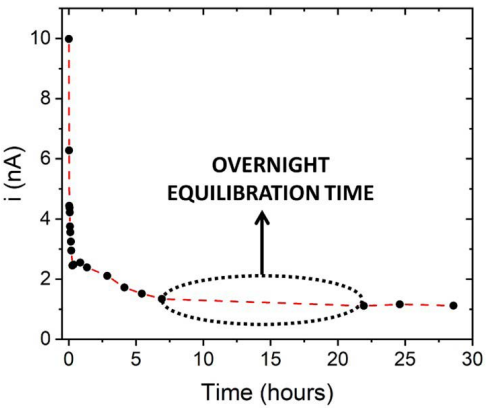

Figure 4.3: Trend of the FeDHN signal vs. time in the presence of a constant EDTA concentration. Experimental: UV-digested seawater; 10 mM HEPPS buffer pH 8.0; 10 µM DHN; 0.5 nM total iron; 1 mM EDTA; T=4°C. Square-wave voltammetry: 30 s deposition time; -0.05 V deposition potential; 10 Hz square-wave frequency; 0.05 $V \cdot s^{-1}$ scan rate.

Furthermore, the possibility to perform the analysis preserving the aliquots at room temperature was assessed. Preliminary experiments showed unreliable results in the trend of experimental data, in accordance with literature data[63]; thus, the equilibration period has been performed at T=4°C for all the experiments reported in this study.

The side reaction coefficients for the FeDHN complex were calibrated for four different DHN concentrations (0.5,1,5,10 µM DHN); moreover, for each of them, three replicate calibrations were performed to assess the precision of the procedure.

The trend of ratio between the peak current for each EDTA addition and the peak current in absence of EDTA $X=i_p/i_{p0}$ vs. $\alpha_{Fe'EDTA}$ is shown in Figure 4.4 (points: experimental data; dashed lines: data fitting with equations 4.16).

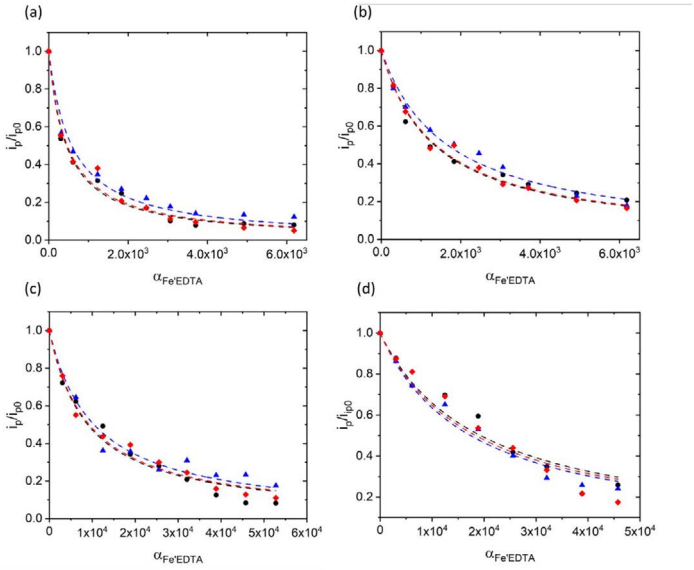

Figure 4.4: Trend of $X=i_p/i_{p0}$ vs. $\alpha_{Fe'EDTA}$ for 0.5 (a), 1 (b), 5 (c) and 10 (d) µM DHN. For each DHN concentration all the three replicate calibrations are shown. equation 4.16 fitted the experimental data (dashed lines) with R^2 between 0.9433 and 0.9897 with a median value of 0.9819. Experimental: UV-digested seawater; 10 mM HEPPS buffer pH 8.0; 10 nM added Fe for 0.5 µM DHN and 5 nM added Fe for the other DHN concentrations; overnight refrigerated equilibration time. Square-wave voltammetry: 30 s deposition time; -0.4 V deposition potential; 0.005 V Voltage step; 10 Hz frequency; 0.05 V·s-1 scan rate.

The mean side reaction coefficients αFe'DHN of the three replicates for each DHN concentration, together with their uncertainties expressed as the standard deviations and the relative standard deviations (RSD%) are listed in Table 4.2.

The $\alpha_{Fe'DHN}$ values reported in Table 4.2 apparently disagreed with literature data[118] where values of 166 and 366 were reported for 0.5 and 1 µM DHN, respectively.

DHN (µM)	$\alpha_{Fe'DHN}$ (mean ± standard deviation)	RSD%
0.5	$(5.0\pm0.7)\cdot10^{2}$	15%
1	$(1.5\pm0.2)\cdot10^{3}$	12%
5	$(9.5\pm0.7)\cdot10^{3}$	7.9%
10	$(1.7\pm0.06)\cdot10^{4}$	3.4%

Table 4.2: Side reaction coefficients αFe'DHN for the FeDHN complex expressed against the inorganic iron. For each DHN concentration the precision is expressed as the standard deviation and the percentage relative standard deviation.

Nevertheless, these literature values were calculated considering the activity coefficients of the ionic species equal to one. Therefore, if the calculation for the side reaction coefficients of the FeDHN complex of this work were repeated neglecting the correction for the ionic strength, values of $(9.01\pm1.3)\cdot10^{1}$, $(2.6\pm0.3)\cdot10^{2}$, $(1.6\pm0.2)\cdot10^{3}$ and $(3.1\pm0.1)\cdot10^{3}$ would be obtained for 0.5, 1, 5 and 10 µM DHN, respectively. The latter values, which were instead in good agreement with literature data, confirmed that neglecting the contribution of the ionic strength in seawater causes an underestimation of the side reaction coefficients. Moreover, as an artificial li-

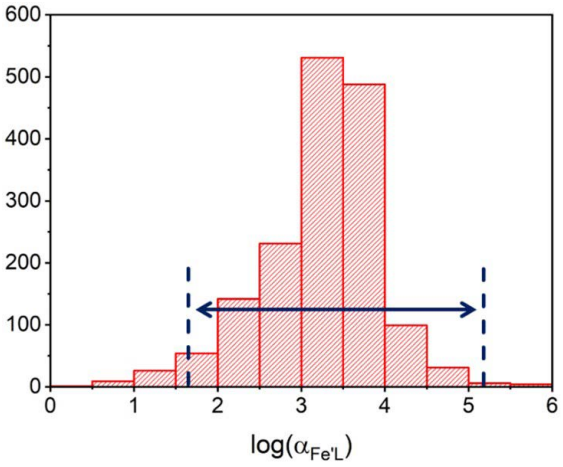

Figure 4.5: Distribution of the around 1600 log(αFe'L) values reported in a recent compilation of iron speciation data in seawater27 for organic iron complexing ligands. Blue lines indicate the range of values detectable by the method here described employing different artificial ligand concentrations.

gand *AL* characterized by a given $\alpha_{Fe'AL}$ may only detect natural ligand following the inequality $0.1 \cdot \alpha_{Fe'AL} < \alpha_{Fe'L} < 10 \cdot \alpha_{Fe'AL}$, thanks to the side reaction coefficient here calculated, the method presented in this thesis is theoretically capable to detect natural ligands with αFe'L in the range of $50\text{-}2 \cdot 10^5$ (1.7-5.2 of the log scale as $\log(\alpha_{Fe'L})$). A comparison between this result and a recent compilation of iron speciation in seawater data[27] demonstrates that 97% of these are included in the $50\text{-}2 \cdot 10^5$ range suggested that the correct detection window was targeted by the method (Figure 4.5).

Regarding the precision of the $\alpha_{Fe'DHN}$ values, the one achieved here was higher with respect to literature data that reported RSD% values in the range of 24-35% for the α_{CuEDTA} [152], as opposite to the 3-15% range obtained for the αFe'DHN here. As a final consideration, the side reaction coefficients linearly increased with the DHN concentration with an R^2=0.9980 confirming the presence of the 1:1 complex as demonstrated in the 3.3.2 section of chapter 3. In particular, the $(1.80 \pm 0.05) \cdot 10^{-9}$ (9.25 on the logarithm scale) slope of the fitted line shown in Figure 4.6 corresponded to the conditional stability constant for the FeDHN complex in seawater ($K'_{Fe'DHN}$) expressed against inorganic iron.

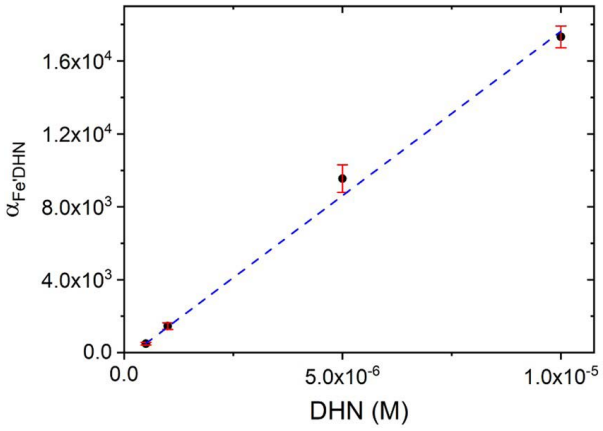

Figure 4.6: Linear trend (R2=0.9980) of the side reaction coefficients αFe'DHN vs. DHN concentration. Data are expressed as medium value of the three replicates calibration ± standard deviation. The (1.80±0.05) ·10-9 (9.25 on the logarithm scale) slope corresponds to the conditional stability constant $K'_{Fe'DHN}$ of the FeDHN complex in seawater (expressed against the inorganic iron).

4.3 Set up and method validation[4]

4.3.1 Blank

Preliminary experiments were employed in the attempt to demonstrate that the trend of the FeDHN peak current vs. the ligand concentration typical of the speciation analysis was only due to the competition for iron complexation between the DHN itself and the organic iron binding ligand present in the seawater sample. Other electroactive complexes, in fact, could interfere with the FeDHN peak, leading to a misinterpretation of the experimental data. Accordingly, a first titration of UV-digested seawater with increasing iron concentration without the DHN showed voltammograms characterized by a total absence of signals (Figure 4.7), confirming that the peak visible during the speciation analysis was only due to reduction of the FeDHN complex and no interference from other species occurred (Figure 4.7).

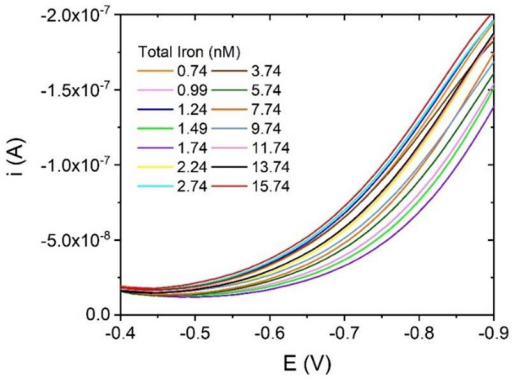

Figure 4.7: Voltammograms of the titration of UV digested seawater with increasing iron concentration in the total absence of 2,3-dihydroxynapthalene. The FeDHN peak at around -0.6 V is totally absent for all the Fe concentration. Measurements are acquired employing the pseudoreference. Experimental: UV-digested seawater; 10 mM HEPPS buffer pH 8.0; 0.74 initial total Fe concentration; overnight refrigerated equilibration time. Square-wave voltammetry: 30 s deposition time; -0.4 V deposition

As the second step, two blank titrations of UV-digested seawater in the presence

This part, except the validation with DTPA, was conducted in collaboration with Professor Luis Laglera in the FI-Trace group laboratories (https://www.fitrace.es/) at the Universitat de les Illes Balears in Palma de Mallorca.

of 1 and 10 µM DHN with increasing iron concentration were performed to assess the selectivity of the method in accordance with previous data[112]. Figure 4.8 shows the voltammograms of the two titrations and the consecutive trend of the peak current vs. iron concentration.

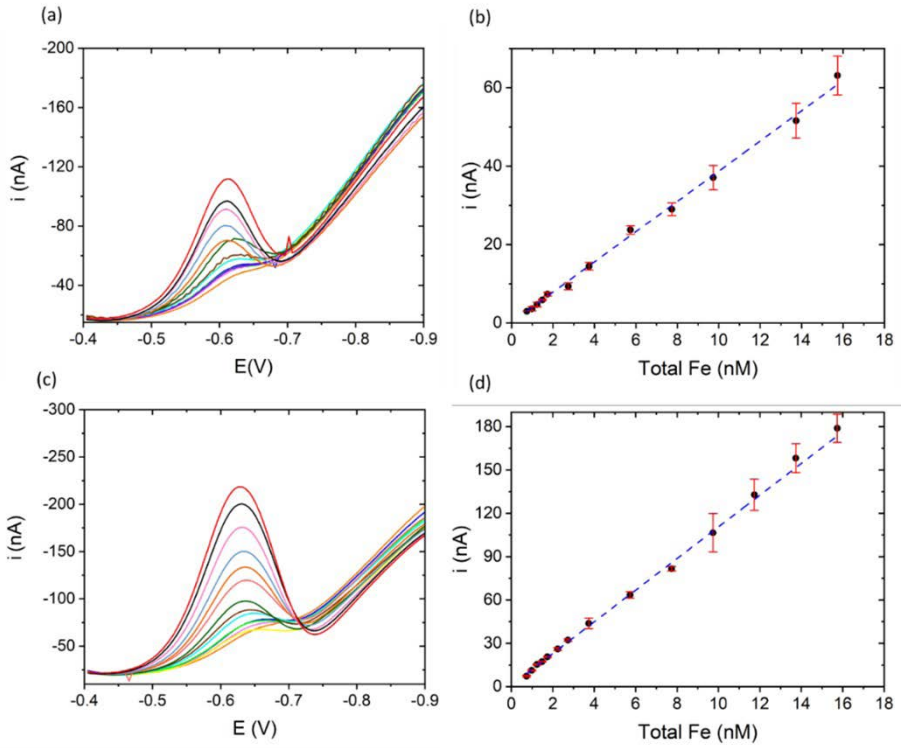

Figure 4.8: Titration of UV-digested seawater and trend of the peak current vs. iron concentration in the presence of 1 (a) and (b), and 10 (c) and (d) µM DHN. Measurements are acquired employing the pseudoreference. Data are expressed as medium value of three replicates measurements ± standard deviation. Experimental: 10 mM HEPPS buffer pH 8.0; 1 and 10 µM DHN; overnight refrigerated equilibration time. Square-wave voltammetry: 30 s deposition time; -0.4 V deposition potential; 0.005 V Voltage step; 10 Hz frequency; 0.05 V·s^{-1} scan rate.

The linear trend, characterized by R^2=0.9961 and R^2=0.9926 for 1 and 10 µM DHN respectively, confirmed that no interference occurred, and the trend of

the seawater titrations was due to the competition between ligands for iron complexation.

4.3.2 Validation with natural and artificial ligands

A validation step followed the verification about the absence of any interference. At first a titration of a seawater sample with trace level of iron containing 5 nM diethylenetriaminepentaacetic acid (DTPA) in the presence of 1 µM 2,3-dihydroxynaphthalene was performed. In particular, the DTPA was chosen as its stability constant for major and trace elements are well-known and the expected side reaction coefficient falls in the previously determined detection window. As in the case of EDTA, when DTPA is employed, all the complexation by trace elements must be considered due to the low concentration of the ligand and its low selectivity for iron. Table 4.3 lists all the DTPA acid dissociation and complex formation constants employed during the calculation.

DTPA			
Species	logK	Species	logK
$HDTPA^{-4}$	11.72	$CaDTPA^{-3}$	12.90
H_2DTPA^{-3}	21.18	$CaHDTPA^{-2}$	19.65
H_3DTPA^{-2}	26.11	$MgDTPA^{-3}$	11.42
H_4DTPA^{-}	29.24	$MgHDTPA^{-2}$	18.91
H^5DTPA	31.46	$Fe(OH)DTPA^{-3}$	40.45
H_6DTPA^{+}	33.05	$FeHDTPA^{-}$	35.21
H_7DTPA_{2+}	37.20	$FeDTPA^{-2}$	31.22

Table 4.3: Stability constants used by the Visual MINTEQ software for the calculation of the stability constants of the DTPA species.

Regarding the trace elements concentrations in seawater (Table 4.4), data from the GEOTRACES database[153] were used.

Element	Concentration (nM)	Element	Concentration (nM)
Al	3.3	Mn	1.6
Ba	42	Ni	3.2
Cd	0.026	Pb	0.015
Co	0.023	Ti	0.049
Cu	0.73	Zn	0.53

Table 4.4: Trace elements concentrations in seawater calculated as mean value of the GEOTRACES data of the GA10 cruise[153].

Moreover, as in the case of EDTA, all the calculations were carried out considering the correction for the ionic strength to avoid any underestimation of the results. The Visual MINTEQ calculation, which employed the stability constants from the NIST database, showed the prevalence of the FeOHDTPA3- species with the corresponding $\log(K'_{FeOHDTPA3-})$ equal to 12.09; otherwise, the concentration of the $FeDTPA^{2-}$ and $FeHDTPA^{-}$ species can be considered as negligible. The 12.09 $\log(K'_{FeOHDTPA3-})$ here calculated apparently disagreed with the 13.6 value reported in literature[154]. Nevertheless, this large difference is explained by the fact that in the cited paper only the major ions were taken into account for the calculation. If the trace elements had not been considered, the $\log(K'_{FeOHDTPA3-})$ would have been 12.9, reducing the difference with the literature value to below one order of magnitude.

Figure 4.9 shows one of the five replicate titrations of DTPA (a) together with its linearization (b) (see Table A.2 of the Appendix III for all the results).

Table 4.5 lists the results obtained during the validation step, expressed as mean value of five replicate titrations ± the standard deviation of the mean; the expected values for the ligand concentration and its stability constant for iron are also reported. The detected ligand concentrations showed an optimal agreement with respect to the expected value, whereas a limited discrepancy was evident regarding the stability constant $\log(K'_{FeOHDTPA3-})$. The latter could be explained considering the errors in the tabulated values of the constants for the EDTA and DTPA species and the errors obtained in the calibration of the side reaction coefficient for the FeDHN complex[152].

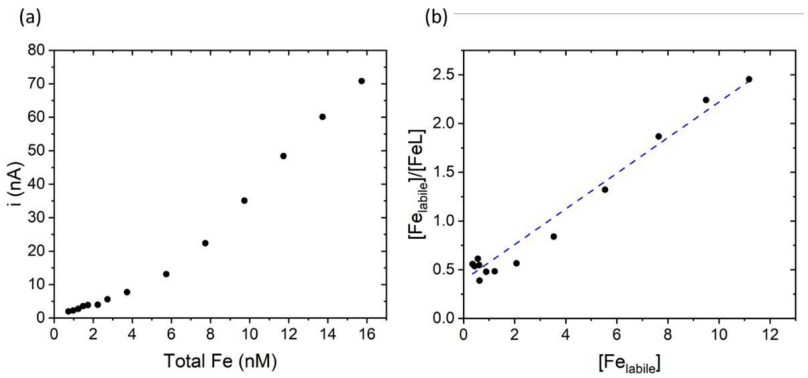

Figure 4.9: Trend of the peak current with the total iron concentration of a 5 nM DTPA titration (a) and its linearization (b). Experimental: matrix: UV-digested seawater; 10 mM HEPPS buffer pH 8.0; 1 µM DHN; 5 nM DTPA, 0.735 nM initial Fe concentration; overnight refrigerated equilibration time. Square-wave voltammetry: 30 s deposition time; -0.4 V deposition potential; 0.005 V Voltage step; 10 Hz frequency; 0.05 V·s^{-1} scan rate.

	EXPECTED		FOUND		
	log(K'$_{FeL}$)	C$_L$	log(K'$_{FeL}$)	C$_L$	n
DTPA	12.09	5	11.82±0.043	5.0±0.21	5
DFO	11.54[115] 11.60-12.10[54]	3	12.54±0.07	3.1±0.25	3
PPIX	11.9±0.5[57]	3	12.21±0.16	2.7±0.13	3
		6	11.91±0.4	6.1±0.15	3

Table 4.5: Results obtained during the validation step in terms of organic iron-binding ligand concentration and its stability constant for iron using both an artificial and two natural ligands compared to the expected values

The method was subsequently validated using two commercially available natural ligands. In particular, the deferoxamine (DFO) as mesylate salt, and the protoporphyrin IX (PPIX) were chosen as they represent two of the main classes of organic iron-binding ligands in seawater[41–43,57,58,155]. Contrary to DTPA, the stability constants for the FeDFO and FePPIX complex were previously determined (see Table 4.5) and they were employed to evaluate the experimental results obtained in the present study. Figure 4.10 shows one of the three replicate titrations of 3 nM DFO, 3 nM PPIX and 6 nM PPIX with their linearization (see Table A.3-A.5 of the Appendix for all the other results).

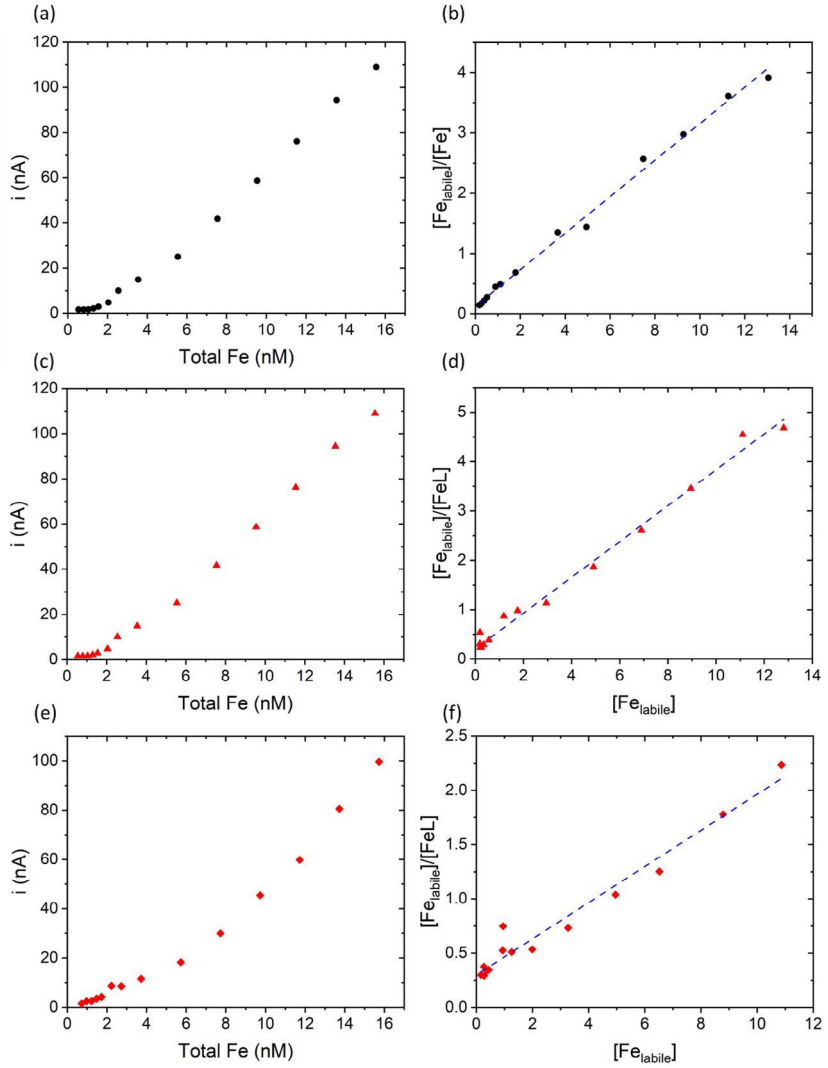

Figure 4.10: Trend of the peak current with the total iron concentration and its linearization for 3 nM DFO (a) and (b), 3 nM PPIX (c) and (d) and 6 nM PPIX (e) and (f) titrations. Experimental: matrix: UV-digested seawater; 10 mM HEPPS buffer pH 8.0; 1 µM DHN; 1.392 nM, 0.544 nM and 0.728 nM initial Fe concentration for the 3 nM DFO, the 3 nM PPIX and the 6 nM PPIX titrations, respectively; overnight refrigerated equilibration time. Square-wave voltammetry: 30 s deposition time; -0.4 V deposition potential; 0.005 V Voltage step; 10 Hz frequency; 0.05 V·s^{-1} scan rate.

All the results are listed in Table 4.5: for both the DFO and the PPIX, the found organic iron-binding ligand concentration and its conditional stability constant for iron were in good agreement with the expected values reported in the table.

4.3.3 Humic Substance

In the last years humic substances have attracted considerable attention of the chemical oceanographers as recent evidences showed their importance in the iron biogeochemical cycle in seawater[156]. Thus, the method was tested for the detection of Humic Acid (the Suwannee River humic Acid standard was employed in this context). Preliminary experiments were employed to verify the absence of interference caused by the Fe-HA complex peak in the voltammograms. The previously developed method which employed bromate as the catalytic enhancer evidenced, in fact, a peak due to the reduction of the FeHS species[119,124]. Therefore, a titration of UV-SW without any other ligand than humic acid with growing iron concentration up to 30 nM was performed. Figure 4.11 displays resulted voltammograms.

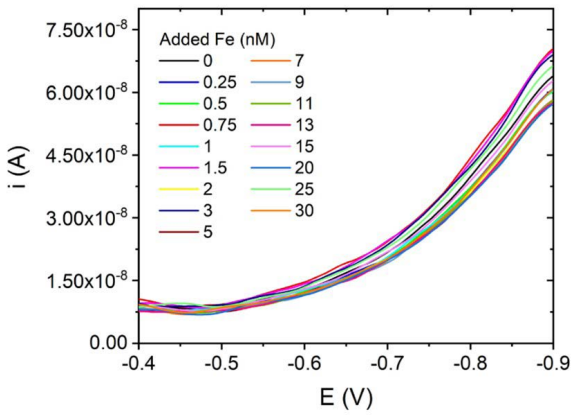

Figure 4.11: Voltammograms of the titration of UV digested seawater with increasing iron concentration in the total absence of 2,3-dihidroxynaphthalene and in the presence of 0.20 mg·L-1 SRHA. No peaks are present. Experimental: 10 mM HEPPS buffer pH 8.0; 0.20 mg·L-1 SRHA; overnight refrigerated equilibration time. Square-wave voltammetry: 30 s deposition time; -0.4 V deposition potential; 0.005 V Voltage step; 10 Hz frequency; 0.05 V·s^{-1} scan rate.

No peaks were present in the voltammograms, even for the higher Fe concentration. Accordingly, no species as the FeHS one could interfere with the FeDHN peak in the detection of humic substances by the CLE-CSV technique. Moreover, the O_2 method cannot be used for the detection of the Fe-HA complex

as done in the case of bromate[63]. UV-digested seawater containing 0.20 mg·L^{-1} SRHA was titrated with increasing iron concentration in the presence of 1 µM DHN. Figure 4.12 shows one of the titrations as an example (see Table A.5 of the Appendix for the results of each titration).

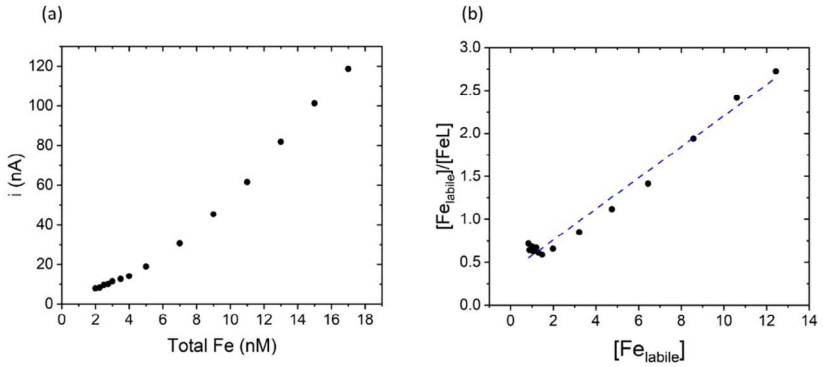

Figure 4.12: Titration (a) and its linearization (b) of 0.20 mg·L^{-1} SRHA. Experimental: 10 mM HEPPS buffer pH 8.0; 1 µM DHN; 1.995 nM initial Fe concentration; overnight refrigerated equilibration time. Square-wave voltammetry: 30 s deposition time; -0.4 V deposition potential; 0.005 V Voltage step; 10 Hz frequency; 0.05 V·s^{-1} scan rate.

As a result, the method was demonstrated to detect the complexing capacity of the humic acid, as a value of 5.8±0.3 nM, or 29±1.3 nmol per milligram of HA, was found and the conditional stability constant K'$_{Fe'HA}$ was calculated as 11.72±0.09. Regarding the comparison with literature data, only Laglera and van den Berg[63] reported the estimation of the HA complexing capacity and of the K' as 32±2.2 nmol·mg^{-1} of HA and 11.1±0.2, respectively. A limited 10 % difference was found in the HA complexing capacity, whereas a higher 0.6 on the logarithm scale discrepancy was found in the calculation of the conditional stability constant. However, it should be highlighted that the different methods employed in the cited paper[63] and in this work (direct detection of the FeHA complex for the complexing capacity and competition with the EDTA for K', and CLE-CSV, respectively) could play a role in the estimation of the complexing capacity and the conditional stability constant.

4.4 Antarctic seawater samples

Six seawater samples from a Ross Sea water column collected between 1 and 736 m depth were employed to test the method for both the detection of the total iron concentration and the metal speciation. Table 4.6 lists all the results expressed as mean ± standard deviation for each sample (Table A.7 of the Appendix lists all the results for each replicate titrations).

Depth (m)	Fe (nM)	CL (nM)	log(K'Fe'L)
1	1.5 ± 0.1	2.6 ± 0.09	12.25 ± 0.2
20	2.0 ± 0.1	4.9 ± 0.2	12.31 ± 0.03
50	1.51 ± 0.05	6.4 ± 0.2	12.05 ± 0.1
100	2.4 ± 0.3	2.9 ± 0.3	12.73 ± 0.3
400	1.8 ± 0.1	5.8 ± 0.1	11.88 ± 0.06
736	2.5 ± 0.5	6.5 ± 0.07	12.33 ± 0.4

Table 4.6: Dissolved total iron concentration and organic iron-binding ligand concentration and its stability constant for iron found in six seawater samples from the Ross Sea (E5 site, 74°40.04' S, 167°18.76' E). Data are all expressed as mean value of three replicates (three replicate titrations were performed for each sample).

One of the titrations of the 1 m depth sample and its linearization is reported as an example in Figure 4.13.

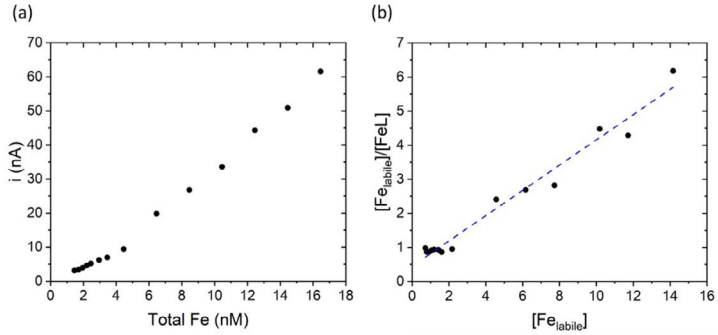

Figure 4.13: Titration (a) and its linearization (b) of the 1 m depth sample from the E5 site (74°40.04' S, 167°18.76' E74°40.04' S, 167°18.76' E) of the Ross Sea. Experimental: 10 mM HEPPS buffer pH 8.0; 1 µM DHN; 1.46 nM initial Fe concentration; overnight refrigerated equilibration time. Square-wave voltammetry: 30 s deposition time; -0.4 V deposition potential; 0.005 V Voltage step; 10 Hz frequency; 0.05 V·s^{-1} scan rate.

The total dissolved iron concentration, organic iron-binding ligand concertation and $logK'_{Fe'L}$ values spanned between 1.5 and 2.5 nM, 2.6 and 6.5 nM, and 11.8 and 12.73, respectively. The total iron concentrations are similar to values previously found in the upper 200 m of the water column in an around 20 nmi away area during the Antarctic summer season[157]. The high degree of variability found in the data is fully explained by the dynamicity of the coastal waters in the Ross Sea during this season due to both riverine inputs and melting pack ice phenomena and physical features like currents[157]. Regarding the $log(K'_{Fe'L})$, the results show good agreement with the 12.17 medium value obtained from a recent compilation about iron speciation data[27], whereas a higher discrepancy was found between the average total iron concentrations (1.9 nM in the present thesis vs. 1.4 nM from literature[27]) as only data from open oceanic waters were reported in the literature. A comparison between the precision of the here proposed method and literature data is another interesting topic to discuss. Besides a few cases, literature reports only one titration for each sample, whereas in the present work at least three replicates measurements were performed. This is the reason why only errors obtained from the linear fitting of the data can be compared. Regarding the concentration of the organic iron-binding ligand, the average percentage standard deviation RSD% values were 4% (n= 18) and 11% (n≈1200) for the here proposed method and literature data, respectively. On the other hand, errors in $log(K'_{Fe'L})$ were 0.17 (n=18, this method) and 0.27 (n≈900, literature data). Nevertheless, despite this apparently important discrepancy between the errors of the new method and literature data, it should be reminded that the latter is only a qualitative comparison, as the dimensions of the two data sets are completely different; moreover, it should be considered that literature data are expected to show a higher variability, because they were obtained by experiments conducted in different laboratories across a time span of 25 years. However, having said that, the precision for both the organic iron-binding ligand concentration and its stability constant for iron resulted comparable or better than data reported in literature.

4.5 Limit of detection

As the final assessment of the technique performances, the limit of detection (LOD) in terms of the lowest detectable ligand concentration was studied. Generally, the LOD calculation requires the evaluation of the standard deviation of the blank[124]. Nevertheless, the linearization procedure applied to the titration of the blank provided very low values for the ligand concentration and, consequently, caused an underestimation of the limit of detection. Therefore, the data obtained during the analysis of the Antarctic seawater samples reported in the previous paragraph of this section were used to achieve a more realistic evaluation of the limit of detection. In this context, a pooled standard deviation spooled from the ligand concentration results of all the 18 titrations of the Antarctic seawater samples were used to estimate the standard deviation of the blank. The LOD estimation formula, proposed by IUPAC (three times the standard deviation of the blank concentration) was then applied. As a result, a spooled of 0.17 nM was calculated and the minimum detectable organic iron-binding ligand concentration was estimated as 0.51 nM. The fitness for the purpose of the method was prompted by the 95% of the literature data[27] which reported organic iron-binding ligand concentrations higher than the estimated value of the limit of detection.

5 UNBUFFERED CLE-CSV METHOD[5]

In the previous chapter, the speciation procedure developed introducing several improvements has been described. In particular, all the parameters characterizing the analysis method have been optimized and applied to the CLE-CSV technique: the addition of bromate as catalytic enhancer was avoided, as the use of atmospheric oxygen directly introduced into the close voltammetric cell was proposed, the analysis time was reduced as well as the required sample volume, which was lowered down to 1 mL per titration aliquot. Nevertheless, some modification could be also introduced to the use of the pH buffer as its removal has not yet been considered. The pH buffer is usually used in all the voltammetric methods for iron detection and speciation in seawater to fix the pH at the value of 8.00. In fact, despite the natural buffer capacity of seawater, primarily due to the presence of the $CO_2/HCO_3^-/CO_3^{2-}$ system, most methods employ the nitrogen purging step which causes the carbon dioxide removal, resulting in a significant raise in the pH value. Consequently, the latter pH increase would lead to a change in both the organic and inorganic speciation of the metal[158–161]. Nevertheless, the method developed and presented in this

[5] [3]Fully reproduced and adapted with permission of Elsevier from Exploring bufferless iron speciation in seawater by Competitive Ligand Equilibration-Cathodic Stripping Voltammetry: does pH control really matter?, Talanta 2021, 122300 (https://doi.org/10.1016/j.talanta.2021.122300) Copyright © 2021 Elsevier B.V. All rights reserved.

thesis is characterized by the removal of the N_2 purging step, as it has been replaced by an atmospheric air purging to introduced oxygen as the catalytic enhancer. In this context, this new method seemed perfectly suited to introduce the simplification of the buffer removal in the procedure. The pH buffer removal in fact, could lead to an improvement in the method, not only regarding a general simplification of the procedure, but also because two problems related to the use of the buffer may be avoided. Firstly, because of the subnanomolar levels of iron in most of seawater samples, the pH buffer should be iron free, requiring in this way a time-consuming purification step. Thus, several (in our case, at least three) overnight equilibrations with colloidal manganese dioxide[118] (see section 6.2 of the Materials & Methods chapter) are required, and the residual iron concentration must be checked after each equilibration, until a satisfactory level of purification is achieved. Secondly, it should be also considered that the pH buffers usually employed in this context (the so-called "*Good Buffers*"[162]), may complex the metal or adsorb onto the electrode surface, affecting in this way the voltammetric signal. Actually, at present, no evidence about the iron complexation by the pH buffer employed (the 4-(2-hydroxyehtyl)-1-piperazinepropanesulfonic acid, HEPPS) has been yet found, but it should be also considered that the buffer surface active behavior and its ability to complex other trace metals could affect the reliability of iron speciation results.

However, before working on a non-buffered method for iron speciation in seawater, a thorough assessment of all the factor that may alter the sample pH were performed as seawater has limited buffering capacity, with an average 2.2±0.3 $mmol \cdot kg^{-1}$ total alkalinity (normalized to a 35 psu salinity)[163]. The first point to be considered was that the bulk pH of the sample should not change during both the equilibration step and the analysis. Thus, as the acidic iron standard solutions added to the aliquots during each titration were a source of H^+, and the new procedure lowered the volume of the sample aliquots down to 1 mL, the decrease in the pH was avoided from one side limiting the volume of the standard addition to below 10 µL, and from the other preserving the iron standard solutions with 1 mM HCl, as opposite to the higher acidic condition

usually employed. Moreover, no bulk pH changes could be observed during the analysis step, since the new method employed a purging step with atmospheric air, avoiding in this way the removal of the carbon dioxide. Secondly, it should be also considered that the pH buffer removal could result in a change in the pH values at the electrode interface during the electron transfer reaction typical of the deposition and sweeping steps. In particular, the interface pH was expected to raise as a consequence of proton consuming due to the oxygen reduction during the deposition step[164–166]. Accordingly, a significant increase in the pH could occur under the experimental conditions typical of the proposed method and its effect was carefully evaluated in the following section of this thesis.

5.1 General effects of the pH buffer removal

The effects of the pH buffer removal were thoroughly investigated to understand if any detrimental consequence on the method performances, especially regarding the speciation procedure, may be observed. Firstly, a 0.1 V shift towards more negative potentials was observed in the absence of buffer. The latter evidence is due to the increase in the interface pH value as a consequence of the oxygen reduction during the deposition step, as explained in the introduction of this chapter and in[164]. Figure 5.1 shows the 0.1 V peak shift for the buffered and non-buffered titrations of the same sample. This phenomenon did not appear to affect the analytical signal as the background current increase, although evident, was limited and did not influence the signal to noise ratio.

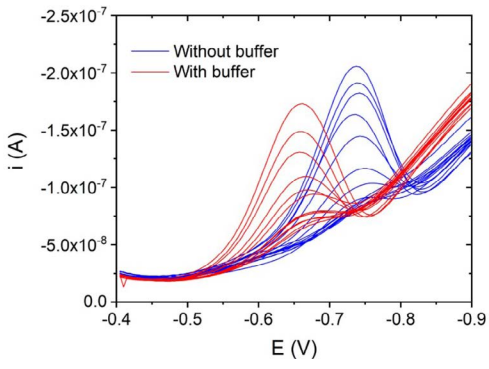

Figure 5.1: Titrations of the same Antarctic seawater sample (74°,40.04' S, 167°,18.76' E; 100 m depth) with (red lines) and without (blue lines) the pH buffer showing the 0.1 V shift towards more negative potentials (only one replicate per aliquot is shown for the sake of clarity). Experimental: 1 µM DHN; 2.43 nM total initial iron concentration; iron additions from 0 to 16 nM; 17 hours refrigerated equilibration period; square-wave voltammetry: 30 s deposition time; 0.4 V deposition potential; 0.005 V Voltage step; 10 Hz frequency; 0.05 V·s^{-1} scan rate.

The impact of the pH buffer removal on the analytical sensitivity is reported in Figure 5.2, together with its trend with the DHN concentration.

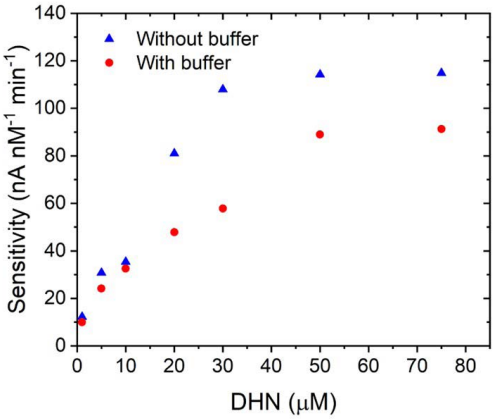

Figure 5.2: Trend of the analytical sensitivity vs. DHN concentration in buffered (red points) and unbuffered (blue points) UV- digested seawater. The sensitivity is reported as the signal of 1 nM iron concentration per minute of deposition time. Experimental: square-wave voltammetry: 30 s deposition time; 0.4 V deposition potential; 0.005 V Voltage step; 10 Hz frequency; 0.05 V·s^{-1} scan rate.

The trend of the sensitivity with the DHN concentration was the same for both buffered and unbuffered UV-digested seawater: it increased up to a maximum and then it levelled off for the highest ligand concentration, as shown in the previous chapters of this thesis. Nevertheless, it should be highlighted that a significant increase in the analytical sensitivity was found when the buffer was removed, especially for the highest DHN concentration. The latter effect could be considered a consequence of the higher pH value registered during the unbuffered analysis, in good agreement with data previously obtained using oxygen[112] and bromate[113] as catalytic enhancer of the signal.

5.2 Calibration of the side reaction coefficient

The side reaction coefficients for the FeDHN complex were again calibrated due to the new experimental conditions employed. Accordingly, competitive titrations against EDTA were performed at same four different DHN concentrations

investigated using the pH buffer (0.5, 1, 5 and 10 µM). Figure 5.3 shows the trend of the ratio $X=i_p/i_{p0}$ vs. the side reaction coefficients $\alpha_{Fe'EDTA}$ which is varied by varying EDTA concentrations.

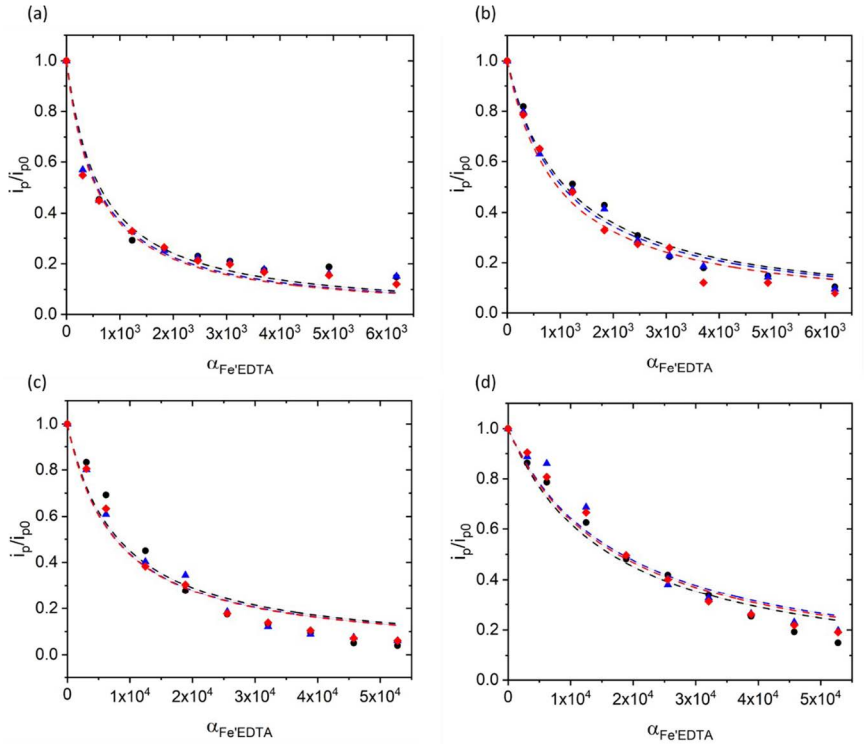

Figure 5.3: Trend of of the ratio $X=i_p/i_{p0}$ vs. $\alpha_{Fe'EDTA}$ for 0.5 (a), 1(b), 5 (c), and 10 (d) µM DHN. Three replicate titrations were performed for each DHN levels. The experimental data (points) were fitted according to equation 4.16. Experimental: UV-digested seawater; total iron concentration 10 nM for 0.5 µM DHN and 5 nM for 1, 5, and 10 µM DHN; 17 hours refrigerated equilibration time; square-wave voltammetry: 30 s deposition time; 0.4 V deposition potential; 0.005 V Voltage step; 10 Hz frequency; 0.05 $V \cdot s^{-1}$ scan rate.

As in the case of the buffered calibrations, the side reaction coefficients αFe'DHN were calculated by fitting the experimental data by equation 4.16; Table 5.1 lists all the results, including the percentage relative standard deviation %RSD.
Data reported in Table 5.1 resulted not statistically different with respect to

DHN (μM)	$\alpha_{Fe'DHN}$ (mean ± standard deviation)	RSD%
0.5	$(5.9\pm0.4)\cdot10^{2}$	6.6%
1	$(1.03\pm0.07)\cdot10^{3}$	7.4%
5	$(7.8\pm0.2)\cdot10^{3}$	3.5%
10	$(1.74\pm0.09)\cdot10^{4}$	5.0%

Table 5.1: Side reaction coefficients values at the four different DHN levels studied. The percentage relative standard deviations were calculated from three replicate titrations for each DHN concentration.

the ones reported in Table 4.2 (section 4.2 of the previous chapter) regarding the calibration of $\alpha_{Fe'DHN}$ using the HEPPS pH buffer. In particular, the $\alpha_{Fe'DHN\ buffered}$ vs. $\alpha_{Fe'DHN\ unbuffered}$ plot (Figure 5.4) evidenced a linear trend (R^2=0.9883, p<0.01, n=4) with the slope not statistically different from 1 (0.989±0.075) and the intercept undistinguishable from 0 (-440±770).

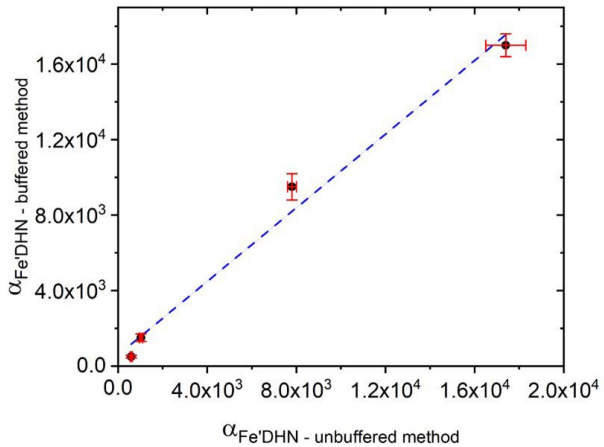

Figure 5.4: Linear trend (R^2=0.9883, p<0.01, n=4) of $\alpha_{Fe'DHN\ buffered}$ vs. $\alpha_{Fe'DHN\ unbuffered}$ showing a 0.989±0.075 slope and a -440±770 intercept. Data are expressed as medium value ± standard deviation of the $\alpha_{Fe'DHN\ buffered}$ (y-axis error bars) and of the $\alpha_{Fe'DHN\ unbuffered}$ (x-axis error bars).

Furthermore, the conditional stability constant for the FeDHN complex, calculated, as before, as the slope of the linear trend obtained by plotting the side reaction coefficient $\alpha_{Fe'DHN}$ vs. the DHN concentration, was identical (9.25 on the log scale) to the one obtained with the buffered method. The latter evidence indicates that the simultaneous equilibria between iron, DHN and EDTA were

not altered by the absence of the pH buffer, at least regarding the around 50 seconds timescale of the analysis, accordingly to the slow kinetics of exchange reactions involving iron and EDTA at trace levels previously demonstrated (see Figure 4.3 of section 4.2 of chapter 4).

5.3 Validation of the unbuffered method

The new experimental conditions, i.e. the pH buffer removal, required a new validation step. In this context the unbuffered method was validated using 5 nM diethylenetriaminepentaacetic acid (DTPA) as artificial ligand, and 3 nM deferoxamine mesylate (DFO), as natural ligand, because a comparison with the validation of the buffered method is required. In particular, it should be reminded that the K'FeL was calculated with the Visual MINTEQ v. 3.1 software in the case of DTPA (see section 4.3.2 of the previous chapter) and was available from literature[57,118] in the case of DFO. The results of the validation experiments, that are listed in Table 5.2, showed the absence of bias in the unbuffered method.

	EXPECTED		FOUND	
	$\log(K'_{FeL})$	C_L	$\log(K'_{FeL})$	C_L
DTPA	12.09	5	11.91±0.04	4.9±0.4
DFO	11.54[115] 11.60-12.10[57,118]	3	11.90±0.07	3.1±0.1

Table 5.2: Results of the speciation validation procedure in unbuffered UVSW. Three replicates titrations were performed for each ligand. Uncertainties are reported as ± sone standard deviation of the three replicates (see Table A.8 and A.9 for the detailed results of each titration).

A comparison between the expected and found values is here required: no statistical difference was found between the expected and found concentrations for both the ligands at the 95% confidence level (n=3, tcal=1.35 and 2.33 for DFO and DTPA, respectively). Regarding the values of the conditional stability constant, a slight discrepancy was, instead, evident. The two ligands require, in this context, two separate comments. Firstly, regarding the DTPA, the 0.18 on log scale difference between the experimental and calculated values may be

ascribed, as in the case of the buffered method, to errors in the tabulated values for the EDTA and DTPA species and in the side reaction coefficient of the FeDHN complex. However, it should be highlighted that the results obtained with the buffered and unbuffered methods were not statistically different at the 95% confidence level. On the other hand, the conditional stability constant for the FeDFO complex log($K'_{Fe'DFO}$) fell in the range of values reported in literature[57,118], even if only values of 11.60 were found with CLE-CSV technique[57,118] and the higher values were obtained applying the so-called kinetic method[57]. As in the case of DTPA, this discrepancy may be due to uncertainties in the tabulated stability constants for the EDTA species and in the calibration of $\alpha_{Fe'DHN}$.

As the final step of the validation procedure, the method was assessed for the detection of humic acid in UV-digested seawater. The absence of any interference was firstly checked: preliminary experiments confirmed the absence of peaks when the DHN is not added to the samples, analogous to what was observed in the presence of the HEPPS pH buffer (section 4.3.3). Subsequently, the same procedure as used with the pH buffer was employed: 0.20 mg·L^{-1} of the Suwannee River Humic Acid (SRHA) was titrated with increasing iron concentration in the presence of 1µM DHN. The resulted HA complexing capacity was 5.5±0.3 nM, or 28±1.5 nmol per milligram of HA; regarding the calculated log$K'_{Fe'SRHA}$, a value of 11.72±0.12 was found (see Table A.10 of the Appendix for the results of the three replicate titrations). No difference was found between the results obtained in the presence or in the absence of the buffer, whereas the same discrepancies were found between the literature data[63,167] and the calculated values of the complexing capacity and the conditional stability constant. This is the reason why the same explanation can be ascribed to justify this difference: only Laglera and van den Berg[63,167] reported data about humic substances, but in the cited papers the complexing capacity and the conditional stability constant were determined by direct detection of the FeSRHA complex and competition against EDTA, respectively, whereas here the CLE-CSV method was applied. However, despite these considerations, the unbuffered method was demonstrated to detect the complexing capacity of humic substances with regard to iron in seawater.

5.4 Comparison between buffered and unbuffered titrations of Antarctic seawater samples

The same six seawater samples from the Ross Sea water column analyzed to test the buffered method were then used to apply the procedure in the absence of the pH buffer. Table 5.3 list the iron speciation data obtained during this step.

Sample depth (m)	Fe (nM)	C_L (nM)	$logK'_{Fe'L}$
1	1.5 ± 0.1	2.8±0.3	12.03±0.13
20	2.0 ± 0.1	5.4±0.05	12.47±0.06
50	1.51 ± 0.05	5.47±0.3	11.91±0.12
100	2.4 ± 0.3	3.3±0.4	12.60±0.4
400	1.8 ± 0.1	5.6±0.6	11.90±0.06
736	2.5 ± 0.5	5.91±0.08	12.10±0.02

Table 5.3: Organic iron binding ligand concentration and its stability constant for iron found in six Antarctic seawater samples from the Ross Sea obtained applying the unbuffered method. Data are reported as ± one standard deviation (see Table A.11 of the Appendix for the detailed results of each sample). Experimental: 1 µM DHN; refrigerated overnight equilibration time; square wave voltammetry: 30 s deposition time; 0.4 V deposition potential; 0.005 V Voltage step; 10 Hz frequency; 0.05 $V \cdot s^{-1}$ scan rate.

In general terms, the differences found between the data reported in Table 5.3 and the ones obtained applying the buffered method (Table 4.6) are relatively small and within the expected random errors typical of the speciation procedures. In fact, the differences measured in this context, that were lower than 15% and 0.23 log scale for C_L and $logK'_{Fe'L}$, respectively, were in good agreement with the uncertainty reported in a recent compilation[27] for speciation data (average RSD% 11% and standard deviation 0.6 log unit from ≈1200 and 900 data for CL and $logK'_{Fe'L}$, respectively). Moreover, the paired t-tests confirmed the absence of bias among the two procedures as no systematic differences were found, showing p values of 0.91 and 0.61 for CL and $logK'_{Fe'L}$, respectively (n=12). Accordingly, as already observed during the calibration of the side reaction coefficients and the validation with both artificial and natural ligands, no systematic differences in the speciation data were introduced by the pH buffer removal. Upon an initial analysis, these data, as well as the speciation data found for iron complexes with

EDTA (section 5.2) and discrete ligands (section 5.3), seemed in contrast with the alteration of the pH in the diffusion layer[164,166]. Nevertheless, it should be considered that the ligand exchange reactions are usually characterized by a slow kinetics. In this context, the approximately 50 seconds spent by the FeL and FeDHN complexes in the diffusion layer at an higher pH value were not enough to affect the equilibrium concentrations[168].

5.5 Effect of the pH buffer removal on the performances and detection capabilities

The titrations of the six Antarctic seawater samples were also useful to evaluate the performances of the unbuffered method and its detection capabilities. A first comment regards the analytical sensitivity. In fact, even if an increase in the analytical sensitivity due to the pH buffer removal was firstly observed and justified (see section 5.1), the sensitivity gain observed in the seawater sample titrations using 1 µM DHN was almost negligible, as it increased from 10.3 $nA \cdot nM^{-1} \cdot min^{-1}$ in unbuffered samples to only 12.6 $nA \cdot nM^{-1} \cdot min^{-1}$ in buffered samples. The lowest detectable ligand concentration was, subsequently, estimated in accordance with the IUPAC recommendation[169]. Thus, a 1.05 nM LOD was calculated as three times the pooled standard deviation of the ligand concentration data from the twelve titrations of the seawater samples (two replicates for each sample). The latter LOD value resulted around twice the 0.51 nM value determined in the presence of the HEPPS pH buffer. Accordingly, the unbuffered method seemed to be characterized by a lower reproducibility, although it should be highlighted that only two titrations per sample were used to estimate the standard deviation in the case of the unbuffered method, opposite to the three used for the buffered one. A lower precision of the unbuffered method is also supported by a F-test conducted on the pooled standard deviations of ligand concentration data for the two groups (buffered vs. unbuffered) at the 0.05 significance level ($F=4.63$, $df_1=6$, $df_2=12$; $F_{crit,\alpha=0.05}=3.00$). Nevertheless, if the highest standard deviation of 0.6, relative to the 400 m depth sample, found with the unbuffered

method, is removed from the calculation, the difference results not significant ($F=2.28$, $df_1=5$, $df_2=12$; $F_{crit,\alpha=0.05}=3.10$). The latter evidence, which showed the high leverage of this datum on the pooled standard deviation, highlighted that a larger sample size would be needed to corroborate or dismiss the difference among the precisions of the buffered and unbuffered methods.

5.6 Equilibration phase kinetics

As the final step in the development of the new method, the increase of the sample throughput by reducing the equilibration time required before the analysis of the titration aliquots was tested. The possibility to reduce the equilibration time is directly connected to the kinetics of the involved chemical equilibria and of the ligand exchange reactions involving natural ligands, as iron rapidly reacts with the artificial one[168]. In this context, the titration of the 20 m depth sample was repeated after 3, 6, 12, 17, and 24 hours equilibration time and the apparent organic iron binding ligand concentration and conditional stability constant for iron were determine as a function of the equilibration time. Figure 5.5 reports the trend of the apparent ligand concentration vs. equilibration time. Figure 5.5 shows that the 6 hours equilibration time was not enough to reach the equilibrium, as well as after twelve hours. Therefore, the equilibration time reduction seemed not to be a good strategy to increase the sample throughput as it would lead to an around 20% bias in the estimated ligand concentration. Instead, experimental data suggested that the equilibrium was achieved after the overnight 17 hours equilibration time and that the results were stable for at least 24 hours. This evidence suggested that up to eight titration per day may be analyzed, making the method exploitable for a large number of samples, typical of the oceanographic studies. On the other hand, regarding the conditional stability constant of the FeL complex, only the titration measured after the three hours equilibration time resulted in a lower estimation of $\log(K'_{Fe'L})$, as a value of 11.93 was calculated, whereas for all the other experiments, $\log(K'_{Fe'L})$ fell in the 12.28-12.46 range, without showing any trend.

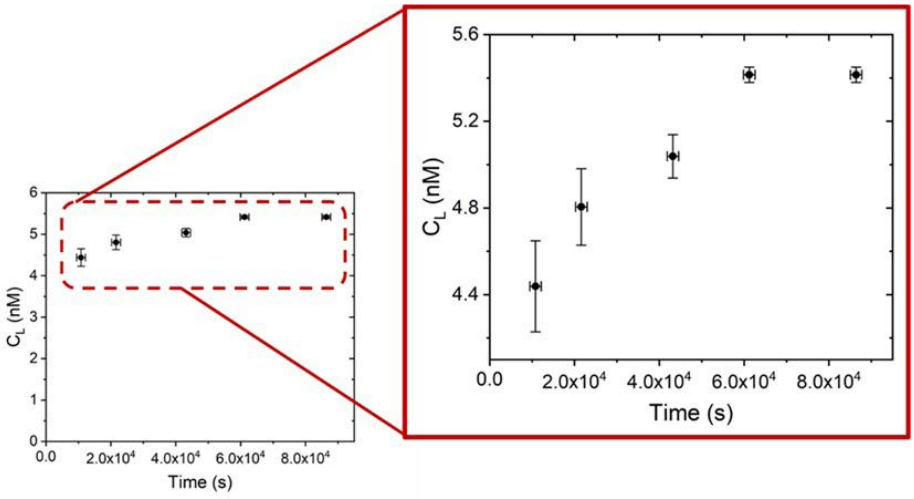

Figure 5.5: Trend of the organic iron binding ligand concentration vs. equilibration time determined by the unbuffered CLE-CSV technique. The equilibration time was assumed as the time interval between the preparation of the titration and the middle of the titration measurements; its error was estimated as ±22.5 minutes, i.e. half of the analysis time. Y-axis errors are reported as one standard deviation calculated from the two replicates. Experimental: 20 m depth Antarctic seawater sample; 2.05 nM initial iron concentration; 1 µM DHN; refrigerated equilibration time (3, 6, 12, 17, and 24 hours); square wave voltammetry: 30 s deposition time; 0.4 V deposition potential; 0.005 V Voltage step; 10 Hz frequency; 0.05 $V \cdot s^{-1}$ scan rate.

6 MATERIALS & METHODS

6.1 Equipment

Voltammetric measurements were mostly performed by a Metrohm VA 757 Computrace voltammetric stand; the latter was equipped with a three electrodes configuration, employing a Hanging Mercury Drop (HMDE) electrode as the working electrode, a silver wire (Sigma-Aldrich, 1 mm diameter, 99.9% purity) as pseudoreference and a graphite counter electrode. A 663 VA Stand voltammeter by Metrohm controlled by a μAUTOLAB III potentiostat and equipped with the same electrodes configuration was employed for measurements that required the split of the forward and backward components of the square-wave voltammograms and for the validation of the speciation method with deferoxamine (DFO), protoporphyrin IX (PPIX) and humic substances[6]. A 1 mL quartz microcell[170] was installed and used unless otherwise noted, and three replicate measurements were performed for each analysis. Table 6.1 lists all the voltammetric parameters employed to perform the experiments.

[6]The validation step, in fact, was perform in the laboratory of the FI-Trace group in collaboration with professor Luis Laglera at the Universitat de les Illes Balears in Palma de Maiorca

	Cyclic Voltammetry	Square-Wave voltammetry without catalytic enhancement (absence of O_2)	Square-Wave voltammetry with catalytic enhancement (presence of O_2)
Purge time (s)	300	300	0
Deposition potential (V)	-0.1[1]	-0.1	-0.4[1]
Deposition time (s)	30	30	30
Equilibration time (s)	10	10	10
Start potential (V)	-0.1	-0.1	-0.4
End Potential (V)	-0.9	-0.9	-0.9
Voltage step (V)	0.005	0.005	0.005
Amplitude (V)	/	0.05	0.05
Frequency (Hz)	/	10[3]	10
Scan rate (V·s-1)	0.15[2]	0.05[3]	0.05

[1] -0.1 V without catalytic enhancement and for the electrochemical characterization; -0.4 V with the catalytic enhancement.

[2] Varied for the ligand symmetry factory α and standard electrochemical rate constant k0 determination.

[3] Varied for the complex symmetry factory α and standard electrochemical rate constant k0 determination.

Table 6.1: Voltammetric parameters employed during all the experiments.

An aquarium air pump was used to introduce atmospheric oxygen as catalytic enhancer with a 2.1 $L \cdot min^{-1}$ into the voltammetric cell. All the voltammetric apparatus, together with the pump, was located under an Aura HZ-72T laminar flow hood from Bioair. The ECDSOFT software was used to treat the voltammograms.

Spectrophotometric measurements were performed by a ThermoScientific Evolution 220 UV-Vis spectrophotometer (instrumental parameters are listed in Table 6.2). The latter was equipped with a ThermoScientific Haake S3 thermostat to keep the temperature constant during the kinetic tests.

Band width (nm)	1	**Data range (nm)**	0.5
Integration time (s)	0.2	**Scan rate (nm·min-1)**	150

Table 6.2: Spectrophotometric parameter employed during the kinetic and stoichiometry experiments

A Bruker 400 MHz NMR equipped with a 5 mm PABBO probe was used during the kinetic experiments using the zg acquisition sequence and a delay time of 15 s accumulating 32 sans. The TOPSPIN software was used to integrate the ^{1}H-NMR spectra.

The pH of the solutions used during the experiments was measured by a VWR MU 6100L pH-meter; the same instrument with a pHenomenal® CO11 conductivity cell from VWR was emplyed to measure the salinity of the seawater samples.

Ultrapure water was produced by a Millipore MilliQ A10 system or by a Sartorius Arium Mini ultrapure water lab system.

Organic matter was removed from the seawater samples, if needed, using a home-made UV digestion system[171] (Figure 6.1) with a 400 W mercury bulb lamp.

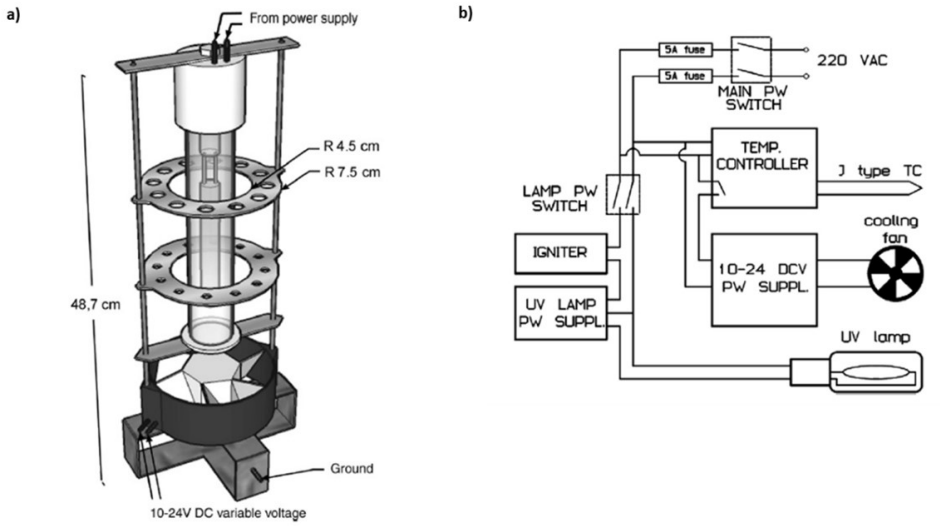

Figure 6.1: Scheme of the UV-digestion system (a) and main components of the control unit and its connections to the UV-digester unit. Pictures from[171]

A Milestone DuoPUR subboiling distillation system was used to produce ultrapure nitric acid[172].

6.2 Materials

All solutions were prepared in LDPE bottles cleaned as suggested for oceanographic studies. They were soaked in three consecutive baths for one week each: firstly 0.8% Nalgene L900 liquid detergent, then 2 M ultrapure HCl (prepared by dilution of the Fluka TraceSELECT reagent, and lastly 2% ultrapure HNO_3 (produced by subboiling distillation from the Sigma-Aldrich reagent).

The 1 M 4-(2-Hydroxyethyl)-1-piperazinepropanesulfonic acid (HEPPS) solution, used as buffer for the voltammetric measurements, was prepared by dissolution of the adequate amount of the solid reagent (Sigma-Aldrich) in ultrapure water. The pH was set to 8.04 (NBS scale) by adding 50% ultrapure NaOH and the so prepared solution was purified by three consecutive overnight equilibrations with the Chelex 100® resin (Sigma-Aldrich), previously cleaned with methanol, ultrapure HCl and ultrapure water.

The 2,3-dihydroxynaphthalene (DHN), which was used as ligand for iron in the voltammetric analyses, was purified by sublimation on a cold finger at a temperature T=100°C (Figure 6.2). This solid was dissolved in ultrapure water up to the final concentration of 10 mM to obtain the stock solution. The latter was prepared every ten days.

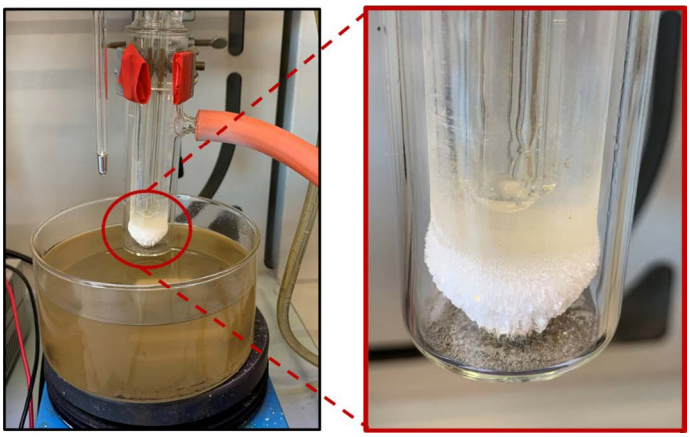

Figure 6.2: System used for the purification of the DHN by sublimation T=100°C with focus on the pure DHN crystals on the cold finger.

The NaOH solution was prepared by dissolving the solid reagent (Sigma-Aldrich, 99.99%, trace metal basis) in ultrapure water and purification by five consecutive overnight equilibrations with MnO_2.
The latter was prepared following the procedure reported in[118] according to the following reaction.

$3\ Mn^{2+} + 2\ MnO_4^- + 4\ OH^- \rightarrow 5\ MnO_2 + 2\ H_2O$

After mixing equal volumes of 0.03 M $MnCl_2$ and 0.02 M $KMnO_4$/0.04 M NaOH, the pH was set to 7.0 (NBS scale) adding more NaOH. The brown MnO_2 obtained was centrifugated three times and taken up in ultrapure water to the final concentration of 0.05 M.
All the iron standards were prepared by dilution from the 1000 $mg \cdot L^{-1}$ ICP iron standard (Fluka, TraceCERT) and subsequent acidification to pH 3 or 3.5 (the latter pH value was used only for voltammetric measurements without the buffer) with 0.1 M ultrapure HCl (prepared from the Fluka, TraceSELECT reagent). For both the pH values, the adequate concentrations of the Fe(III) standards were chosen considering the $k_{sp} = 1.1 \cdot 10^{-36}$ of the $Fe(OH)_3$ species in order to avoid any Fe(III) precipitation.
The adequate amount of solid (Sigma-Aldrich) was dissolved in ultrapure water to obtain the 10 mM stock solution of ethylenediaminetetraacetic (EDTA), diethylenetriaminepentaacetic acid (DTPA) and deferoxamine (DFO).
The Humic Acid (HA) stock solution was prepared by dissolution of the adequate amount of the Suwannee River standard reference in 100 µL of ultrapure NaOH and dilution in ultrapure water.
Protoporphyrin IX (PPIX) stock solution was prepared by dissolving the solid with 0.1 M ultrapure HCl and diluting with ultrapure water to the final stock solution concentration.

6.3 Sampling and methods

6.3.1 Sampling

The seawater sample called SAFe D2 used for the validation of the new instrumental configuration was collected during the SAFe cruise (Sampling and Analysis of Fe[129]. The consensus value for the total iron concentration of this sample was 0.91±0.02 nM.

Otherwise, the seawater samples used to apply the speciation method were collected in the Ross Sea during the 2011/2012 Italian expedition in Antarctica. Six samples from a water column at depths between 1 and 736 m of the E5 site (74°40.04' S – 167°18.76' E) were chosen (Figure 6.3).

Figure 6.3: Antarctica Maps showing the E5 site with the pink star

All samples were filtered by a Teflon apparatus using polycarbonate membranes (diameter 142 mm, porosity 0.42 µm) under a laminar flow hood.

The seawater samples from Antarctica have been granted by the Antarctic Environmental Specimen Bank (BCAA) of the Italian Antarctic Research Program (PNRA) and the University of Genoa.

6.3.2 Set up and validation

6.3.2.1 Sensitivity

The sensitivity was preliminary evaluated in ultrapure water and then in seawater by square-wave voltammetry following the same procedure. 10 mL of water were added with 10 mM pH 8 HEPPS buffer and the adequate amount of DHN. 1 mL of the latter solution was transferred into the voltammetric cell and three replicate measurements acquired. Measurements were then acquired after each of the two consecutive 0.3 nM Fe additions. The sensitivity was calculated as the slope of the calibration line and it was normalized by the deposition time employed during the analysis. This procedure was repeated for different DHN concentration, between 1 and 100 µM, and square-wave frequency, between 5 and 100 Hz. The trend of the sensitivity moving from ultrapure water and seawater was also estimated: seawater was diluted with ultrapure water with growing dilution factor and the sensitivity evaluated for each solution.

6.3.2.2 Limit of detection

The limit of detection (LOD) of the new method was evaluated both in ultrapure water and seawater after a deep cleaning step of the voltammetric cell for different DHN concentration (between 1 and 100 µM). 1 mL of the blank solution, containing water with 10 mM pH 8 HEPPS buffer and the proper amount ligand was transferred into the voltammetric cell and ten replicates measurements acquired. Voltammograms were also acquired after a 0.3 nM iron addition to check the sensitivity as the LOD was calculated according to equation 6.1.

$$LOD=3\sigma_{blank}/solpe_{calibration\ line} \quad (6.1)$$

6.3.2.3 Method validation

The new method was validated by measuring the total iron concentration of a reference sample. 10 mL of the SAFe D2 sample were acidified to pH 1.5 with ultrapure HCl for 12 hours and subsequently neutralized using ultrapure 1 M NaOH. A 10x dilution was applied to test the method for the detection of

ultratrace levels of iron. 10 mM pH 8 HEPPS buffer and 10 µM DHN were then added. 1 mL of the so-prepared sample was transferred into the voltammetric cell and the total iron concentration was quantified after two consecutive 0.3 nM iron additions. A subtraction of the total iron concentration of the blank (HCl, NaOH and HEPPS) from the results was mandatory to obtain the correct value.

6.3.3 Method characterization

6.3.3.1 Kinetic studies

The degradation of the 2,3-dihydroxynaphthalene was followed by both UV-Vis spectroscopy and ^{1}H-NMR spectrometry.

UV-Vis kinetic tests were performed on 0.2 mM DHN solutions prepared form the solid at different pH values, between 6 and 11. The pH was set to the proper value by adding 1M HCl or NaOH. Kinetic tests at pH between 6 and 8 were characterized by the acquisition of one spectrum every 15 minutes, whereas, for higher pH values tests, spectra were acquired every 30 minutes. The instrumental parameters characterizing these experiments are listed in Table 6.2.

^{1}H-NMR spectrometry experiments were conducted on 10 mM DHN solutions at pH 5, which is its natural pH, and at pH 8.0, which is the pH condition used during the voltammetric measurements. Regarding pH 8, two different solutions were prepared and analyzed: the first one was preserved at room temperature during the dead time between the acquisitions, while the second at T=4°C. Dimethyl sulfoxide (DMSO) was used as the internal standard and added to the solutions up to the concentration of 10 mM. The singlet peak at 7.31 ppm, which corresponded to hydrogens 1 and 4 of the naphthalene ring of the DHN was integrated with respect to the singlet peak at 2.30 ppm.

The latter, which was set to 1.000, corresponded the hydrogen of the dimethyl sulfoxide and was constant during the kinetic tests. Preliminary experiments were conducted to set the acquisition rate, which was higher for tests at pH 8 as DHN, at these conditions, was characterized by a higher degradation rate. Total

acquisition time was 312 hours (13 days) for pH 5 experiments, and 402.5 hours (about 17 days) for pH 8 ones.

6.3.3.2 Complex stoichiometry

The classical spectrophotometric methods, the Job's[130,131] and the Mole-Ratio[132] ones, were firstly used to study the stoichiometry of the FeDHN complex. The Job's method, also called method of continuous variations, was based on the acquisition of the UV-Vis spectra of solutions with *[DHN]/[Fe]* ratios between 0.1 and 10 at different pH values (2-10). Otherwise, the Mole-Ratio method was performed varying the *[DHN]/[Fe]* ratios between 0 and 5, maintaining the iron concentration constant. For both methods, the graph of the absorbance vs. the *[DHN]/[Fe]* ratio of each experiment gave a curve with the maximum in correspondence of the stoichiometric ratio between DHN and Fe.

The stoichiometric ratio of the FeDHN complex in the presence of trace concentration of Fe was determined by square-wave voltammetry methods. Two experiments, with and without catalytic enhancement, of the signal were performed. The experiments were characterized by constant iron concentration (100 nM and 0.37 nM without and with the catalytic enhancement, respectively, as the catalyzed method was characterized by a much higher analytical sensitivity) and increasing DHN concentration. The peak current of the FeDHN reduction peak was measured for each DHN addition and data were fitted with equation 3.4, as reported in section 3.1.2 of chapter 3[131–133].

6.3.3.3 Adsorption properties

Cyclic voltammetry without the catalytic enhancement of the signal was used to study the adsorption phenomena of the ligand itself and the FeDHN complex onto the electrode surface. The adsorption of the 2,3-dihydroxynaphthalene in the absence of iron was firstly studied. A pH 8 buffered solution was employed and DHN concentration was varied between 10 and 210 µM. The current of the peak at around -0.2 V, related to the reduction of the DHN, was measured for

each DHN concentration and the surface coverage Γ was calculated according to equation 3.8). Trend of Γ with the DHN concentration was fitted with the Langmuir isotherm model (equation 3.10) to obtain the adsorption parameters of the ligand.

A similar procedure was applied to determine the adsorption parameters of the FeDHN complex. Seven experiments characterized by different DHN concentration, between 5 and 200 µM were set up. For each experiment, the iron concentration was varied between 90 and 1890 nM. The current of the peak of FeDHN complex was measured for each iron addition, the surface coverage of the electrode by the complex calculated following equation 3.8 and data fitted with the multicomponent Langmuir isotherm model (equation 3.11).

6.3.3.4 Standard electrochemical rate constant

As the backward peak in cyclic voltammogram was missing for the FeDHN complex, square-wave voltammetry was used to determine its symmetry factor and standard electrochemical rate constant. A pH 8 buffered solution containing 5 µM DHN and 54 nM iron was analyzed, and the square-wave frequency changed between 10 and 150 Hz. The peak current of the FeDHN complex was measured for each frequency (f) and its trend with $\log(f^{-1})$ gave a maximum in the correspondence of the so-called fmax. The latter was used for the calculation of k0FeDHN according to equation 3.16. Regarding the symmetry factor of the FeDHN complex, the same experiments were performed and the backward and forward components of the square-wave voltammograms registered. α^0 was calculated according to the empirical equation 3.17.

6.3.3.5 Catalytic constant

The catalytic constant was calculated following the equation $k'_{cat}/[oxidant]$ (with k'_{cat} apparent catalytic constant) estimating the concentration of the oxidant at the electrode surface. Otherwise, the calculation of the apparent catalytic constant was based on the assumption that $sensitivity=i_p \cdot [Complex]$

using equation 3.19. Experiments were performed on a pH 8 buffered solution containing 0.37 nM Fe using both 1 and 10 cell volumes to compare the results. 2,3-dihydroxynaphthalene was added to the solution with concentrations between 150 µM and 500 µM, condition in which all the iron is complexed by the ligand.

6.3.4 Speciation analyses

6.3.4.1 Determination of the total iron concentration

The application of the competitive ligand equilibration-cathodic stripping voltammetry as method for iron speciation in seawater required the preliminary determination of the total iron concentration of each seawater sample.

Firstly, each seawater sample was acidified to pH 1.5 by adding 12 M ultrapure HCl (Fluka, TraceSELECT) for at least 12 hours to make all the iron available for the analyses. The proper amount of pH 8 HEPPS buffer and DHN added to the final concentration of 10 mM and 10 µM, respectively were added. Samples were then neutralized using 1M ultrapure NaOH (prepared as described in the previous paragraph). The former procedure was used following the method validated by Laglera et al in [113]. 1 mL of the so prepared solution was transferred into the voltammetric cell and three replicates measurements were acquired using the instrumental parameters reported in Table 6.1. The sensitivity was calibrated by repeating the same measurements after two consecutive additions of 0.3 nM Fe and the total iron concentration was consequentially calculated. The value of the total iron concentration for each sample was obtained after the subtraction of the 0.31 nM blank iron concentration (HCl, NaOH and HEPPS).

Figure 6.4 shows a calibration line used for the determination of the total iron concentration as an example: data are expressed as medium value of five replicate measurements ± standard deviation.

It should be also reminded that the same procedure was repeated to determine the total iron concentration of the blank, also for the ligands used for the validation of the speciation method.

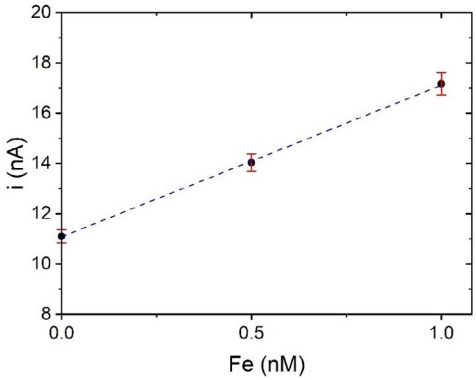

Figure 6.4: Determination of the total iron concentration of the 50 m depth sample from the Ross Sea water column (E5 site, 74°40.04' S – 167°18.76' E). The sensitivity was calibrated by two consecutive 0.5 nM Fe addition. Data are expressed as medium value of five replicate measurements ± standard deviation. Experimental: seawater; 10 mM HEPPS buffer pH 8.0; 1 µM DHN; two 0.5 nM Fe addition to calibrate the sensitivity. Square-wave voltammetry: -0.4 V deposition potential; 10 Hz square-wave frequency; 0.05 V·s^{-1} scan rate.

6.3.4.2 Calibration of the side reaction coefficient $\alpha_{Fe'DHN}$

The calibration of the side reaction coefficient $\alpha_{Fe'DHN}$ for the FeDHN species, needed to calculate the stability constant $K'_{Fe'DHN}$ of the complex required titrations of pretreated seawater samples with a competitive ligand. Ethylenediaminetetraacetic acid (EDTA) was accordingly chosen, as its stability constant for most metal ions are well-known. Seawater was previously UV-digested for 4 hours to remove the organic matter. Subsequentially, 10 mL of the UV-digested samples were added with 10 mM pH 8 HEPPS buffer and the adequate amount of DHN and iron. Experiments at four different DHN concentrations were set up: 0.5, 1, 5 and 10 µM. Iron concentration was 10 nM for the lower DHN concentration and 5 for the others. The so prepared solutions were divided in 10 aliquots, 1 mL each, using preequilibrated vials, and the latter were titrated with increasing EDTA concentrations, between 5 and 100 µM for 0.5 and 1 µM DHN and between 50 and 800 µM for 5 and 10 µM DHN. After the

overnight equilibration time (around 17 hours) at T=4°C to avoid the degradation of the DHN, measurements were acquired following the ascending order with respect to the EDTA concentration. Figure 6.5 reports the scheme of the titration employed for the calibration of the side reaction coefficient.

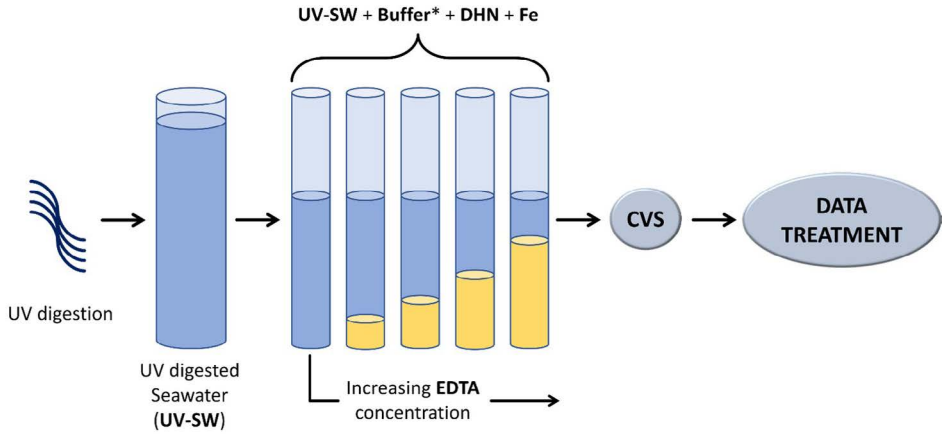

Figure 6.5: scheme of the titration of the CLE-CSV procedure.

The side reaction coefficient of the FeDHN complex for the four ligand concentrations was calculated by fitting the i_p/i_{p0} vs. $\alpha_{Fe'EDTA}$ graph with equation (4.16). In particular, the $\alpha_{Fe'EDTA}$ values for the different EDTA concentrations used during the experiments were calculated employing the Visual MINTEQ software (3.1 version).

6.3.4.3 Validation and application to real samples

The validation of the new method for iron speciation based on the CLE-CSV procedure required the titration of previously pretreated seawater samples containing a known amount of an organic Fe-binding ligand with known or calculable conditional stability constants for iron. In this context, diethylenetriaminepentaacetic acid was used as artificial ligand as its stability

constant for iron could be calculated using the Visual MINTEQ software, and deferoxamine and protoporphyrin IX were employed as natural ligand, present in seawater, as their constants for iron were well-known from the literature.
After the 4 hours UV-digestion, 15 mL of UVSW were added with 10 mM pH 8 HEPPS, 1 µM DHN and the adequate amount of the proper organic Fe-binding ligand as follow: 5 nM DTPA, 3 nM DFO, and 3 and 6 nM PPIX. The so-prepared solutions were divided in 15 aliquots, 1 mL each, in 15 preequilibrated vials, and titrated with increasing iron concentration, up to 15 nM. Measurements were acquired after the refrigerated overnight equilibration time by transferring the aliquots into the voltammetric cell following the increasing order with respect to the iron concentration. Data were treated as reported in the 4.1.3 section of chapter 4. Three replicates analysis were done for each ligand. The same procedure was applied to test the method for humic substances detection, introducing into the solutions 0.2 $mg \cdot L^{-1}$ of SRHA.
Real samples were analyzed following the validated procedure. Figure 6.6 reports the titration scheme.

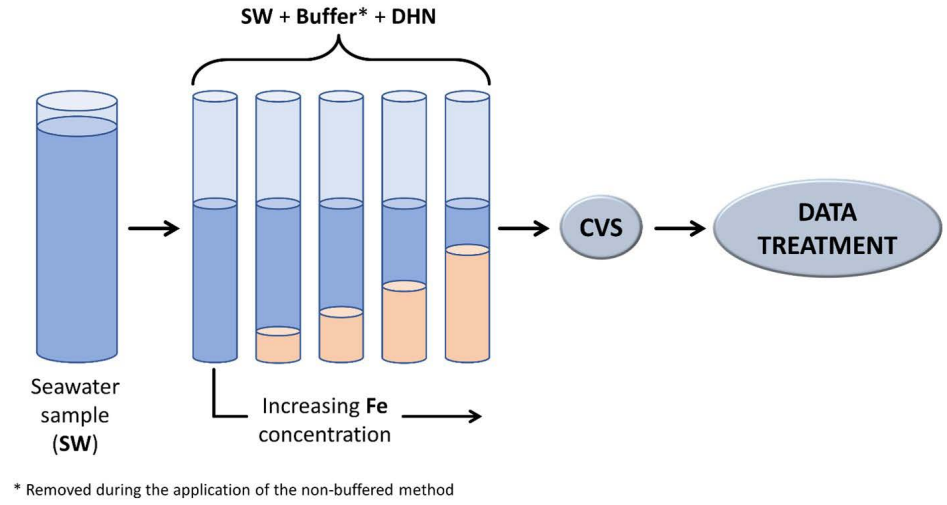

Figure 6.6: scheme of the titration procedure used for the determination of the side reaction coefficient.

15 mL of each seawater sample was added with 10 mM pH 8 HEPPS and 1 µM DHN. The solution was divided into 15 aliquots in 15 preequilibrated vials and the latter titrated with increasing iron concentrations. After the overnight refrigerated equilibration time, aliquots were transferred into the voltammetric cell and the analysis was performed following the increasing order with respect of iron concentration. Before starting each titration measurement, three blank measurements were performed for the microcell conditioning. Each sample was analyzed three times and data treated as reported in the 4.1.3 paragraph of chapter 4.

All the procedures reported in the present section were repeated in the total absence of the HEPPS buffer to assess the unbuffered method.

7 CONCLUSION

7.1 Major outcomes

The aim of this project was the development, optimization and characterization of a new method based on the competitive ligand equilibration-cathodic stripping voltammetry procedure for iron speciation in seawater able to overcome the drawbacks of the already existing methods. A completely new hardware configuration was at first developed: a silver wire pseudoreference was for the first time introduced replacing the traditional Ag/AgCl 3M KCl reference electrode, and atmospheric oxygen, which was used as the catalytic enhancer was directly introduced into the "closed" cell by an air pump. All the here summarized modifications led to a great simplification of the instrumental configuration, ensuring on the other hand analytical performances fully satisfactory for trace and ultratrace levels both in terms of detection capabilities and signal stability.

Before applying the new instrumental configuration to the development of the new method for iron speciation in seawater, a complete characterization of the chemical and electrochemical features of the method was performed. This step was basically dictated by the lack of information on the chemical and electrochemical features of the system: generally, a protocol for the characterization of a voltammetric method seemed to be missing in the literature. A systematic approach for the characterization of adsorptive stripping

voltammetry methods with catalytic enhancement of the signal was accordingly proposed for the first time, involving both the characterization of the chemical and the electrochemical features. Firstly, the quantitative study of the degradation of the ligand used as iron chelator, in our case the 2,3-dihydroxynaphthalene, was fundamental to set the proper experimental conditions in terms of analysis time and storage temperature of stock solutions. The study of DHN degradation proved a challenging task and required the use of proton Nuclear Magnetic Resonance (^{1}H-NMR). A significant loss in the ligand concentration was evidenced at pH 8 when the sample was preserved at room temperature and a significant deterioration of the speciation analysis results was observed under these conditions (i.e. equilibration time at room temperature). DHN degradation was prevented when the same solution was preserved at T=4°C and in the dark. The latter evidence demonstrated the need to perform the equilibration period at 4°C in the dark.

Secondly, the stoichiometry of the complex adsorbed onto the electrode surface was determined under the conditions relevant for the AdCSV method which involves trace and ultratrace concentrations of the metal, in the range of nM-pM, in the presence of a 1000-fold ligand excess. The latter condition usually favors the formation of complexes characterized by the lowest metal-ligand ratio: a 1:1 stoichiometry ratio between iron and DHN was, in fact, found by studying electrochemical measurements. Otherwise, the use of traditional spectrophotometric methods, i.e. the Job's and the mole-ratio methods, led to misleading results, suggesting the presence of 1:3 complexes when metal to ligand ratio in the range 1:10-10:1 are used.

The simultaneous adsorption of the complex and of the ligand on the electrode surface was subsequently investigated. The multicomponent Langmuir isotherm was used as a simpler, monocomponent modelling approach may be employed only if the ligand does not adsorb onto the electrode surface. As a result, this approach suggested that the competition between the ligand and the complex for the electrode surface did not occur even under the highest employed ligand concentrations, showing that also high concentration of the ligand may be

employed to ensure high sensitivity values.

As the final step of this part of the work, the electron transfer kinetics (k^0) and catalytic enhancement (k'_{cat}) were simultaneously studied to completely characterize the electrode reaction and gave full insight into the intimate mechanism responsible for the high sensitivity. In particular, the ratio between the catalytic and the standard electrochemical rate constant was lower than 2, meaning that the signal was mostly controlled by the catalytic effect.

The CLE-CSV method for iron speciation in seawater was subsequently developed. Firstly, as a completely new instrumental configuration was applied to develop a CLE-CSV method, the side reaction coefficients for the FeDHN complex was calibrated for four DHN concentration by competition with EDTA. In particular, the resulted values for the side reaction coefficients were calculated showing a higher precision with respect with literature data, as the relative standard deviation RSD% was in the 3%-15% range.

The method was then successfully validated using an artificial and two natural ligands, namely DTPA, DFO and PPIX respectively, and tested for the detection of humic substances. In particular, the results of the validation step demonstrated the capability of the method to correctly determine the complexing capacity and stability constant of both discrete and more complex organic iron binding ligands.

The subsequent application to six Antarctic seawater samples from a Ross Sea water column suggested the possibility to apply the method to organic iron speciation in seawater samples.

The possibility to perform the iron speciation in seawater analysis by the CLE-CSV procedure developed in the total absence of the pH buffer was finally investigated, requiring the calibration and validation steps to be performed again. The side reaction coefficient of the FeDHN complex was calibrated for the four DHN concentration previously used, obtaining values not distinguishable from the side reaction coefficients obtained in the presence of the pH buffer. The method was then validated using known ligands (DTPA and DFO) and tested for the detection of humic substances obtaining results not different from the

expected values and from the results obtained in the presence of the pH buffer. Accordingly, the unbuffered method was demonstrated to be able to determine the concentration and the conditional stability constant for both artificial and natural iron ligands, including humic substances. Moreover, the unbuffered method was tested for the analysis of the same Antarctic seawater samples and the results were comparable to the ones obtained when the pH buffer was used. The major advantage of the proposed unbuffered method was the in situ disentanglement of the equilibration and analysis environment. The iron fraction bounded to the added ligand and adsorbed onto the electrode surface, in fact, was detected at pH values around 8.5, where the sensitivity is optimal, whereas the equilibration was performed at the natural pH value of the sample. The present protocol is expected to greatly benefit the speciation analysis of samples with circumneutral to slightly acidic pH, as the voltammetric measurements are performed with the optimal sensitivity, while at the same time, the samples are preserved at the natural pH during the equilibration time.

7.2 Comparison with existing methods

Table 7.1 lists all the CLE-CSV methods for iron speciation in seawater introduced since 1994, together with their main features (analysis time and required sample size) and performances (detection capabilities and sensitivity).

An analytical sensitivity of around 13 $nA \cdot nM^{-1} \cdot min^{-1}$ for 1 µM DHN was obtained applying the unbuffered DHN/O_2 method. The latter result is sevenfold higher than the sensitivity obtained with the same ligand concentration (1 µM DHN) using bromate instead of atmospheric oxygen. In fact, the bromate method resulted in a 1.9 $nA \cdot nM^{-1} \cdot min^{-1}$ sensitivity[118]. Moreover, the around 13 $nA \cdot nM^{-1} \cdot min^{-1}$ sensitivity value resulted 25% lower than the 17 $nA \cdot nM^{-1} \cdot min^{-1}$ one obtained with 10 µM TAC[110] and comparable to the 15 $nA \cdot nM^{-1} \cdot min^{-1}$ one obtained with 1-5 µM NN[105]. On the other hand, the use of SA as ligand and bromate as catalytic enhancer led to an extreme sensitivity, in the 40-180 $nA \cdot nM^{-1} \cdot min^{-1}$ range for a 25 µM SA[121]. Nevertheless, it should be highlighted that these great values

Ligand	Purge (s)	Deposition time (s)	Total analysis time (min)	Sensitivity (nA· nM^{-1}·min^{-1})	LOD (pM)	Catalytic enhancer	Ligand (µM)	$log\alpha_{Fe'L}$	Equilibration time	Sample volume (mL)	Other	Ref.
NN	n.a.	a	a	a		Hydrogen peroxide	1-5	00.5-2.5	Overnight		Addition of SDS to the samples	105
	200	300-500	305-425	0.64-1.1		None	5	2.5			Drop surface 0.52 mm^2	115
	240	240	290	1.0		None	20				Large Hg drop	116
	n.a.	30	48	1.5[b]		Bromate	5	2.5			Drop surface 0.5 mm^2	117
SA	0	120	86	2.6-4.4	24-30 (300s, 5 µM SA)	Atmospheric oxygen	1-40	0.83-2.9 (2-100 µM SA)			Drop surface 0.5 mm^2	120
	0	120-300	98-206	40-180	10 (600 s, 27.5 µM SA	Probably armospheric oxygen	25	1.78	2 h	100	Drop surface 3.34 mm^2	121
TAC	240	120-600	216-504	17	100 (300 s, 10 µM TAC)	None	10	2.40	5 h - overnight	240	Scan speed 10 V/s	110
DHN	300	90	249	1.9 (0.5 µM DHN)	n.a.	Bromate	0.25,1	1.84-2.56	Overnight	125		118
	300	120	267	n.a.	n.a.	None	0.5		Overnight	120		124
	0	30	29	10.3 (1 µM DHN)	10 (1-10 µM DHN)	Atmospheric oxygen	0.5-10	2.7-4.2	Overnight	12	Drop surface 0.56 mm^2	c
	0	30	29	12.6 (1 µM DHN)	/	Atmospheric oxygen	0.5-10	2.7-4.2	Overnight	12	Drop surface 0.56 mm^2	d

a. the deposition time for speciation analysis is not reported and sensitivity cannot be calculated: presumably, dep. time is 60 s, total analysis time ≈ 48 min and sensitivity ≈2.5 nA· nM^{-1}·min^{-1} (see also[107]); b. estimated from[108]; c. buffered method developed in the present thesis; d. Unbuffered method developed in the present thesis

Table 7.1 CLE-CSV methods for iron speciation in seawater introduced since 1994 and their analytical performances.

were obtained using a huge mercury drop as electrode (3.34 mm^2). Beside sensitivity, the limit of detection of the technique is a fundamental parameter to consider when iron speciation in seawater is involved. The limit of detection calculated as *3xblank standard deviation/slope of the calibration line* was used during the comparison as the minimum detectable ligand concentration was estimated only in the present work. As a result, the new method featured the best LOD value independently of the ligand concentration, 10 pM for both 1 and 10 µM DHN for a 30 seconds deposition time. This could be related to an extreme stability of the signal, thanks to the new instrumental configuration (close analysis cell and pseudoreference replacing the traditional Ag/AgCl electrode) opposite to methods characterized by higher sensitivities but affected by lower signal reproducibility. A similar LOD value was only achieved with 25 µM SA and a 600 seconds deposition time[121]. Another relevant benefit introduced by the novel method was the extreme reduction of the analysis time. The use of atmospheric oxygen as the catalytic enhancer avoided the need of nitrogen purging of the sample aliquots, reducing the analysis time by 300 seconds per aliquots, as common to the later evolution of the SA method[120,121]. Moreover, the deposition time was three or four times lower than the ones previously used with DHN (90 and 120 seconds in[118] and[119], respectively), and four-twenty times lower with respect to the SA (120-300 seconds[120,121]) and TAC (120-600 seconds[110]) methods. All of these improvements resulted in an analysis time of only 30 minutes for the measurements of a twelve aliquots titration. Furthermo-

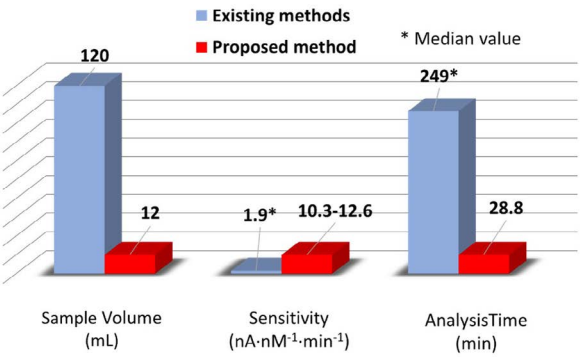

Figure 7.1: general comparison between the present method and all the other existing methods.

re, the new method avoided the addition of several chemicals, as no hydrogen peroxide or bromate were added to the samples, and the pH buffer was totally removed in the unbuffered version of the method. As a final remark, Figure 7.1 summarizes all the benefits introduced by the new method.

7.3 Relevance to existing speciation analysis procedures

The here described approach may be extended to already existing and used procedures for both the speciation of iron and other metals in seawater. The modifications introduced to the hardware configuration, in fact, may also be used when SA, TAC or NN are used as iron chelators. In particular, the use of the microcell would lead from one side to a tenfold sample size reduction and, from the other, could improve the detection capabilities, as explained in chapter 3. The use of a pseudoreference electrode would also simplify the overall hardware setting.

On the other hand, the possibility to remove the pH buffer in the existing procedures requires a more careful discussion. Starting from the speciation method employing SA[120,121], the unbuffered procedure could be easily adopted because this method also avoids the nitrogen purging step before the analysis as the here presented one. The same cannot be said regarding the use of NN[105,106,115,116] and TAC[110] as the pH buffer removal would cause a raise in the pH value, up to 9.1, due to the CO_2 removal. Nevertheless, as proved in chapter 5, only a limited rearrangement of the species distribution is expected following the raise in the pH value, as the kinetics of ligand exchange is typically slow. It should be highlighted that the sensitivity is expected to increase with the pH, when TAC is employed, whereas it decreases above pH 8.5, when NN is involved. Contrarily, the unpurged procedure would avoid the raise in the pH value, but oxygen reduction signals would raise the baseline current. Nevertheless, the peak potential of both $FeTAC_2$ (-0.53V,[110]) and $FeNN_3$ (-0.58V,[115]) complexes in seawater falls in a potential range were the baseline current due to the reduction of oxygen is stable and limited (around 30 nA in the –0.55V / –0.65V range in our

experimental conditions).
Accordingly, the unbuffered method proposed in the present thesis could be generally employed in iron speciation analysis by CLE-CSV, avoiding the purging step also when other iron chelators are employed, although thorough testing is required to confirm such hypothesis.

7.4 Future perspectives

Regarding the future perspectives and developments of this project, the proposed method should be thoroughly tested to detect the complexing properties of other natural ligands (e.g. exopolysaccharides EPS, porphyrins, domoic and phytic acids, and transferrin), and the results obtained from the speciation analysis of different natural ligand pools (e.g. as found in coastal and open oceanic waters) compared with existing data. Furthermore, the analysis of a large number of samples is required to fully assess the fit for purpose of the developed CLE-CSV method, as only six seawater samples were analyzed in the present work.
Furthermore, a thorough comparison between all the existing methods could provide a full picture of all the pros and cons of this method. In this context an intercomparison exercise, i.e. the application of all the existing methods using all the four iron chelators (NN, TAC, SA, DHN) on the same samples set, which could be a water column or a transect, could be useful to assess the merits of these procedures.
Further developments regarding the here presented method may be focused on the development of an unbuffered reverse titration (RT) procedure, which allows the speciation analysis for samples with high and similar iron and organic iron-binding ligands concentrations. In particular, the possibility to develop an RT unbuffered procedure seems feasible, even if it should be firstly set-up and then tested and validated.
Regarding the analytical aspects of the technique, the slow degradation kinetics of the 2,3-dihydroxynaphthalene represents the most relevant complication of

the procedure. Despite it is easily dealt with by preserving the samples in the fridge at 4°C during the equilibration time, this drawbacks may be solved by introducing one or more electron withdrawing substituent(s) on the naphthalene ring, as they could lead to a less easily oxidizable species. The complexing properties of this species and the ensuing performances should be carefully evaluated as performances similar to the ones afforded by unsubstituted DHN cannot be a priori assumed.

Further hardware development may be also foreseen. In particular, the procedure automatization would represent a great step forward in the throughput of speciation analysis, which are labor and time consuming, especially when a large number of samples are analyzed. In this context, the whole system should be carefully studied as the use of the microcell would require a dedicated system for the transfer of the sample aliquots. Moreover, the use of substituted, less easily oxidizable DHN species could be helpful to avoid the refrigerated equilibration time, which could result difficult to implement in an automated system.

APPENDIX

	Temperature (K)		pH	
	Beginning	End	Beginning	End
pH 6	297.85	298.25	6.15	6.18
pH 7	298.25	298.35	7.02	7.11
pH 8	298.25	298.25	8.14	8.16
pH 9	298.15	298.75	9.12	9.08
pH 10	298.75	298.45	10.05	10.05
pH 11	297.75	298.15	11.04	11.02

Table A.1: temperature and pH values at the beginning and at the end of the UV-Visible kinetic tests for pH values between 6 and 11

Equations used to determine the stoichiometry

$i=i_{max}\cdot(K[L]/(K[L]+1))$ (A.1) only the 1:1 complex forms and is electroactive;

$i=i_{max}\cdot(K[L]/(K[L]+\beta_1[L]^2+1))$ (A.2) the 1:1 and 1:2 species form but only the 1:1 one is electroactive;

$i=i_{max}\cdot((K[L]+\beta_1[L]^2)/(K[L]+\beta_1[L]^2+1))$ (A.3) the 1:1 and 1:2 species form and are electroactive;

$i=i_{max}\cdot(K[L]/(K[L]+\beta_1[L]^2+\beta_3[L]^3+1))$ (A.4) the 1:1, 1:2 and 1:3 species form and the 1:1 is the only electroactive;

$i=i_{max}\cdot((K[L]+\beta_1[L]^2)/(K[L]+\beta_1[L]^2+\beta_3[L]^3+1))$ (A.5) the 1:1, 1:2 and 1:3 species form and 1:1 and 1:2 are electroactive.

$i=i_{max}\cdot((K[L]+\beta_1[L]^2+\beta_3[L]^3)/(K[L]+\beta_1[L]^2+\beta_3[L]^3+1))$ (A.6) the 1:1, 1:2 and 1:3 species form and are electroactive.

Table A.2-A7 report the detailed result for each titration acquired using the buffered method.

Replicate	C_L	$logK'_{Fe'L}$
1	4.64±0.30	11.79±0.05
2	4.39±0.37	11.78±0.07
3	5.39±0.45	11.87±0.09
4	4.89±0.33	11.85±0.06
5	5.47±0.437	11.83±0.07

Table A.2: Results of the titrations performed during the validation step using 5 nM diethylenetriaminepentaacetic acid.

Replicate	C_L	$logK'_{Fe'L}$
1	2.82±0.06	12.62±0.13
2	3.15±0.07	12.52±0.13
3	3.31±0.07	12.48±0.11

Table A.3: Results of the titrations performed during the validation step using 3 nM deferoxamine.

Replicate	C_L	$logK'_{Fe'L}$
1	2.58±0.1	12.22±0.12
2	2.24±0.15	9.98±0.16
3	2.76±0.07	12.36±0.11

Table A.4: Results of the titrations performed during the validation step using 3 nM protoporphyrin IX.

Replicate	C_L	$logK'_{Fe'L}$
1	6.11±0.38	12.08±0.13
2	6.30±0.33	11.81±0.05
3	6.01±0.35	11.86±0.06

Table A.4: Results of the titrations performed during the validation step using 6 nM protoporphyrin IX.

Replicate	C_L	$logK'_{Fe'L}$
1	5.88±0.66	11.66±0.07
2	6.04±0.41	11.68±0.06
3	5.53±0.23	11.82±0.05

Table A.6: Results of the titrations performed during the test of the method for the detection of 0.20 mg·L^{-1} humic acid.

Sample depth (m)	Replicate	C_L	$logK'_{Fe'L}$
1	1	2.70±0.13	12.08±0.12
	2	2.60±0.12	12.24±0.14
	3	2.51±0.08	12.44±0.16
20	1	4.87±0.14	11.91±0.07
	2	5.10±.12	12.06±0.09
	3	4.66±.11	12.31±0.07
50	1	6.54±0.27	11.91±0.07
	2	6.31±0.39	12.06±0.09
	3	6.22±0.19	12.18±0.07
100	1	3.12±0.09	13.05±0.4
	2	2.70±0.06	12.50±0.1
	3	2.94±0.11	12.64±0.3
400	1	5.73±0.49	11.93±0.08
	2	5.94±0.58	11.95±0.09
	3	5.88±0.49	11.83±0.08
736	1	6.59±0.21	12.23±0.1
	2	6.46±0.32	12.10±0.09
	3	6.31±0.21	12.12±0.08

Table A.7: Ross Sea water column seawater samples titrations results.

Table A.8-A.11 list the detailed results obtained during the development of the unbuffered method.

Replicate	C_L	$logK'_{Fe'L}$
1	4.50±0.47	11.82±0.15
2	5.10±0.47	11.98±0.19
3	5.19±0.55	11.95±0.24

Table A.8: Results of the titrations performed during the validation step using 5 nM diethylenetriaminepentaacetic acid.

Replicate	C_L	$logK'_{Fe'L}$
1	2.97±0.01	11.94±0.11
2	3.10±0.13	11.86±0.11
3	3.21±0.13	11.99±0.12

Table A.9: Results of the titrations performed during the validation step using 3 nM deferoxamine.

Replicate	C_L	$logK'_{Fe'L}$
1	5.74±0.50	11.62±0.12
2	5.24±0.22	11.86±0.10
3	5.58±0.33	11.69±0.11

Table A.10: Results of the titrations performed during the test of the method for the detection of 0.20 $mg \cdot L^{-1}$ humic acid.

Sample depth (m)	Replicate	C_L	$logK'_{Fe'L}$
1	1	3.03±0.19	11.93±0.12
	2	2.56±0.20	12.12±0.2
20	1	5.46±0.10	12.42±0.1
	2	5.39±0.14	12.51±0.13
50	1	5.27±0.37	12.00±0.1
	2	5.67±0.17	11.82±0.09
100	1	3.58±0.11	12.86±0.14
	2	2.95±0.07	12.33±0.33
400	1	6.04±0.47	11.85±0.11
	2	5.24±0.29	11.94±0.13
736	1	5.96±0.30	12.11±0.12
	2	5.85±0.25	12.08±0.11

Table A.11: Ross Sea water column seawater samples titrations results.

REFERENCES

(1) de Baar, H. J. W.; Bathmannt, U.; Smetacek, V.; Löscher, B. M.; Veth, C. Importance of Iron for Plankton Blooms and Carbon Dioxide Drawdown in the Southern Ocean. Nature. 1995. https://doi.org/10.1038/373412a0.

(2) Martin, J. H. Glacial-Interglacial CO2 Change the Iron Hypothesis. Paleoceanography 1990, 5 (1), 1–13.

(3) Martin, J. H.; Fitzwater, S. E. Iron Deficiency Limits Phytoplankton Growth in the North-East Pacific Subarctic. Nature 1988, 331 (6154), 341–343. https://doi.org/10.1038/331341a0.

(4) de Baar, H. J. W. Von Liebig's Law of the Minimum and Plankton Ecology (1899–1991). Prog. Oceanogr. 1994, 33 (4), 347–386. https://doi.org/10.1016/0079-6611(94)90022-1.

(5) Boyd, P. W.; Jickells, T.; Law, C. S.; Blain, S.; Boyle, E. A.; Buesseler, K. O.; Coale, K. H.; Cullen, J. J.; de Baar, H. J. W.; Follows, M.; et al. Mesoscale Iron Enrichment Experiments 1993-2005: Synthesis and Future Directions. Science (80-.). 2007, 315 (5812), 612–617. https://doi.org/10.1126/science.1131669.

(6) Longhurst, A. R.; Glen Harrison, W. The Biological Pump: Profiles of Plankton Production and Consumption in the Upper Ocean. Prog. Oceanogr. 1989, 22 (1), 47–123. https://doi.org/10.1016/0079-6611(89)90010-4.

(7) Tagliabue, A.; Bowie, A. R.; Boyd, P. W.; Buck, K. N.; Johnson, K. S.; Saito, M. A. The Integral Role of Iron in Ocean Biogeochemistry. Nature. 2017. https://doi.org/10.1038/nature21058.

(8) Coale, K. H. Effects of Iron, Manganese, Copper, and Zinc Enrichments on Productivity and Biomass in the Subarctic Pacific. Limnol. Oceanogr. 1991. https://doi.org/10.4319/lo.1991.36.8.1851.

(9) de Baar, H.; Buma, A.; Nolting, R.; Cadee, G.; Jacques, G.; Treguer, P. On Iron Limitation of the Southern Ocean: Experimental Observations in the Weddell and Scotia Seas. Mar. Ecol. Prog. Ser. 1990. https://doi.org/10.3354/meps065105.

(10) Buma, A. G. J.; de Baar, H. J. W.; Nolting, R. F.; van Bennekom, A. J. Metal Enrichment Experiments in the Weddell-Scotia Seas: Effects of Iron and Manganese on Various Plankton Communities. Limnol. Oceanogr. 1991, 36 (8), 1865–1878. https://doi.org/10.4319/lo.1991.36.8.1865.

(11) Martin, J. H.; Fitzwater, S. E.; Gordon, R. M. Iron Deficiency Limits Phytoplankton Growth in Antarctic Waters. Global Biogeochem. Cycles 1990, 4 (1), 5–12. https://doi.org/10.1029/GB004i001p00005.

(12) Coale, K. H.; Johnson, K. S.; Fitzwater, S. E.; Gordon, R. M.; Tanner, S.; Chavez, F. P.; Ferioli, L.; Sakamoto, C.; Rogers, P.; Millero, F.; et al. A Massive Phytoplankton Bloom Induced by an Ecosystem-Scale Iron Fertilization Experiment in the Equatorial Pacific Ocean. Nature 1996, 383 (6600), 495–501. https://doi.org/10.1038/383495a0.

(13) Martin, J. H.; Coale, K. H.; Johnson, K. S.; Fitzwater, S. E.; Gordon, R. M.; Tanner, S. J.; Hunter, C. N.; Elrod, V. A.; Nowicki, J. L.; Coley, T. L.; et al. Testing the Iron Hypothesis in Ecosystems of the Equatorial Pacific Ocean. Nature 1994, 371 (6493), 123–129. https://doi.org/10.1038/371123a0.

(14) Dixon, J. L. Macro and Micro Nutrient Limitation of Microbial Productivity in Oligotrophic Subtropical Atlantic Waters. Environ. Chem. 2008, 5 (2), 135. https://doi.org/10.1071/EN07081.

(15) Boyd, P. W.; Watson, A. J.; Law, C. S.; Abraham, E. R.; Trull, T.; Murdoch, R.; Bakker, D. C. E.; Bowie, A. R.; Buesseler, K. O.; Chang, H.; et al. A Mesoscale Phytoplankton Bloom in the Polar Southern Ocean Stimulated by Iron Fertilization. Nature 2000. https://doi.org/10.1038/35037500.

(16) Gervais, F.; Riebesell, U.; Gorbunov, M. Y. Changes in Primary Productivity and Chlorophyll a in Response to Iron Fertilization in the Southern Polar Frontal Zone. Limnol. Oceanogr. 2002. https://doi.org/10.4319/lo.2002.47.5.1324.

(17) Hoffmann, L. J.; Peeken, I.; Lochte, K.; Assmy, P.; Veldhuis, M. Different Reactions of Southern Ocean Phytoplankton Size Classes to Iron Fertilization. Limnol. Oceanogr. 2006. https://doi.org/10.4319/lo.2006.51.3.1217.

(18) Smetacek, V.; Klaas, C.; Strass, V. H.; Assmy, P.; Montresor, M.; Cisewski, B.; Savoye, N.; Webb, A.; D'Ovidio, F.; Arrieta, J. M.; et al. Deep Carbon Export from a Southern Ocean Iron-Fertilized Diatom Bloom. Nature 2012. https://doi.org/10.1038/nature11229.

(19) Peloquin, J.; Hall, J.; Safi, K.; Smith, W. O.; Wright, S.; van den Enden, R. The Response of Phytoplankton to Iron Enrichment in Sub-Antarctic HNLCLSi Waters: Results from the SAGE Experiment. Deep. Res. Part II Top. Stud. Oceanogr. 2011. https://doi.org/10.1016/j.dsr2.2010.10.021.

(20) Takeda, S.; Obata, H. Response of Equatorial Pacific Phytoplankton to Subnanomolar Fe Enrichment. Mar. Chem. 1995. https://doi.org/10.1016/0304-4203(95)00037-R.

(21) Banse, K. Rates of Phytoplankton Cell Division in the Field and in Iron Enrichment Experiments. Limnol. Oceanogr. 1991, 36 (8), 1886–1898. https://doi.org/10.4319/lo.1991.36.8.1886.

(22) Chisholm, S. W.; Morel, F. M. M. What Controls Phytoplankton Production in Nutrient-Rich Areas of the Open Sea? Limonology Oceanogr. 1991.

(23) Aumont, O.; Bopp, L. Globalizing Results from Ocean in Situ Iron Fertilization Studies. 2006, 20 (June), 1–15. https://doi.org/10.1029/2005GB002591.

(24) Keller, D. P.; Feng, E. Y.; Oschlies, A. Potential Climate Engineering Effectiveness and Side Effects during a High Carbon Dioxide-Emission Scenario. Nat. Commun. 2014, 5 (1), 3304. https://doi.org/10.1038/ncomms4304.

(25) Lauderdale, J. M.; Braakman, R.; Forget, G.; Dutkiewicz, S.; Follows, M. J. Microbial Feedbacks Optimize Ocean Iron Availability. Proc. Natl. Acad. Sci. U. S. A. 2020. https://doi.org/10.1073/pnas.1917277117.

(26) Anderson, R.; Henderson, G. PROGRAM UPDATE | GEOTRACES—A Global Study of the Marine Biogeochemical Cycles of Trace Elements and Their Isotopes. Oceanography 2005, 18 (3), 76–79. https://doi.org/10.5670/oceanog.2005.31.

(27) Caprara, S.; Buck, K. N.; Gerringa, L. J. A.; Rijkenberg, M. J. A.; Monticelli, D. A Compilation of Iron Speciation Data for Open Oceanic Waters. Front. Mar. Sci. 2016, 3 (NOV). https://doi.org/10.3389/fmars.2016.00221.

(28) Cutter, G. A.; Casciotti, K. L.; Croot, P. L.; Geibert, W.; Heimbürger, L. E.; Lohan, M.; Planquette, H.; van de Flierdt, T. Sampling and Sample-Handling Protocols for GEOTRACES Cruises. 2017.

(29) Wells, M. L. The Level of Iron Enrichment Required to Initiate Diatom Blooms in HNLC Waters. Mar. Chem. 2003. https://doi.org/10.1016/S0304-4203(03)00055-0.

(30) Schlosser, C.; Croot, P. L. Application of Cross-Flow Filtration for Determining the Solubility of Iron Species in Open Ocean Seawater. Limnol. Oceanogr. Methods 2008. https://doi.org/10.4319/lom.2008.6.630.

(31) Baalousha, M.; Stolpe, B.; Lead, J. R. Flow Field-Flow Fractionation for the Analysis and Characterization of Natural Colloids and Manufactured Nanoparticles in Environmental Systems: A Critical Review. Journal of Chromatography A. 2011. https://doi.org/10.1016/j.chroma.2011.04.063.

(32) Byrne, R. H.; Kester, D. R. Solubility of Hydrous Ferric Oxide and Iron Speciation in Seawater. Mar. Chem. 1976, 4 (3), 255–274. https://doi.org/10.1016/0304-4203(76)90012-8.

(33) Kuma, K.; Nishioka, J.; Matsunaga, K. Controls on Iron(III) Hydroxide Solubility in Seawater: The Influence of PH and Natural Organic Chelators. Limnol. Oceanogr. 1996. https://doi.org/10.4319/lo.1996.41.3.0396.

(34) Liu, X.; Millero, F. J. The Solubility of Iron in Seawater. Mar. Chem. 2002, 77, 43–54. https://doi.org/10.1016/S0304-4203(01)00074-3.

(35) Schlosser, C.; de la Rocha, C. L.; Streu, P.; Croot, P. L. Solubility of Iron in the Southern Ocean. Limnol. Oceanogr. 2012. https://doi.org/10.4319/lo.2012.57.3.0684.

(36) Millero, F. J.; Yao, W.; Aicher, J. The Speciation of Fe(II) and Fe(III) in Natural Waters. Mar. Chem. 1995. https://doi.org/10.1016/0304-4203(95)00024-L.

(37) Gledhill, M.; van den Berg, C. M. G. Measurement of the Redox Speciation of Iron in Seawater by Catalytic Cathodic Stripping Voltammetry. Mar. Chem. 1995. https://doi.org/10.1016/0304-4203(95)00026-N.

(38) Perdue, E. M.; Reuter, J. H.; Parrish, R. S. A Statistical Model of Proton Binding by Humus. Geochim. Cosmochim. Acta 1984. https://doi.org/10.1016/0016-7037(84)90060-7.

(39) Susetyo, W.; Dobbs, J. C.; Carreira, L. A.; Azarraga, L. V.; Grimm, D. M. Development of a Statistical Model for Metal-Humic Interactions. Anal. Chem. 1990. https://doi.org/10.1021/ac00212a005.

(40) Grimm, D. M.; Azarraga, L. V.; Carreira, L. A.; Susetyo, W. Continuous Multiligand Distribution Model Used to Predict the Stability Constant of Cu(II) Metal Complexation with Humic Material from Fluorescence Quenching Data. Environ. Sci. Technol. 1991. https://doi.org/10.1021/es00020a010.

(41) Amin, S. A.; Green, D. H.; Hart, M. C.; Kupper, F. C.; Sunda, W. G.; Carrano, C. J. Photolysis of Iron-Siderophore Chelates Promotes Bacterial-Algal Mutualism. Proc. Natl. Acad. Sci. 2009, 106 (40), 17071–17076. https://doi.org/10.1073/pnas.0905512106.

(42) Cabaj, A.; Kosakowska, A. Iron-Dependent Growth of and Siderophore Production by Two Heterotrophic Bacteria Isolated from Brackish Water of the Southern Baltic Sea. Microbiol. Res. 2009, 164 (5), 570–577. https://doi.org/10.1016/j.micres.2007.07.001.

(43) Vraspir, J. M.; Butler, A. Chemistry of Marine Ligands and Siderophores. Ann. Rev. Mar. Sci. 2009, 1 (1), 43–63. https://doi.org/10.1146/annurev.marine.010908.163712.

(44) Stintzi, A.; Barnes, C.; Xu, J.; Raymond, K. N. Microbial Iron Transport via a Siderophore Shuttle: A Membrane Ion Transport Paradigm. Proc. Natl. Acad. Sci. 2000, 97 (20), 10691–10696. https://doi.org/10.1073/pnas.200318797.

(45) Mawji, E.; Gledhill, M.; Milton, J. A.; Zubkov, M. V.; Thompson, A.; Wolff, G. A.; Achterberg, E. P. Production of Siderophore Type Chelates in Atlantic Ocean Waters Enriched with Different Carbon and Nitrogen Sources. Mar. Chem. 2011, 124 (1–4), 90–99. https://doi.org/10.1016/j.marchem.2010.12.005.

(46) Barbeau, K.; Rue, E. L.; Bruland, K. W.; Butler, A. Photochemical Cycling of Iron in the Surface Ocean Mediated by Microbial Iron(III)-Binding Ligands. Nature 2001. https://doi.org/10.1038/35096545.

(47) Barbeau, K.; Rue, E. L.; Trick, C. G.; Bruland, K. W.; Butler, A. Photochemical Reactivity of Siderophores Produced by Marine Heterotrophic Bacteria and Cyanobacteria Based on Characteristic Fe(III) Binding Groups. Limnol. Oceanogr. 2003. https://doi.org/10.4319/lo.2003.48.3.1069.

(48) Sandy, M.; Butler, A. Microbial Iron Acquisition: Marine and Terrestrial Siderophores. Chem. Rev. 2009. https://doi.org/10.1021/cr9002787.

(49) Martinez, J. S. Self-Assembling Amphiphilic Siderophores from Marine Bacteria. Science (80-.). 2000, 287 (5456), 1245–1247. https://doi.org/10.1126/science.287.5456.1245.

(50) Martinez, J. S.; Carter-Franklin, J. N.; Mann, E. L.; Martin, J. D.; Haygood, M. G.; Butler, A. Structure and Membrane Affinity of a Suite of Amphiphilic Siderophores Produced by a Marine Bacterium. Proc. Natl. Acad. Sci. U. S. A. 2003. https://doi.org/10.1073/pnas.0637444100.

(51) Martinez, J. S.; Butler, A. Marine Amphiphilic Siderophores: Marinobactin Structure, Uptake, and Microbial Partitioning. J. Inorg. Biochem. 2007, 101 (11–12), 1692–1698. https://doi.org/10.1016/j.jinorgbio.2007.07.007.

(52) Xu, G.; Martinez, J. S.; Groves, J. T.; Butler, A. Membrane Affinity of the Amphiphilic Marinobactin Siderophores. J. Am. Chem. Soc. 2002. https://doi.org/10.1021/ja026768w.

(53) Owen, T.; Pynn, R.; Martinez, J. S.; Butler, A. Micelle-to-Vesicle Transition of an Iron-Chelating Microbial Surfactant, Marinobactin E. Langmuir 2005. https://doi.org/10.1021/la0519352.

(54) Martin, J. D.; Ito, Y.; Homann, V. V.; Haygood, M. G.; Butler, A. Structure and Membrane Affinity of New Amphiphilic Siderophores Produced by Ochrobactrum Sp. SP18. JBIC J. Biol. Inorg. Chem. 2006, 11 (5), 633–641. https://doi.org/10.1007/s00775-006-0112-y.

(55) Homann, V. V.; Sandy, M.; Tincu, J. A.; Templeton, A. S.; Tebo, B. M.; Butler, A. Loihichelins A-F, a Suite of Amphiphilic Siderophores Produced by the Marine Bacterium Halomonas LOB-5. J. Nat. Prod. 2009. https://doi.org/10.1021/np800640h.

(56) Homann, V. V.; Edwards, K. J.; Webb, E. A.; Butler, A. Siderophores of Marinobacter Aquaeolei: Petrobactin and Its Sulfonated Derivatives. BioMetals 2009. https://doi.org/10.1007/s10534-009-9237-0.

(57) Witter, A. E.; Hutchins, D. A.; Butler, A.; Luther, G. W. Determination of Conditional Stability Constants and Kinetic Constants for Strong Model Fe-Binding Ligands in Seawater. Mar. Chem. 2000, 69 (1–2), 1–17. https://doi.org/10.1016/S0304-4203(99)00087-0.

(58) Hunter, K. A.; Boyd, P. W. Iron-Binding Ligands and Their Role in the Ocean Biogeochemistry of Iron. Environ. Chem. 2007. https://doi.org/10.1071/EN07012.

(59) Rijkenberg, M. J. A.; Gerringa, L. J. A.; Carolus, V. E.; Velzeboer, I.; de Baar, H. J. W. Enhancement and Inhibition of Iron Photoreduction by Individual Ligands in Open Ocean Seawater. Geochim. Cosmochim. Acta 2006. https://doi.org/10.1016/j.gca.2006.03.004.

(60) Rue, E.; Bruland, K. Domoic Acid Binds Iron and Copper: A Possible Role for the Toxin Produced by the Marine Diatom Pseudo-Nitzschia. Mar. Chem. 2001. https://doi.org/10.1016/S0304-4203(01)00053-6.

(61) Hassler, C. S.; Schoemann, V.; Nichols, C. M.; Butler, E. C. V.; Boyd, P. W. Saccharides Enhance Iron Bioavailability to Southern Ocean Phytoplankton. Proc. Natl. Acad. Sci. U. S. A. 2011. https://doi.org/10.1073/pnas.1010963108.

(62) Gyurcsik, B.; Nagy, L. Carbohydrates as Ligands: Coordination Equilibria and Structure of the Metal Complexes. Coord. Chem. Rev. 2000, 203 (1), 81–149. https://doi.org/10.1016/S0010-8545(99)00183-6.

(63) Laglera, L. M.; Van Den Berg, C. M. G. Evidence for Geochemical Control of Iron by Humic Substances in Seawater. Limnol. Oceanogr. 2009. https://doi.org/10.4319/lo.2009.54.2.0610.

(64) Jickells, T. D.; An, Z. S.; Andersen, K. K.; Baker, A. R.; Bergametti, C.; Brooks, N.; Cao, J. J.; Boyd, P. W.; Duce, R. A.; Hunter, K. A.; et al. Global Iron Connections between Desert Dust, Ocean Biogeochemistry, and Climate. Science. 2005. https://doi.org/10.1126/science.1105959.

(65) de Baar, H. J. W.; De Jong, J. T. M. Distributions, Sources and Sinks of Iron in Seawater. In The biogeochemistry of iron in seawater; 2001; pp 123–153.

(66) Poulton, S. W.; Raiswell, R. The Low-Temperature Geochemical Cycle of Iron: From Continental Fluxes to Marine Sediment Deposition. Am. J. Sci. 2002. https://doi.org/10.2475/ajs.302.9.774.

(67) Boyle, E. A.; Edmond, J. M.; Sholkovitz, E. R. The Mechanism of Iron Removal in Estuaries. Geochim. Cosmochim. Acta 1977. https://doi.org/10.1016/0016-7037(77)90075-8.

(68) Boyle, E. A.; Bergquist, B. A.; Kayser, R. A.; Mahowald, N. Iron, Manganese, and Lead at Hawaii Ocean Time-Series Station ALOHA: Temporal Variability and an Intermediate Water Hydrothermal Plume. Geochim. Cosmochim. Acta 2005, 69 (4), 933–952. https://doi.org/10.1016/j.gca.2004.07.034.

(69) Bennett, S. A.; Achterberg, E. P.; Connelly, D. P.; Statham, P. J.; Fones, G. R.; German, C. R. The Distribution and Stabilisation of Dissolved Fe in Deep-Sea Hydrothermal Plumes. Earth Planet. Sci. Lett. 2008. https://doi.org/10.1016/j.epsl.2008.01.048.

(70) Tagliabue, A.; Bopp, L.; Dutay, J. C.; Bowie, A. R.; Chever, F.; Jean-Baptiste, P.; Bucciarelli, E.; Lannuzel, D.; Remenyi, T.; Sarthou, G.; et al. Hydrothermal Contribution to the Oceanic Dissolved Iron Inventory. Nat. Geosci. 2010. https://doi.org/10.1038/ngeo818.

(71) Klunder, M. B.; Laan, P.; Middag, R.; De Baar, H. J. W.; van Ooijen, J. C. Dissolved Iron in the Southern Ocean (Atlantic Sector). Deep. Res. Part II Top. Stud. Oceanogr. 2011. https://doi.org/10.1016/j.dsr2.2010.10.042.

(72) Wu, J.; Wells, M. L.; Rember, R. Dissolved Iron Anomaly in the Deep Tropical-Subtropical Pacific: Evidence for Long-Range Transport of Hydrothermal Iron. Geochim. Cosmochim. Acta 2011. https://doi.org/10.1016/j.gca.2010.10.024.

(73) Resing, J. A.; Sedwick, P. N.; German, C. R.; Jenkins, W. J.; Moffett, J. W.; Sohst, B. M.; Tagliabue, A. Basin-Scale Transport of Hydrothermal Dissolved Metals across the South Pacific Ocean. Nature 2015, 523 (7559), 200–203. https://doi.org/10.1038/nature14577.

(74) German, C. R.; Campbell, A. C.; Edmond, J. M. Hydrothermal Scavenging at the Mid-Atlantic Ridge: Modification of Trace Element Dissolved Fluxes. Earth Planet. Sci. Lett. 1991, 107 (1), 101–114. https://doi.org/10.1016/0012-821X(91)90047-L.

(75) Toner, B. M.; Fakra, S. C.; Manganini, S. J.; Santelli, C. M.; Marcus, M. A.; Moffett, J. W.; Rouxel, O.; German, C. R.; Edwards, K. J. Preservation of Iron(II) by Carbon-Rich Matrices in a Hydrothermal Plume. Nat. Geosci. 2009. https://doi.org/10.1038/ngeo433.

(76) Sander, S. G.; Koschinsky, A. Metal Flux from Hydrothermal Vents Increased by Organic Complexation. Nat. Geosci. 2011. https://doi.org/10.1038/ngeo1088.

(77) Yücel, M.; Gartman, A.; Chan, C. S.; Luther, G. W. Hydrothermal Vents as a Kinetically Stable Source of Iron-Sulphide-Bearing Nanoparticles to the Ocean. Nat. Geosci. 2011. https://doi.org/10.1038/ngeo1148.

(78) Gartman, A.; Findlay, A. J.; Luther, G. W. Nanoparticulate Pyrite and Other Nanoparticles Are a Widespread Component of Hydrothermal Vent Black Smoker Emissions. Chem. Geol. 2014. https://doi.org/10.1016/j.chemgeo.2013.12.013.

(79) Raiswell, R.; Tranter, M.; Benning, L. G.; Siegert, M.; De'ath, R.; Huybrechts, P.; Payne, T. Contributions from Glacially Derived Sediment to the Global Iron (Oxyhydr)Oxide Cycle: Implications for Iron Delivery to the Oceans. Geochim. Cosmochim. Acta 2006. https://doi.org/10.1016/j.gca.2005.12.027.

(80) Kirchman, D. L. Microbial Ferrous Wheel. Nature 1996, 383 (6598), 303–304. https://doi.org/10.1038/383303a0.

(81) Haygood, M. G.; Holt, P. D.; Butler, A. Aerobactin Production by a Planktonic Marine Vibrio Sp. Limnology and Oceanography. 1993. https://doi.org/10.4319/lo.1993.38.5.1091.

(82) Wilhelm, S. Ecology of Iron-Limited Cyanobacteria: A Review of Physiological Responses and Implications for Aquatic Systems. Aquat. Microb. Ecol. 1995, 9, 295–303. https://doi.org/10.3354/ame009295.

(83) Strzepek, R. F.; Maldonado, M. T.; Higgins, J. L.; Hall, J.; Safi, K.; Wilhelm, S. W.; Boyd, P. W. Spinning the "Ferrous Wheel": The Importance of the Microbial Community in an Iron Budget during the FeCycle Experiment. Global Biogeochem. Cycles 2005, 19 (4). https://doi.org/10.1029/2005GB002490.

(84) Barbeau, K.; Moffett, J. W.; Caron, D. A.; Croot, P. L.; Erdner, D. L. Role of Protozoan Grazing in Relieving Iron Limitation of Phytoplankton. Nature 1996. https://doi.org/10.1038/380061a0.

(85) Maranger, R.; Bird, D. F.; Price, N. M. Iron Acquisition by Photosynthetic Marine Phytoplankton from Ingestion Bacteria. Nature 1998. https://doi.org/10.1038/24352.

(86) Lee, B. G.; Fisher, N. S. Release Rates of Trace Elements and Protein from Decomposing Planktonic Debris. 1. Phytoplankton Debris. J. Mar. Res. 1993. https://doi.org/10.1357/0022240933223774.

(87) Sarthou, G.; Vincent, D.; Christaki, U.; Obernosterer, I.; Timmermans, K. R.; Brussaard, C. P. D. The Fate of Biogenic Iron during a Phytoplankton Bloom Induced by Natural Fertilisation: Impact of Copepod Grazing. Deep Sea Res. Part II Top. Stud. Oceanogr. 2008, 55 (5–7), 734–751. https://doi.org/10.1016/j.dsr2.2007.12.033.

(88) Mioni, C. E.; Poorvin, L.; Wilhelm, S. W. Virus and Siderophore-Mediated Transfer of Available Fe between Heterotrophic Bacteria: Characterization Using an Fe-Specific Bioreporter. Aquat. Microb. Ecol. 2005. https://doi.org/10.3354/ame041233.

(89) Nodwell, L. M.; Price, N. M. Direct Use of Inorganic Colloidal Iron by Marine Mixotrophic Phytoplankton. Limnol. Oceanogr. 2001. https://doi.org/10.4319/lo.2001.46.4.0765.

(90) Lohan, M. C.; Aguilar-Islas, A. M.; Bruland, K. W. Direct Determination of Iron in Acidified (PH 1.7) Seawater Samples by Flow Injection Analysis with Catalytic Spectrophotometric Detection: Application and Intercomparison. Limnol. Oceanogr. Methods 2006. https://doi.org/10.4319/lom.2006.4.164.

(91) Measures, C. I.; Yuan, J.; Resing, J. A. Determination of Iron in Seawater by Flow Injection Analysis Using In-Line Preconcentration and Spectrophotometric Detection. Mar. Chem. 1995, 50 (1–4), 3–12. https://doi.org/10.1016/0304-4203(95)00022-J.

(92) Kolotyrkina, I. Y.; Shpigun, L. K.; Zolotov, Y. A.; Malahoff, A. Application of Flow Injection Spectrophotometry to the Determination of Dissolved Iron in Sea-Water. Analyst 1995. https://doi.org/10.1039/AN9952000201.

(93) Obata, H.; Karatani, H.; Nakayama, E. Automated Determination of Iron in Seawater by Chelating Resin Concentration and Chemiluminescence Detection. Anal. Chem. 1993. https://doi.org/10.1021/ac00059a007.

(94) Sarthou, G.; Baker, A. R.; Blain, S.; Achterberg, E. P.; Boye, M.; Bowie, A. R.; Croot, P.; Laan, P.; De Baar, H. J. W.; Jickells, T. D.; et al. Atmospheric Iron Deposition and Sea-Surface Dissolved Iron Concentrations in the Eastern Atlantic Ocean. Deep. Res. Part I Oceanogr. Res. Pap. 2003. https://doi.org/10.1016/S0967-0637(03)00126-2.

(95) Elrod, V. A.; Johnson, K. S.; Coale, K. H. Determination of Subnanomolar Levels of Iron(II) and Total Dissolved Iron in Sea Water by Flow Injection Analysis with Chemiluminescence Detection. Anal. Chem. 1991. https://doi.org/10.1021/ac00009a011.

(96) Hirata, S.; Yoshihara, H.; Aihara, M. Determination of Iron(II) and Total Iron in Environmental Water Samples by Flow Injection Analysis with Column Preconcentration of Chelating Resin Functionalized with N-Hydroxyethylethylenediamine Ligands and Chemiluminescence Detection. In Talanta; 1999. https://doi.org/10.1016/S0039-9140(99)00061-2.

(97) Obata, H.; Karatani, H.; Matsui, M.; Nakayama, E. Fundamental Studies for Chemical Speciation of Iron in Seawater with an Improved Analytical Method. Mar. Chem. 1997. https://doi.org/10.1016/S0304-4203(96)00082-5.

(98) Bruland, K. W.; Franks, R. P.; Knauer, G. A.; Martin, J. H. Sampling and Analytical Methods for the Determination of Copper, Cadmium, Zinc, and Nickel at the Nanogram per Liter Level in Sea Water. Anal. Chim. Acta 1979, 105, 233–245. https://doi.org/10.1016/S0003-2670(01)83754-5.

(99) Gordon, R. M.; Coale, K. H.; Johnson, K. S. Iron Distributions in the Equatorial Pacific: Implications for New Production. Limnol. Oceanogr. 1997. https://doi.org/10.4319/lo.1997.42.3.0419.

(100) Saager, P. M.; De Baar, H. J. W.; Burkill, P. H. Manganese and Iron in Indian Ocean Waters. Geochim. Cosmochim. Acta 1989. https://doi.org/10.1016/0016-7037(89)90348-7.

(101) Riley, J. P.; Taylor, D. The Concentrations of Cadmium, Copper, Iron, Manganese, Molybdenum, Nickel, Vanadium and Zinc in Part of the Tropical North-East Atlantic Ocean. Deep. Res. Oceanogr. Abstr. 1972. https://doi.org/10.1016/0011-7471(72)90024-1.

(102) Kingston, H. M.; Barnes, I. L.; Brady, T. J.; Rains, T. C.; Champ, M. A. Separation of Eight Transition Elements from Alkali and Alkaline Earth Elements in Estuarine and Seawater with Chelating Resin and Their Determination by Graphite Furnace Atomic Absorption Spectrometry. Anal. Chem. 1978, 50 (14), 2064–2070. https://doi.org/10.1021/ac50036a031.

(103) Sohrin, Y.; Iwamoto, S. I.; Akiyama, S.; Fujita, T.; Kugii, T.; Obata, H.; Nakayama, E.; Goda, S.; Fujishima, Y.; Hasegawa, H.; et al. Determination of Trace Elements in Seawater by Fluorinated Metal Alkoxide Glass-Immobilized 8-Hydroxyquinoline Concentration and High-Resolution Inductively Coupled Plasma Mass Spectrometry Detection. Anal. Chim. Acta 1998. https://doi.org/10.1016/S0003-2670(98)00074-9.

(104) Akatsuka, K.; McLaren, J. W.; Lam, J. W.; Berman, S. S. Determination of Iron and Ten Other Trace Elements in the Open Ocean Seawater Reference Material NASS-3 by Inductively Coupled Plasma Mass Spectrometry. J. Anal. At. Spectrom. 1992, 7 (6), 889. https://doi.org/10.1039/ja9920700889.

(105) Gledhill, M.; van den Berg, C. M. G. Determination of Complexation of Iron(III) with Natural Organic Complexing Ligands in Seawater Using Cathodic Stripping Voltammetry. Mar. Chem. 1994, 47 (1), 41–54. https://doi.org/10.1016/0304-4203(94)90012-4.

(106) van den Berg, C. M. G.; Nimmo, M.; Abollino, O.; Mentasti, E. The Determination of Trace Levels of Iron in Seawater, Using Adsorptive Cathodic Stripping Voltammetry. Electroanalysis 1991, 3 (6), 477–484. https://doi.org/10.1002/elan.1140030606.

(107) Yokoi, K.; van den Berg, C. M. G. The Determination of Iron in Seawater Using Catalytic Cathodic Stripping Voltammetry. Electroanalysis 1992. https://doi.org/10.1002/elan.1140040113.

(108) Aldrich, A. P.; Van Den Berg, C. M. G. Determination of Iron and Its Redox Speciation in Seawater Using Catalytic Cathodic Stripping Voltammetry. Electroanalysis 1998. https://doi.org/10.1002/(SICI)1521-4109(199805)10:6<369::AID-ELAN369>3.0.CO;2-W.

(109) Rue, E. L.; Bruland, K. W. Complexation of Iron(III) by Natural Organic Ligands in the Central North Pacific as Determined by a New Competitive Ligand Equilibration/Adsorptive Cathodic Stripping Voltammetric Method. Mar. Chem. 1995, 50 (1–4), 117–138. https://doi.org/10.1016/0304-4203(95)00031-L.

(110) Croot, P. L.; Johansson, M. Determination of Iron Speciation by Cathodic Stripping Voltammetry in Seawater Using the Competing Ligand 2-(2-Thiazolylazo)-p-Cresol (TAC). Electroanalysis 2000, 12 (8), 565–576. https://doi.org/10.1002/(SICI)1521-4109(200005)12:8<565::AID-ELAN565>3.0.CO;2-L.

(111) Obata, H.; Van den Berg, C. M. G. Determination of Picomolar Levels of Iron in Seawater Using Catalytic Cathodic Stripping Voltammetry. Anal. Chem. 2001, 73 (11), 2522–2528. https://doi.org/10.1021/ac001495d.

(112) Caprara, S.; Laglera, L. M.; Monticelli, D. Ultrasensitive and Fast Voltammetric Determination of Iron in Seawater by Atmospheric Oxygen Catalysis in 500 Ul Samples. Anal. Chem. 2015, 87 (12), 6357–6363. https://doi.org/10.1021/acs.analchem.5b01239.

(113) Laglera, L. M.; Santos-Echeandía, J.; Caprara, S.; Monticelli, D. Quantification of Iron in Seawater at the Low Picomolar Range Based on Optimization of Bromate/Ammonia/Dihydroxynaphtalene System by Catalytic Adsorptive Cathodic Stripping Voltammetry. Anal. Chem. 2013, 85 (4), 2486–2492. https://doi.org/10.1021/ac303621q.

(114) van den Berg, C. M. G.; Huang, Z. Q. Determination of Iron in Seawater Using Cathodic Stripping Voltammetry Preceded by Adsorptive Collection with the Hanging Mercury Drop Electrode. J. Electroanal. Chem. 1984, 177 (1–2), 269–280. https://doi.org/10.1016/0022-0728(84)80228-4.

(115) Boye, M.; Van Den Berg, C. M. G.; De Jong, J. T. M.; Leach, H.; Croot, P.; De Baar, H. J. W. Organic Complexation of Iron in the Southern Ocean. Deep. Res. Part I Oceanogr. Res. Pap. 2001. https://doi.org/10.1016/S0967-0637(00)00099-6.

(116) Witter, A. E.; Lewis, B. L.; Luther, G. W. Iron Speciation in the Arabian Sea. Deep. Res. Part II Top. Stud. Oceanogr. 2000. https://doi.org/10.1016/S0967-0645(99)00152-6.

(117) Boye, M.; Aldrich, A. P.; Van Den Berg, C. M. G.; De Jong, J. T. M.; Veldhuis, M.; De Baar, H. J. W. Horizontal Gradient of the Chemical Speciation of Iron in Surface Waters of the Northeast Atlantic Ocean. Mar. Chem. 2003, 80 (2–3), 129–143. https://doi.org/10.1016/S0304-4203(02)00102-0.

(118) van den Berg, C. M. G. Chemical Speciation of Iron in Seawater by Cathodic Stripping Voltammetry with Dihydroxynaphthalene. Anal. Chem. 2006, 78 (1), 156–163. https://doi.org/10.1021/ac051441.

(119) Laglera, L. M.; Battaglia, G.; van den Berg, C. M. G. Effect of Humic Substances on the Iron Speciation in Natural Waters by CLE/CSV. Mar. Chem. 2011, 127 (1–4), 134–143. https://doi.org/10.1016/j.marchem.2011.09.003.

(120) Abualhaija, M. M.; van den Berg, C. M. G. Chemical Speciation of Iron in Seawater Using Catalytic Cathodic Stripping Voltammetry with Ligand Competition against Salicylaldoxime. Mar. Chem. 2014, 164, 60–74. https://doi.org/10.1016/j.marchem.2014.06.005.

(121) Buck, K. N.; Moffett, J.; Barbeau, K. A.; Bundy, R. M.; Kondo, Y.; Wu, J. The Organic Complexation of Iron and Copper: An Intercomparison of Competitive Ligand Exchange-Adsorptive Cathodic Stripping Voltammetry (CLE-ACSV) Techniques. Limnol. Oceanogr. Methods 2012, 10 (7), 496–515. https://doi.

org/10.4319/lom.2012.10.496.

(122) Hassler, C.; Cabanes, D.; Blanco-Ameijeiras, S.; Sander, S. G.; Benner, R. Importance of Refractory Ligands and Their Photodegradation for Iron Oceanic Inventories and Cycling. Mar. Freshw. Res. 2020. https://doi.org/10.1071/MF19213.

(123) Sander, S. G.; Tian, F.; Ibisanmi, E. B.; Currie, K. I.; Hunter, K. A.; Frew, R. D. Spatial and Seasonal Variations of Iron Speciation in Surface Waters of the Subantarctic Front and the Otago Continental Shelf. Mar. Chem. 2015. https://doi.org/10.1016/j.marchem.2014.09.001.

(124) Laglera, L. M.; Battaglia, G.; van den Berg, C. M. G. Determination of Humic Substances in Natural Waters by Cathodic Stripping Voltammetry of Their Complexes with Iron. Anal. Chim. Acta 2007. https://doi.org/10.1016/j.aca.2007.07.059.

(125) Inzelt, G.; Lewenstam, A.; Scholz, F. Handbook of Reference Electrodes; 2013. https://doi.org/10.1007/978-3-642-36188-3.

(126) Sanvito, F.; Pacileo, L.; Monticelli, D. Fostering and Understanding Iron Detection at the Ultratrace Level by Adsorptive Stripping Voltammetry with Catalytic Enhancement. Electroanalysis 2019, 31 (2). https://doi.org/10.1002/elan.201800675.

(127) Mirčeski, Valentin; Komorsky-Lovric, Sebojka; Lovric, M. Square-Wave Voltammetry. Theory and Application; Springer, 2007.

(128) Vettorelo, S. N.; Garay, F. Theory of Square-Wave Catalytic Adsorptive Stripping Voltammetry . How to Obtain Mechanistic Information from Experimental Data. J. Electroanal. Chem. 2018, 826 (July), 125–132. https://doi.org/10.1016/j.jelechem.2018.08.024.

(129) Johnson, K. S.; Elrod, V.; Fitzwater, S.; Plant, J.; Boyle, E.; Bergquist, B.; Bruland, K.; Aguilar-Islas, A.; Buck, K.; Lohan, M.; et al. Developing Standards for Dissolved Iron in Seawater. Eos, Trans. Am. Geophys. Union 2007, 88 (11), 131–132. https://doi.org/doi:10.1029/2007EO110003.

(130) Job, P. Formation and Stability of Inorganic Complexes in Solution. Ann. Chim. 1928, 9, 113–203.

(131) Renny, J. S.; Tomasevich, L. L.; Tallmadge, E. H.; Collum, D. B. Method of Continuous Variations : Applications of Job Plots to the Study of Molecular Associations in Organometallic Chemistry Angewandte. Angew. Chemie Int. Ed. 2013, 52, 11998–12013. https://doi.org/10.1002/anie.201304157.

(132) Cornard, J. P.; Boudet, A. C.; Merlin, J. C. Complexes of Al (III) with 3'4 ' -Dihydroxy-Flavone: Characterization , Theoretical and Spectroscopic Study. Spectrochim. Acta Par A 2001, 57, 591–602.

(133) Freiser, H. Concepts & Calculations in Analytical Chemistry A Spreadsheet Approach; 1992.

(134) Biçer, E.; Arat, C. A Voltammetric Study on the Aqueous Electrochemistry of Acid Red 1 (Azophloxine). Croat. Chem. Acta 2009, 82 (3), 583–593.

(135) Martel, D.; Sojic, N.; Kuhn, A. A Simple Student Experiment for Teaching Surface Electrochemistry: Adsorption of Polyoxometalate on Graphite Electrodes. J. Chem. Educ. 2002, 79 (3), 349–352. https://doi.org/10.1021/ed079p349.

(136) Graham, D. The Characterization of Physical Adsorption Systems. I. The Equilibrium Function and Standard Free Energy of Adsorption. J. Phys. Chem. 1953, 57 (7), 665–669. https://doi.org/10.1021/j150508a014.

(137) Papageorgiou, S. K.; Katsaros, F. K.; Kouvelos, E. P.; Kanellopoulos, N. K. Prediction of Binary Adsorption Isotherms of Cu 2 + , Cd 2 + and Pb 2 + on Calcium Alginate Beads from Single Adsorption Data. J. Hazard. Mater. 2009, 162, 1347–1354. https://doi.org/10.1016/j.jhazmat.2008.06.022.

(138) Laviron, E. General Expression of the Linear Potential Sweep Voltammogram in the Case of Diffusionless Electrochemical Systems. J. Chem. Educ. 1979, 101, 19–28.

(139) Mirčeski, V.; Gulaboski, R. Surface Catalytic Mechanism in Square-Wave Voltammetry. Electroanalysis 2001, 13 (16), 1326–1334. https://doi.org/10.1002/1521-4109(200111)13:16<1326::AID-ELAN1326>3.0.CO;2-S.

(140) Nicholson, R. S.; Shain, I. Theory of Stationary Electrode Polarography: Single Scan and Cyclic Methods Applied to Reversible, Irreversible, and Kinetic Systems. Anal. Chem. 1964. https://doi.org/10.1021/ac60210a007.

(141) Mirčeski, V.; Gulaboski, R. The Surface Catalytic Mechanism: A Comparative Study with Square-Wave and Staircase Cyclic Voltammetry. J. Solid State Electrochem. 2003. https://doi.org/10.1007/s10008-002-0290-7.

(142) Horak, V.; Foster, F. V.; de Levie, R.; Jones, J. W.; Svoronos, P. Generation and Trapping of 2,3-Naphthoquinone. Tetrahedron Lett. 1981, 22 (37), 3577–3578. https://doi.org/10.1016/S0040-4039(01)81962-6.

(143) Quentel, F.; Mirčeski, V. Catalytic Adsorptive Stripping Voltammetry of Molybdenum: Redox Kinetic Measurements. Electroanalysis 2004, 16 (20), 1690–1696. https://doi.org/10.1002/elan.200303015.

(144) Quentel, F.; Mirčeski, V.; Laouenan, A.; Elleouet, C.; Madec, C. L. Square-Wave Voltammetry of the Molybdenum-1,10 Phenanthroline-Fulvic Acids Complex: Redox Kinetics Measurements. Electroanalysis 2003, 15 (4), 270–277. https://doi.org/10.1002/elan.200390034.

(145) van den Berg, C. M. G.; Donat, J. R. Determination and Data Evaluation of Copper Complexation by Organic Ligands in Sea Water Using Cathodic Stripping Voltammetry at Varying Detection Windows. Anal. Chim. Acta 1992. https://doi.org/10.1016/0003-2670(92)85181-5.

(146) Van Den Berg, C. M. G.; Nimmo, M. Determination of Interactions of Nickel with Dissolved Organic Material in Seawater Using Cathodic Stripping Voltammetry. Sci. Total Environ. 1987. https://doi.org/10.1016/0048-9697(87)90415-3.

(147) Zhang, H.; Van Den Berg, C. M. G.; Wollast, R. The Determination of Interactions of Cobalt (II) with Organic Compounds in Seawater Using Cathodic Stripping Voltammetry. Mar. Chem. 1990. https://doi.org/10.1016/0304-4203(90)90049-I.

(148) van den Berg, C. M. G.; Kramer, J. R. Determination of Complexing Capacities of Ligands in Natural Waters and Conditional Stability Constants of the Copper Complexes by Means of Manganese Dioxide. Anal. Chim. Acta 1979. https://doi.org/10.1016/S0003-2670(01)83711-9.

(149) Van Den Berg, C. M. G. Determination of Copper Complexation with Natural Organic Ligands in Seawater by Equilibration with MnO2 I. Theory. Mar. Chem. 1982, 11 (4), 307–322. https://doi.org/10.1016/0304-4203(82)90028-7.

(150) Ružić, I. Theoretical Aspects of the Direct Titration of Natural Waters and Its Information Yield for Trace Metal Speciation. Anal. Chim. Acta 1982, 140 (1), 99–113. https://doi.org/10.1016/S0003-2670(01)95456-X.

(151) Hudson, R. J. M.; Covault, D. T.; Morel, F. M. M. Investigations of Iron Coordination and Redox Reactions in Seawater Using 59Fe Radiometry and Ion-Pair Solvent Extraction of Amphiphilic Iron Complexes. Mar. Chem. 1992. https://doi.org/10.1016/0304-4203(92)90035-9.

(152) Monticelli, D.; Dossi, C.; Castelletti, A. Assessment of Accuracy and Precision in Speciation Analysis by Competitive Ligand Equilibration-Cathodic Stripping Voltammetry (CLE-CSV) and Application to Antarctic Samples. Anal. Chim. Acta 2010, 675 (2), 116–124. https://doi.org/10.1016/j.aca.2010.07.009.

(153) Schlitzer, R.; Anderson, R. F.; Dodas, E. M.; Lohan, M.; Geibert, W.; Tagliabue, A.; Bowie, A.; Jeandel, C.; Maldonado, M. T.; Landing, W. M.; et al. The GEOTRACES Intermediate Data Product 2017. Chem. Geol. 2018. https://doi.org/10.1016/j.chemgeo.2018.05.040.

(154) Gledhill, M.; Gerringa, L. J. A. The Effect of Metal Concentration on the Parameters Derived from Complexometric Titrations of Trace Elements in Seawater—a Model Study. Front. Mar. Sci. 2017. https://doi.org/10.3389/fmars.2017.00254.

(155) Velasquez, I.; Nunn, B. L.; Ibisanmi, E.; Goodlett, D. R.; Hunter, K. A.; Sander, S. G. Detection of Hydroxamate Siderophores in Coastal and Sub-Antarctic Waters off the South Eastern Coast of New Zealand. Mar. Chem. 2011.

https://doi.org/10.1016/j.marchem.2011.04.003.

(156) Whitby, H.; Planquette, H.; Cassar, N.; Bucciarelli, E.; Osburn, C. L.; Janssen, D. J.; Cullen, J. T.; González, A. G.; Völker, C.; Sarthou, G. A Call for Refining the Role of Humic-like Substances in the Oceanic Iron Cycle. Sci. Rep. 2020. https://doi.org/10.1038/s41598-020-62266-7.

(157) Rivaro, P.; Ardini, F.; Grotti, M.; Aulicino, G.; Cotroneo, Y.; Fusco, G.; Mangoni, O.; Bolinesi, F.; Saggiomo, M.; Celussi, M. Mesoscale Variability Related to Iron Speciation in a Coastal Ross Sea Area (Antarctica) during Summer 2014. Chem. Ecol. 2019. https://doi.org/10.1080/02757540.2018.1531987.

(158) Millero, F. J.; Woosley, R.; Ditrolio, B.; Waters, J. Effect of Ocean Acidification on the Speciation of Metals in Seawater. Oceanography. 2009. https://doi.org/10.5670/oceanog.2009.98.

(159) Shi, D.; Xu, Y.; Hopkinson, B. M.; Morel, F. M. M. Effect of Ocean Acidification on Iron Availability to Marine Phytoplankton. Science (80-.). 2010. https://doi.org/10.1126/science.1183517.

(160) Gledhill, M.; Achterberg, E. P.; Li, K.; Mohamed, K. N.; Rijkenberg, M. J. A. Influence of Ocean Acidification on the Complexation of Iron and Copper by Organic Ligands in Estuarine Waters. Mar. Chem. 2015. https://doi.org/10.1016/j.marchem.2015.03.016.

(161) Ye, Y.; Völker, C.; Gledhill, M. Exploring the Iron-Binding Potential of the Ocean Using a Combined PH and DOC Parameterization. Global Biogeochem. Cycles 2020. https://doi.org/10.1029/2019GB006425.

(162) Good, N. E.; Winget, G. D.; Winter, W.; Connolly, T. N.; Izawa, S.; Singh, R. M. M. Hydrogen Ion Buffers for Biological Research. Biochemistry 1966. https://doi.org/10.1021/bi00866a011.

(163) Pilson, M. E. Q. An Introduction to the Chemistry of the Sea, Second edi.; Cambridge University Press, 2013.

(164) Laglera, L. M.; Caprara, S.; Monticelli, D. Towards a Zero-Blank, Preconcentration-Free Voltammetric Method for Iron Analysis at Picomolar Concentrations in Unbuffered Seawater. Talanta 2016, 150, 449–454. https://doi.org/10.1016/j.talanta.2015.12.060.

(165) Aguilar, D.; Galceran, J.; Companys, E.; Puy, J.; Parat, C.; Authier, L.; Potin-Gautier, M. Non-Purged Voltammetry Explored with AGNES. Phys. Chem. Chem. Phys. 2013. https://doi.org/10.1039/c3cp52836g.

(166) Tercier-Waeber, M.-L.; Buffle, J. Submersible Online Oxygen Removal System Coupled to an in Situ Voltammetric Probe for Trace Element Monitoring in Freshwater. Environ. Sci. Technol. 2000, 34 (18), 4018–4024. https://doi.org/10.1021/es000033e.

(167) van den Berg, C. M. G. Evidence for Organic Complexation of Iron in Seawater. Mar. Chem. 1995. https://doi.org/10.1016/0304-4203(95)00032-M.

(168) Laglera, L. M.; Filella, M. The Relevance of Ligand Exchange Kinetics in the Measurement of Iron Speciation by CLE-AdCSV in Seawater. Mar. Chem. 2015. https://doi.org/10.1016/j.marchem.2014.09.005.

(169) Currie, L. A. Nomenclature in Evaluation of Analytical Methods Including Detection and Quantification Capabilities (IUPAC Recommendations 1995). Anal. Chim. Acta 1999. https://doi.org/10.1016/S0003-2670(99)00104-X.

(170) Monticelli, D.; Laglera, L. M.; Caprara, S. Miniaturization in Voltammetry: Ultratrace Element Analysis and Speciation with Twenty-Fold Sample Size Reduction. Talanta 2014. https://doi.org/10.1016/j.talanta.2014.04.024.

(171) Monticelli, D.; Carugati, G.; Castelletti, A.; Recchia, S.; Dossi, C. Design and Development of a Low Cost, High Performance UV Digester Prototype: Application to the Determination of Trace Elements by Stripping Voltammetry. Microchem. J. 2010, 95 (2), 158–163. https://doi.org/10.1016/j.microc.2009.11.002.

(172) Monticelli, D.; Castelletti, A.; Civati, D.; Recchia, S.; Dossi, C. How to Efficiently Produce Ultrapure Acids. Int. J. Anal. Chem. 2019, 2019, 1–5. https://doi.org/10.1155/2019/5180610.

LIST OF PUBLICATIONS

1) Sanvito, F.; Pacileo, L.; Monticelli, D. Fostering and Understanding Iron Detection at the Ultratrace Level by Adsorptive Stripping Voltammetry with Catalytic Enhancement, Electroanalysis 2019, 31 (2). https://doi.org/10.1002/elan.201800675.

2) Sanvito, F.; Maspero, A., Monticelli, D. Strategies for the characterization and optimization of adsorptive stripping voltammetry with catalytic enhancement for ultratrace element determination: The case of iron 2,3-dihydroxynaphthalene complex with catalytic enhancement by atmospheric oxygen, Electrochimica Acta, 321 (2019) 134653. https://doi.org/10.1016/j.electacta.2019.134653.

3) Sanvito, F.; Monticelli, D. Fast iron speciation in seawater by catalytic Competitive Ligand Equilibration-Cathodic Stripping Voltammetry with tenfold sample size reduction, Analytica Chimica Acta, 1113 (2020) 9–17. https://doi.org/10.1016/j.aca.2020.04.002.

4) Sanvito, F.; Monticelli, D. Exploring bufferless iron speciation in seawater by Competitive Ligand Equilibration-Cathodic Stripping Voltammetry: does pH control really matter?, Talanta, (2021) 122300, https://doi.org/10.1016/j.talanta.2021.122300

COMMUNICATIONS TO CONFERENCES

1) Recent evolutions in ultratrace iron detection in seawater by catalytic adsoprtive stripping voltammetry, D. Monticelli*, L. Pacileo, F. Sanvito (*presenting author), 17th International conference on Electroanalysis, Rodos (Greece), 03-07/06/2018

2) Determination of ultratrace iron in seawater: new developments of a catalytic adsorptive stripping voltammetry method, F. Sanvito*, L. Pacileo, D.Monticelli (*presenting author), XXVII Congresso della Divisione di Chimica Analitica della Società Chimica Italiana, Bologna, 16-20/09/2018

3) A novel procedure for the fast iron speciation in seawater, F. Sanvito*, D. Monticelli (*presenting author), XXVIII Congresso della Divisione di Chimica Analitica della Società Chimica Italiana, Bari, 22-26/09/2018

4) A novel Competitive Ligand Equilibration-Cathodic Stripping Vomtammetry (CLE-CSV) procedure for the fast and ultrasensitive iron speciation in seawater with tenfold sample size reduction, F. Sanvito*, L. M. Laglera, D. Monticelli (*presenting author), Ocean Sciences Meeting, San Diego-California (USA), 16-21/02/2020

ACKNOWLEDGMENTS

Professor Damiano Monticelli
Professor Angelo Maspero

Professor Luis Laglera Baquer

Laboratorio Analitica Como

FI-Trace Group

RINGRAZIAMENTI

Per anni ho pensato a come avrei scritto quest'ultima parte della tesi, a chi avrei voluto dire grazie e a chi avrei dovuto dire grazie. Ho scritto e cancellato decine di volte queste righe e solo ora mi rendo conto di quanto poco possano servire queste parole per esprimere la mia più sincera e profonda gratitudine. Per questo motivo ho deciso di chiudere questo percorso con una semplice riflessione.

Sono passati otto anni e mezzo, ormai quasi nove, da quando una ragazzina diciannovenne impaurita e piena di dubbi ha varcato le porte dell'Università. Di quella ragazzina in me ormai è rimasto ben poco, sono cambiata, sono cresciuta, e sono riuscita ad arrotondare qualche spigolo di troppo che avevo.

Sono stati nove anni sulle montagne russe, ci sono stati tanti momenti felici e di grandi soddisfazioni, che porterò per sempre nel cuore, ma, non lo nego, ci sono stati anche tanti momenti di scoforto. Più volte ho pensato che avrei abbandonato questo percorso, più volte ho pensato che avrei lasciato vincere il senso di sconfitta o di inadeguatezza che mi accompagna per mano. E invece ho vinto io, sono arrivata alla fine, soddisfatta, con la consapevolezza che più di così non sarei stata in grado di fare.

Tante persone mi hanno accompagnata in questi anni, chi in silenzio e da un angolino e chi invece facendomi sentire la propria costante presenza. Alcune hanno avuto la pazienza di supportarmi in ogni singolo secondo, facendomi da guida e mostrandomi la strada, anche quando mi sentivo totalmente persa. Alcune mi hanno teso la mano quando stavo sprofondando e hanno gioito con me quando raggiungevo uno degli obiettivi che mi ero prefissata. Alcune persone sono entrate nella mia vita come un tornado facendomi capire il senso di un'amicizia vera e pura, altre invece hanno preferito fare un passo indietro e

andarsene.
A tutti voi va il mio più grande e sincero grazie, perchè avete contribuito a rendere questi anni indimenticabili e a rendere me la persona che sono, forte e fragile allo stesso tempo.
Infine un grazie a me stessa, per aver osato, per essere uscita dai miei schemi e per avercela fatta.
E a tutti quelli che mi chiedono "*Rifaresti mai il dottorato?*" rispondo che si, lo rifarei e non cambierei nulla, nemmeno una virgola, perchè ho realizzato tanti dei miei sogni che custodivo segretamente con gelosia, perchè ho imparato cose che altrimenti non avrei mai imparato e vissuto esperienze che altrimenti non avrei mai vissuto.